

INTERIM PROGRESS REPORT:  
FITNESS-FOR-SERVICE CRITERIA FOR ASSESSING THE SIGNIFICANCE OF  
FATIGUE CRACKS IN OFFSHORE STRUCTURES

---

Y. W. Cheng

Fracture and Deformation Division  
Center for Materials Science  
National Bureau of Standards  
U.S. Department of Commerce  
Boulder, Colorado 80303

February 1985

Sponsored by  
U.S. Department of Interior  
Minerals Management Service  
12203 Sunrise Valley Drive  
Reston, Virginia 22091

## SUMMARY

This report contains results of a research program to develop a technical basis for assessing the significance of fatigue cracks that are found during in-service inspection of offshore structures. The program was sponsored by the Minerals Management Service, U.S. Department of the Interior and the research was conducted at the National Bureau of Standards.

Research results are reported in detail in the five technical papers that make up this report. Each individual paper completes a specific task. Specific goals and approaches are described in the introduction to each paper. Highlights of the results are summarized as follows:

1. An automated fatigue crack growth rate test system has been developed that can be used for tests under constant- and variable-amplitude loadings.
2. A digital simulation of broad-band signal from a power spectrum characteristic of the North Sea environments was developed to apply random-amplitude loading. Experimental results validated an equivalent-stress model of fatigue crack growth under random-amplitude loading.
3. Simplified methods of evaluating the irregularity factor of a power spectrum were derived.
4. The linear-elastic fracture mechanics analysis of fatigue crack growth at stress concentrations appeared to be adequate in yielded regions caused by monotonic loading but having a linear stress-strain relation under cyclic loading. Small-crack behavior was observed in an ABS grade EH36 steel when crack length was less than 1.5 mm in air and less than

3 mm in 3.5 percent NaCl solution. The problem of small-crack behavior was accounted for by adding an intrinsic crack length to the actual physical crack length.

5. The tensile overload retardation effects on fatigue crack growth rates were similar in elastic regions and at the edges of a yielded hole; in air and in 3.5 percent NaCl solution. Tensile overload prior to crack initiation appeared to retard subsequent fatigue crack growth in stress concentration areas. The retardation was explained by the presence of beneficial residual stresses and crack closure.

A future report will incorporate these technical findings into a procedure for calculating fatigue crack growth in offshore structures under realistic conditions.

## CONTENTS

	page
SUMMARY .....	i
INTRODUCTION .....	1
AN AUTOMATED FATIGUE CRACK GROWTH TEST SYSTEM .....	6
Abstract .....	7
Introduction .....	8
The FCGR Test Method .....	8
Equipment for the Automated FCGR Test System .....	9
Applications .....	10
Constant-Load-Amplitude FCGR Test .....	11
Near-Threshold FCGR Test .....	14
Variable-Load-Amplitude FCGR Test .....	16
Summary .....	16
Acknowledgments .....	17
References .....	17
List of Figures .....	19
SPECTRUM-LOADING FATIGUE-CRACK GROWTH FOR A SHIP STEEL IN SALTWATER ..	24
Abstract .....	25
Introduction .....	26
Load Spectrum .....	27
Simulation of Load-Time Histories .....	27
Experimental Procedures .....	29
Test Material and Specimens .....	29
Test Apparatus and Environments .....	29
Loading Conditions .....	30
Experimental Results and Discussion .....	31
Constant-Load-Amplitude Tests .....	31
Spectrum-Loading Tests .....	31
Conclusions .....	34
Acknowledgments .....	35
References .....	35
List of Tables .....	38
List of Figures .....	39
ESTIMATION OF IRREGULARITY FACTOR FROM A POWER SPECTRUM .....	50
Abstract .....	51
Introduction .....	52
Irregularity Factor .....	53
Evaluation of Irregularity Factor from A Power Spectrum .....	54

## CONTENTS (continued)

	page
Direct Integration of Power Spectral Density Function .....	54
Estimation from Characteristic Width and Center Frequency of the Power Spectrum .....	55
Summary .....	59
Acknowledgments .....	59
References .....	60
Appendix .....	61
List of Tables .....	62
List of Figures .....	63
 FATIGUE CRACK GROWTH AT AREAS OF STRESS CONCENTRATIONS .....	 73
Abstract .....	74
Introduction .....	75
Experimental Procedures .....	77
Test Material .....	77
Specimen Preparation .....	77
Loading Conditions .....	78
Test Environments and Crack-Length Measurements .....	78
Experimental Results and Discussion .....	79
Strain Survey .....	79
FCGR at Edges of A Yielded Hole in Air .....	81
FCGR at Edges of A Yielded Hole in Saltwater .....	82
Summary and Conclusions .....	83
Acknowledgments .....	84
References .....	84
List of Tables .....	86
List of Figures .....	87
 HIGH/LOW AMPLITUDE EFFECTS ON FATIGUE CRACK GROWTH RATES OF A SHIP STEEL IN AIR AND IN SALTWATER .....	 97
Abstract .....	98
Introduction .....	99
Experimental Procedures .....	100
Test Material .....	100
Specimen Preparation .....	100
Loading Conditions .....	101
Test Environments and Crack-Length Measurements .....	102
Experimental Results and Discussion .....	103
Strain Survey .....	103
Effects of High/Low Amplitude on FCGR in Air .....	104
Effects of High/Low Amplitude on FCGR in Saltwater .....	107
Effects of Tensile Overload Prior to Crack Initiation on FCGR .....	107

## CONTENTS (continued)

	page
Summary and Conclusions .....	108
Acknowledgments .....	109
References .....	109
List of Tables .....	110
List of Figures .....	111

## INTRODUCTION

Offshore structures are designed to withstand the cyclic stresses caused by wave loading. The possibility of fatigue cracking, however, exists either due to the presence of undetected defects in the as-fabricated structure or due to cyclic stresses during service. If a fatigue crack is detected during the in-service inspection of an offshore structure, a methodology is needed to assess its significance with respect to the safety of the facility. This need was clearly identified by the Committee on Offshore Energy of the Marine Board. The Committee's recommendations to the U.S. Department of the Interior for implementing a post-installation inspection program for fixed steel structures included: "Develop procedures and standards for acceptance of remedial actions carried out in response to the results of an inspection." In consideration of this need, NBS is conducting a research program for the Minerals Management Service with the following overall objective:

To develop a technical basis for recommending remedial actions to be taken in the event that a fatigue crack is discovered during in-service inspection of an offshore structure.

The basis on which remedial actions are to be taken is the fatigue crack growth (FCG) behavior under service conditions. The desired representation of FCG behavior will be fatigue crack length-vs-time curves, such as schematically shown in Figure 1. FCG behavior is best described by the fracture mechanics approach, in which fatigue crack growth rates,  $da/dN$ , are correlated to the applied stress intensity factor range,  $\Delta K$ ,

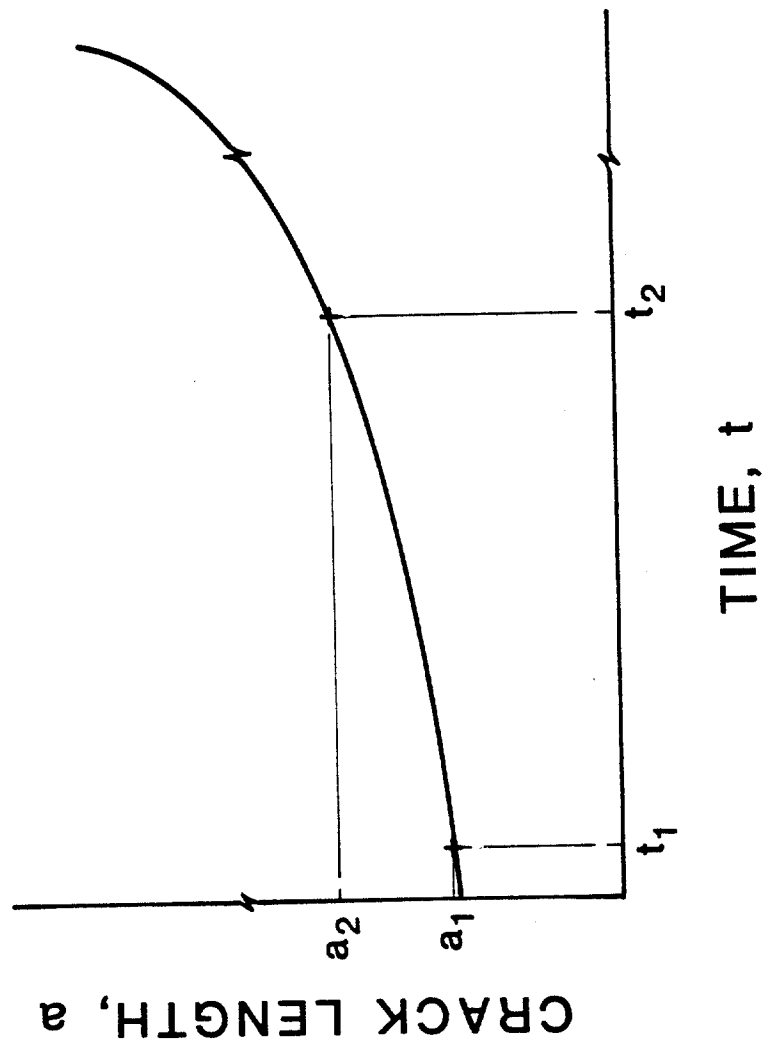


Fig. 1



$$\frac{da}{dN} = C (\Delta K)^m \quad (1)$$

where C and m are material parameters and are evaluated from laboratory specimen tests.  $\Delta K$  is a function of the applied stress range,  $\Delta S$ , the crack length, a, and a geometrical factor, F,

$$\Delta K = \Delta S \sqrt{\pi a} F \quad (2)$$

Integration of equation (1) gives crack length-vs-time (a-vs-t) results.

From equations (1) and (2), one must know the values of C, m,  $\Delta S$ , a, and F in order to evaluate FCG behavior. Referring to Figure 2 and equations (1) and (2), the basic ingredients for fatigue damage assessment are service loading history (reflected in  $\Delta S$ ), component K-solution (reflected in F), and material da/dN data (reflected in C and m) and crack length, a, found by inspection of the structure. Problems associated with the service loading history are calculation of stress range and cycle counting in cases of irregular loading histories, such as sea loadings on offshore structures. The determination and modeling of each piece of information relevant to evaluation of FCG in an offshore structure is a major task by itself and even with all the basic information available, crack growth calculation is not as straightforward as an integration of equation (1) because of load-sequence interaction effects. Understanding of load-sequence interaction effects is necessary.

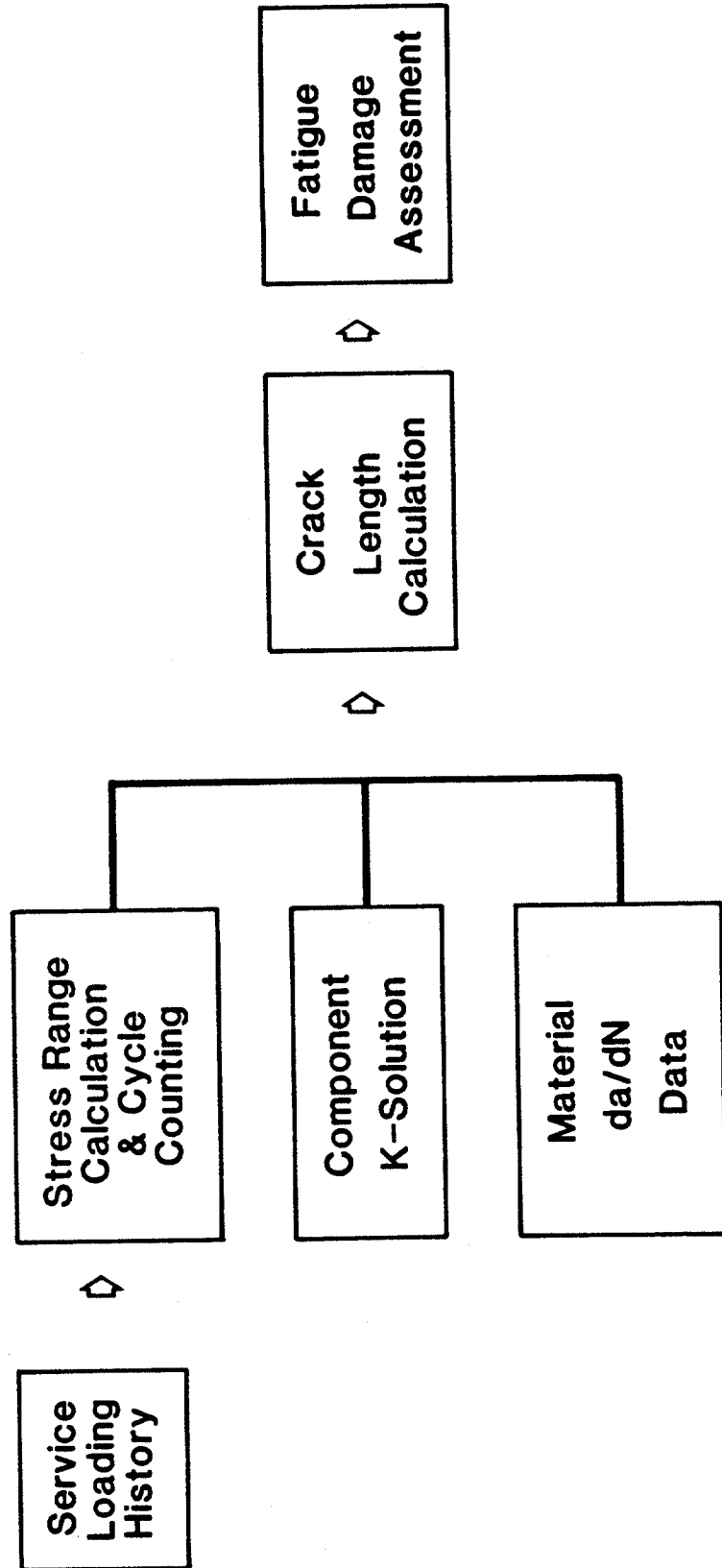


Fig 2

Owing to the complexity involved in fatigue analysis and limited resources available, the major portion of this research program has focused primarily on development, improvement, and verification of models for FCG analysis under random-amplitude loading. The specific output of this program is a procedure for performing the stress range calculation and cycle counting, to determine  $\Delta S$  and  $N$  in equations (1) and (2). The research results are given in five technical papers that follow in this report.

The additional detailed information needed for accurate FCG analysis of specific offshore structural components, such as service loading histories, component K-solutions, and material  $da/dN$  data, must be sought in the literature, especially the results from the European research program on the fatigue behavior of welded tubular joints in offshore structures for the North Sea and from the fabricators and operators of individual structure.

AN AUTOMATED FATIGUE CRACK GROWTH RATE TEST SYSTEM\*+

Yi-Wen Cheng  
David T. Read

Fracture and Deformation Division  
National Bureau of Standards  
Boulder, Colorado

Key Words: automated test system; compliance technique; fatigue crack growth rate; fatigue of materials; near-threshold fatigue test; variable-load-amplitude fatigue test.

\*Contribution of NBS; not subject to copyright.

+Submitted for publication in the Proceedings of the Symposium on Automated Test Methods for Fracture and Fatigue Crack Growth, November 7-8, 1983, Pittsburgh, Pennsylvania.

Accepted for publication in ASTM STP

## ABSTRACT

An automated fatigue crack growth rate (FCGR) test system has been developed that can be used for tests of constant-load-amplitude FCGR above  $10^{-8}$  m/cycle (ASTM E647-83) at normal ( $\sim 10$  Hz) or low ( $\sim 0.1$  Hz) cyclic frequencies and for tests of near-threshold and variable-load-amplitude FCGR. The test system consists of a minicomputer, a programmable arbitrary waveform generator, a servohydraulic test frame, and a programmable digital oscilloscope. The crack length is measured using the compliance technique; the FCGR and the stress intensity factor range are calculated and plotted automatically during the test.

## INTRODUCTION

Fatigue crack growth rate (FCGR) data are used for material characterization and for fracture mechanics reliability analysis of structures subjected to cyclic loading. A standard test method for measuring such data above  $10^{-8}$  m/cycle under constant-amplitude loading has been developed and published in the 1983 Annual Book of ASTM Standards under the designation ASTM E647-83.

With the increased interest in near-threshold FCGR<sup>1,2</sup> and FCGR under environmental influences at low cyclic frequencies<sup>3</sup>, the demand for FCGR measurements has increased. Obtaining such data can be tedious and time-consuming. An automated FCGR test system, such as that described in this paper, allows testing to proceed, data to be taken, and loads to be altered in the absence of an operator.

The automated test system minimizes testing time and operator attention. Data scatter is reduced owing to higher precision in crack length measurement and better control in data point spacing<sup>4</sup>. Because the testing is interactive and automatic in nature, the procedure is relatively easy to follow and requires minimal operator training. Finally, this approach eliminates subjective interpretation and influence of the experimenter.

## THE FCGR TEST METHOD

The sequence of the FCGR test is: first, obtain the raw data, namely, fatigue crack length,  $a$ , versus elapsed fatigue cycles,  $N$ ; then, reduce  $a$  and  $N$  data to a plot of  $da/dN$  versus  $\Delta K$ , where  $da/dN$  is the FCGR in m/cycle and  $\Delta K$  is the crack-tip stress-intensity factor range in  $\text{MPa}\cdot\text{m}^{1/2}$ . Typical outputs are presented in Figure 1.

The number of elapsed fatigue cycles can be obtained from counters (electronic or mechanical) or conversion from time elapsed at the actual testing frequency. The methods of crack length measurement are complicated

and have been a subject of extensive study<sup>5,6</sup>. Although several methods of crack length measurement have been developed, some require specialized equipment not commonly available in mechanical testing laboratories. The compliance technique, however, requires only monitoring of the load cell and the clip gage outputs, which is routinely achieved in mechanical testing. Compliance is defined as the specimen deflection per unit load, which is a function of crack length for a given material and specimen geometry. The load and deflection signals (voltages) can be interfaced to a computer. Because of the simple instrumentation and the need in our laboratory for environmental chambers for cryogenic temperature and saltwater corrosion-fatigue tests, the compliance technique was chosen to measure the crack length.

#### EQUIPMENT FOR THE AUTOMATED FCGR TEST SYSTEM

A schematic of the automated FCGR test system is shown in Figure 2. Figure 2 also shows the sequence of operation and interaction between various components. The test system consists of a closed-loop servo-controlled hydraulic mechanical testing machine, a programmable digital oscilloscope, a programmable arbitrary waveform generator, and a minicomputer.

The machine control unit, which is included in the hydraulic mechanical test machine, includes a servo-control system, a feedback system, two dc conditioners, and a valve drive. A nonprogrammable function generator with an electronic pulse counter is usually built into the machine control unit of a commercially available mechanical testing machine. Signal amplifiers and a load cell are also included in the mechanical testing machine.

The programmable digital oscilloscope contains two 15-bit 100-kHz digitizers and it serves as an analog-to-digital (A/D) converter. In addition to its high speed A/D conversion rate, this oscilloscope features the ability to instantaneously freeze and hold data in memory. The problems encountered with

slower A/D converters, such as interruptions during the test<sup>7</sup> and low test frequencies<sup>8</sup> are eliminated because of the high A/D conversion rate and the freeze-and-hold ability of this oscilloscope. For the near-threshold and the variable-load-amplitude FCGR tests, load levels vary with time and a programmable function generator is needed. For these tests, the programmable arbitrary waveform generator is used. The present programmable waveform generator is not connected to a cycle-counting device and the fatigue cycle counts are inferred from the cyclic frequency<sup>\*</sup> and the time elapsed, as given by the computer. For the constant-load-amplitude FCGR test, the built-in function generator is used.

Included in the minicomputer are a cathode-ray-tube (CRT) terminal, a line printer, a dual floppy disk storage unit, and a digital plotter. The minicomputer uses the 16-bit word and has 128K words of memory. The minicomputer also contains an internal clock that reads to 1/60 s. The IEEE-488/GPIB is used for the interface between the computer and the programmable digital oscilloscope and between the computer and the programmable arbitrary waveform generator.

#### APPLICATIONS

In the following discussion, attention is focused on how the test system described above is used to conduct the FCGR tests. Requirements on grips, fixtures, specimen design, and specimen preparation are detailed in ASTM E647-83 and other proposed standards<sup>3,9</sup> and are not discussed in this paper.

---

\*The frequency used for cycle calculations is checked with a frequency meter; the typical error in frequency is 50 ppm.



### Constant-Load-Amplitude FCGR Test

The test system described in the previous section can be programmed to run the constant-load-amplitude FCGR test. The operational details, implementing the procedures set forth by ASTM E647-83, are described in this section.

As shown in Figure 3, the input parameters are fed by the operator into the computer through the CRT terminal. The input parameters include specimen identification, specimen dimensions, Young's modulus, selected time interval for measuring crack length, minimum load level for compliance measurement, load levels, and test frequency. The time interval for measuring crack length must be kept to a value small enough that every increment of crack growth will not exceed the recommended values as prescribed in ASTM E647-83. The minimum load level for compliance measurement is used to eliminate the possible crack closure effects<sup>10</sup>, which have a significant effect on the accuracy of crack length measurement.

The precracked specimen is fatigue cycled under the prescribed loading conditions and cyclic frequency. A typical frequency is 10 Hz. When the preselected time interval (typical value is 1 minute) for crack length measurement is reached, the computer requests the load-versus-deflection data from the programmable digital oscilloscope, which freezes the load-deflection data in the memory instantaneously, and correlates the data to a straight line using a linear least-squares fit. A linear correlation coefficient of 0.999 or better is usually obtained. From the resulting compliance, the instantaneous crack length is computed using the appropriate expression for the compliance calibration of the specimen<sup>11</sup>. The precision of the crack length measurement is typically within 0.04 mm.

The inferred crack length, which is obtained from the measured compliance, published compliance calibrations, and published Young's modulus, usually does not agree exactly with the actual crack length for a given material and specimen geometry. The exact reasons for the discrepancy between the inferred and the actual crack lengths are not clear and have been discussed in references 12 and 13. Correction factors to the compliance calibration have been used to obtain more accurate physical crack length predictions.

An alternative way of correcting the mismatch between the inferred and the actual crack lengths is to adopt an "effective modulus" for the material. The effective modulus,  $E_{eff}$ , is deduced from a known crack length in a given specimen geometry and compliance calibration. Typically,  $E_{eff}$  is deduced from one well-defined crack front that is visible on a post-test fracture surface. The crack front at the end of fatigue precracking or at the final fatigue crack length is generally used. The effective modulus approach, which is used in our laboratory, thus forces agreement between the inferred and the actual crack lengths and compensates for any errors regardless of source<sup>13</sup>.

The portion of the load-versus-deflection curve used for compliance calculation is from the specified minimum load level to a value corresponding to 95 percent of the maximum load. The typical minimum load level used for compliance calculation is the mean load (load signal midpoint). It should be noted, however, that the specific value of the minimum load level used for a given material, specimen geometry, and load ratio must be larger than crack closure loads. The reason for excluding the upper 5 percent of the load for calculation is that the clip gage tends to vibrate, and noise in the clip-gage signal increases at the maximum load during the high-frequency test.

The increment of crack growth (the difference between the current

measured crack length and the last recorded crack length) is checked against specified values which are within the recommended values of ASTM E647-83. A value of 0.5 mm is typically specified for a 25.4-mm-thick standard compact-type specimen. If the increment of crack growth is equal to or greater than the specified value, the computer calculates  $N$ ,  $\Delta K$ , and  $da/dN$ ; the digital plotter plots the data points  $(a, N)$  and  $(da/dN, \Delta K)$  on the  $a$ -versus- $N$  and on the  $da/dN$ -versus- $\Delta K$  graphs, such as shown in Figure 1; the line printer prints the value of calculated compliance, the linear least-squares correlation coefficient,  $a$ ,  $N$ ,  $da/dN$ , and  $\Delta K$  results. All the resulting data are stored on floppy disks for post-test analyses.

During the test, the point-to-point data reduction technique is used to calculate  $\Delta K$  and  $da/dN$  from  $a$  and  $N$ . Usually the results are consistent with minimum scatter, as those shown in Figure 1. If the results of  $\Delta K$  versus  $da/dN$  scatter, the seven-point incremental polynomial method is used to smooth the results after the test is completed.

The computer programs for post-test analyses include the following capabilities:

1. Reducing  $a$ -versus- $N$  data to  $\Delta K$ -versus- $da/dN$  by the seven-point incremental polynomial method;
2. Converting units;
3. Plotting data in desired units;
4. Plotting data in desired coordinate ranges;
5. Plotting data for several different specimens on one graph (for comparison);
6. Calculating the material constants  $C$  and  $n$  in the Paris equation<sup>14</sup>,  $da/dN = C(\Delta K)^n$ , and drawing the regression line through the data.

All computer programs, including the data acquisition routines, were written in the PDP-11 Fortran language.

### Near-Threshold FCGR Test

The computer programs used in the constant-load-amplitude FCGR test, with some modifications, can be used for near-threshold FCGR tests. The major difference in procedures between the two tests is that the load levels in the near-threshold FCGR test decrease according to the initial  $\Delta K$  value (in the K-decreasing test technique). The load levels are calculated from the following equations<sup>9</sup>:

$$\Delta K = \Delta K_0 \exp[C'(a - a_0)] \quad (1)$$

$$\Delta P = BW^{\frac{1}{2}} \Delta K / f_1(a/W) \quad \text{for compact-type specimen} \quad (2)$$

$$\Delta P = B \Delta K / f_2(a/W) \quad \text{for center-cracked-tension specimen} \quad (3)$$

$$P_{\max} = \Delta P / (1 - R); P_{\min} = P_{\max} R \quad (4)$$

where  $P_{\max}$  = maximum load

$P_{\min}$  = minimum load

$R = P_{\min} / P_{\max}$

$B$  = specimen thickness

$W$  = specimen width

$a$  = the current crack length

$a_0$  = the crack length at the beginning of the test

$$f_1(a/W) = [2 + (a/W)] [0.886 + 4.64(a/W) - 13.32(a/W)^2 + 14.72(a/W)^3 - 5.6(a/W)^4] / [1 - (a/W)^{1.5}]$$

$$f_2(a/W) = [(\pi a/W^2) \sec(\pi a/W)]^{\frac{1}{2}}$$

$\Delta K$  = current crack-tip stress-intensity range

$\Delta K_0$  = crack-tip stress-intensity range at the beginning of the test

$C'$  = negative constant

A typical value of  $C'$  is  $-0.08 \text{ mm}^{-1}$  which gives satisfactory results with no apparent anomalous crack growth for AISI 300-series stainless steels.

The flow chart describing the automated near-threshold FCGR test is summarized in Figure 4. After each crack length measurement, the crack length is compared with the last stored crack length to ensure that a specified measurable small amount of crack growth has occurred. If this is not done, then some unnecessary load level adjustments will take place because of scatter in the crack length measurement. After the crack length has increased a certain amount (for example, 0.13 mm), the new  $\Delta K$  is calculated according to equation (1) and the new crack length is stored. The load levels are then adjusted using equations (2), (3), and (4).

In high-frequency fatigue testing, which is desirable in the near-threshold FCGR test, hydraulic lag might be a problem. This results in the specimen not being actually subjected to the load range commanded by the computer (or waveform generator). The problem is usually corrected by using proper signal conditioners and gain settings. However, overprogramming is sometimes necessary to overcome the persistent hydraulic lag. During the overprogramming process, which is done by trial-and-error method, the computer monitors the values of  $P_{\max}$  and  $P_{\min}$  through the programmable digital oscilloscope and makes necessary changes to achieve the desired values of  $P_{\max}$  and  $P_{\min}$ . The overprogramming is done whenever there is a hydraulic lag problem.

If the measured crack-growth increment, which is the difference between the current measured crack length and the last recorded crack length, is equal to or greater than specified values, which are within the recommended values<sup>8</sup>, the values of  $N$ ,  $\Delta K$ , and  $da/dN$  are calculated and the results are printed, plotted, and stored. A value of 0.5 mm is typically specified for a 25.4-mm-thick standard compact-type specimen. The previously mentioned computer programs for post-test analyses are also applicable for analyzing the data obtained in the near-threshold FCGR test.

### Variable-Load-Amplitude FCGR Test

The automated FCGR test system is also used in the variable-load-amplitude FCGR test. The procedures used in this application are similar to those described in the previous two sections.

The computer reads the prerecorded load-time history from the floppy disks and controls the hydraulic machine through the programmable waveform generator. At a preselected time interval, the crack length is measured. A typical interval is 30 minutes for an average test frequency of 0.1 Hz. The desired output in the variable-load-amplitude FCGR test is time versus crack length. The results are printed, plotted, and stored for post-test analyses.

The present system has two limitations in the application of variable-load-amplitude FCGR testing. One is that the waveform generator needs about 0.1 s for changing one command to another, and this limits the average frequency to about 1 Hz. This will result in a situation of holding about 0.1 s at the peak loads when higher test frequencies are used. In a corrosive or a high temperature environment, in which hold time at peak load is important, this might introduce anomalous fatigue crack growth. The other is the limited storage capacity of the floppy disks, which can only store a certain amount of load-time pairs. The present system uses soft disks which can store about 18,000 load-time pairs. If longer load-time histories are desired, other means of storage devices, such as hard disks must be used.

### SUMMARY

An automated FCGR test system has been developed that can be used for tests of constant-load-amplitude FCGR above  $10^{-8}$  m/cycle (ASTM E647-83), near-threshold FCGR, and variable-load-amplitude FCGR. The test system offers considerable time savings in data acquisition and in data reduction. The test procedure is relatively easy to follow and enables technicians to produce data

with less scatter (with respect to the non-computer-aided technique), because higher precision in crack length measurement, and better control in data point spacing are obtained, while manual data interpretation and data fitting are eliminated.

#### ACKNOWLEDGMENTS

Mr. J. C. Moulder of NBS is acknowledged for helpful discussions on the interface between the computer and the instruments. The work was supported by the Department of Interior, Minerals Management Service, and the Department of Energy, Office of Fusion Energy.

#### REFERENCES

1. Fatigue Thresholds: Fundamentals and Engineering Applications, J. Backlund, A. F. Blour, and C. J. Beevers, eds., Engineering Materials Advisory Services, Chameleon Press, London, United Kingdom (1982).
2. R. J. Bucci, "Development of a Proposed ASTM Standard Test Method for Near-Threshold Fatigue Crack Growth Rate Measurement," in: Fatigue Crack Growth Measurement and Data Analysis, ASTM STP 738, S. J. Hudak, Jr. and R. J. Bucci, eds., American Society for Testing and Materials, Philadelphia, Pennsylvania (1981), pp. 5-28.
3. T. W. Crooker, F. D. Bogar, and G. R. Yoder, "Standard Method of Test for Constant-Load-Amplitude Fatigue Crack Growth Rates in Marine Environments," NRL Memorandum Report 4594 (August 6, 1981).
4. R. P. Wei, W. Wei, and G. A. Miller, "Effect of Measurement Precision and Data-Processing Procedure on Variability in Fatigue Crack Growth-Rate Data," Journal of Testing and Evaluation, Vol. 7, No. 2 (March 1979), pp. 90-95.
5. The Measurement of Crack Length and Shape During Fracture and Fatigue, C. J. Beevers, ed., Engineering Materials Advisory Services, Chameleon Press, London, United Kingdom (1980).
6. Advances in Crack Length Measurement, C. J. Beevers, ed., Engineering Materials Advisory Services, Chameleon Press, London, United Kingdom (1981).
7. Y.-W. Cheng, "A Computer-Interactive Fatigue Crack Growth Rate Test Procedure," in: Materials Studies for Magnetic Fusion Energy Applications at Low Temperatures-VI, R. P. Reed and N. J. Simon, eds., NBSIR 83-1690, National Bureau of Standards, Boulder, Colorado (1983), pp. 41-51.

8. J. J. Ruschau, "Fatigue Crack Growth Rate Data Acquisition System for Linear and Nonlinear Fracture Mechanics Applications," Journal of Testing and Evaluation, Vol. 9, No. 6 (Nov. 1981), pp. 317-323.
9. "Proposed ASTM Test Method for Measurement of Fatigue Crack Growth Rates," in: Fatigue Crack Growth Measurement and Data Analysis, ASTM STP 738, S. J. Hudak, Jr. and R. J. Bucci, eds., American Society for Testing and Materials, Philadelphia, Pennsylvania (1981), pp. 340-356.
10. W. Elber, "The Significance of Fatigue Crack Closure," in: Damage Tolerance in Aircraft Structures, ASTM STP 486, M. S. Rosenfeld, ed., American Society for Testing and Materials, Philadelphia, Pennsylvania (1971), pp. 230-242.
11. S. J. Hudak, Jr., A. Saxena, R. J. Bucci, and R. C. Malcolm, "Development of Standards of Testing and Analyzing Fatigue Crack Growth Rate Data," AFML-TR-78-40, Air Force Materials Laboratory, Wright-Patterson Air Force Base, Ohio (May 1978).
12. T. Nicholas, N. E. Ashbaugh, and T. Weerasooriya, "On the Use of Compliance for Determining Crack Length in the Inelastic Range," to be published in ASTM STP 833.
13. R. L. Tobler and W. C. Carpenter, "A Numerical and Experimental Verification of Compliance Functions for Compact Specimens," to be published in Engineering Fracture Mechanics.
14. P. C. Paris and F. Erdogan, "A Critical Analysis of Crack Propagation Laws," Transactions of ASME, Journal of Basic Engineering, series D, Vol. 85, No. 3 (1963), pp. 528-534.



## LIST OF FIGURES

- Figure 1. Data outputs from the automated FCGR test.
- Figure 2. Schematic of the automated FCGR test system.
- Figure 3. Summary flow chart of the automated constant-load-amplitude FCGR test.
- Figure 4. Summary flow chart of the automated near-threshold FCGR test.

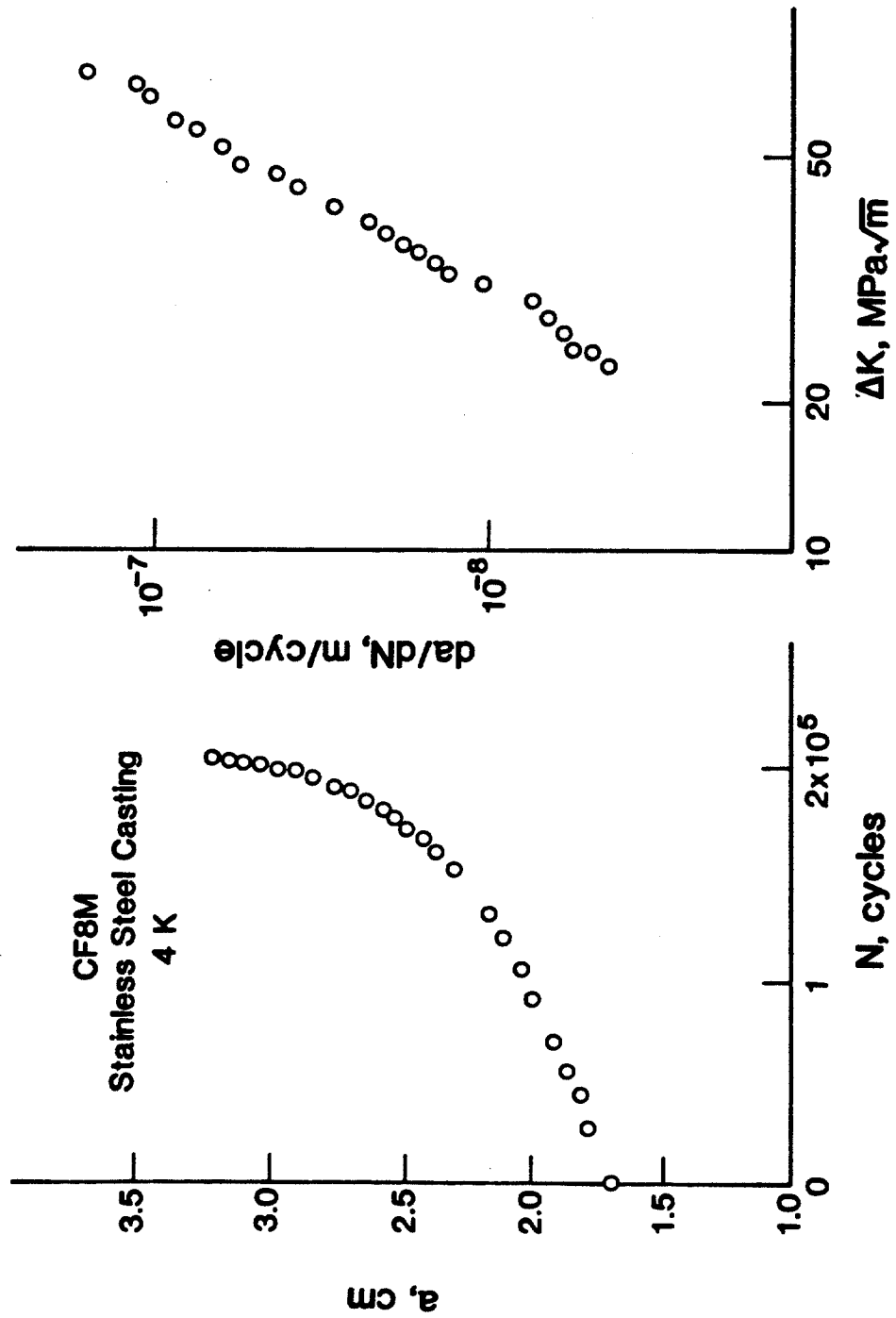


Figure 1. Data outputs from the automated FCGR test.

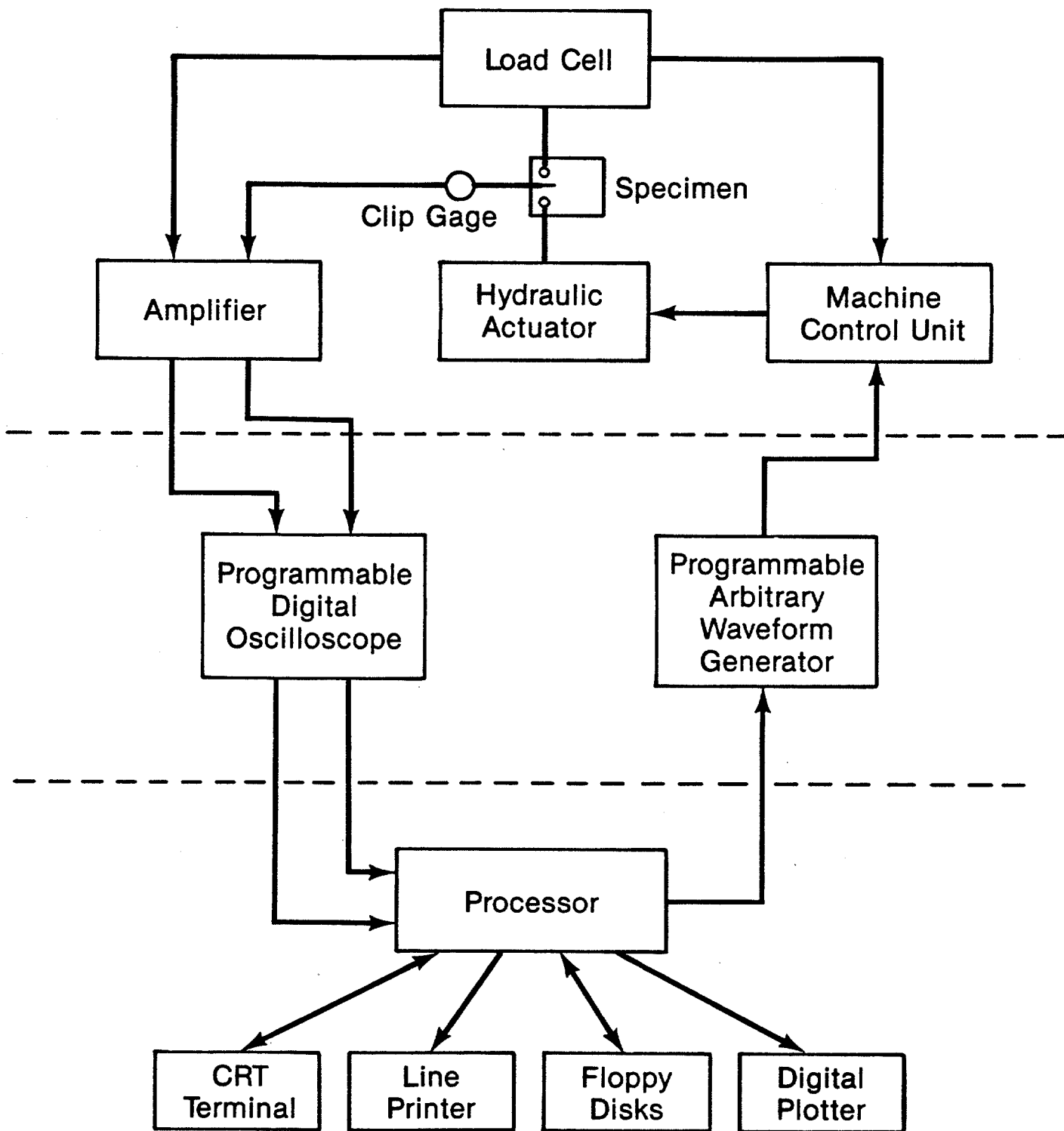


Figure 2. Schematic of the automated FCGR test system.

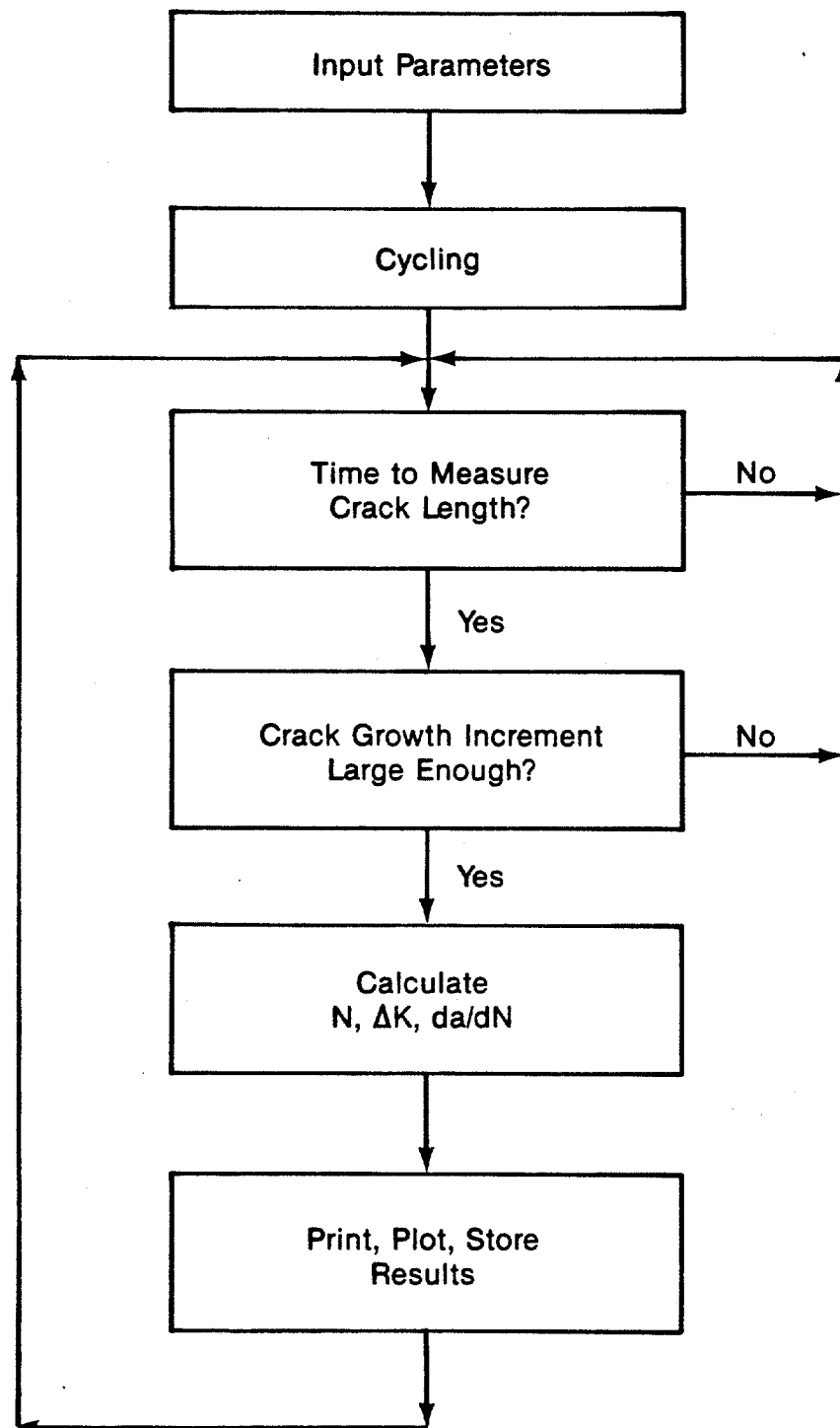


Figure 3. The summary flow chart of the automated constant-load-amplitude FCGR test.

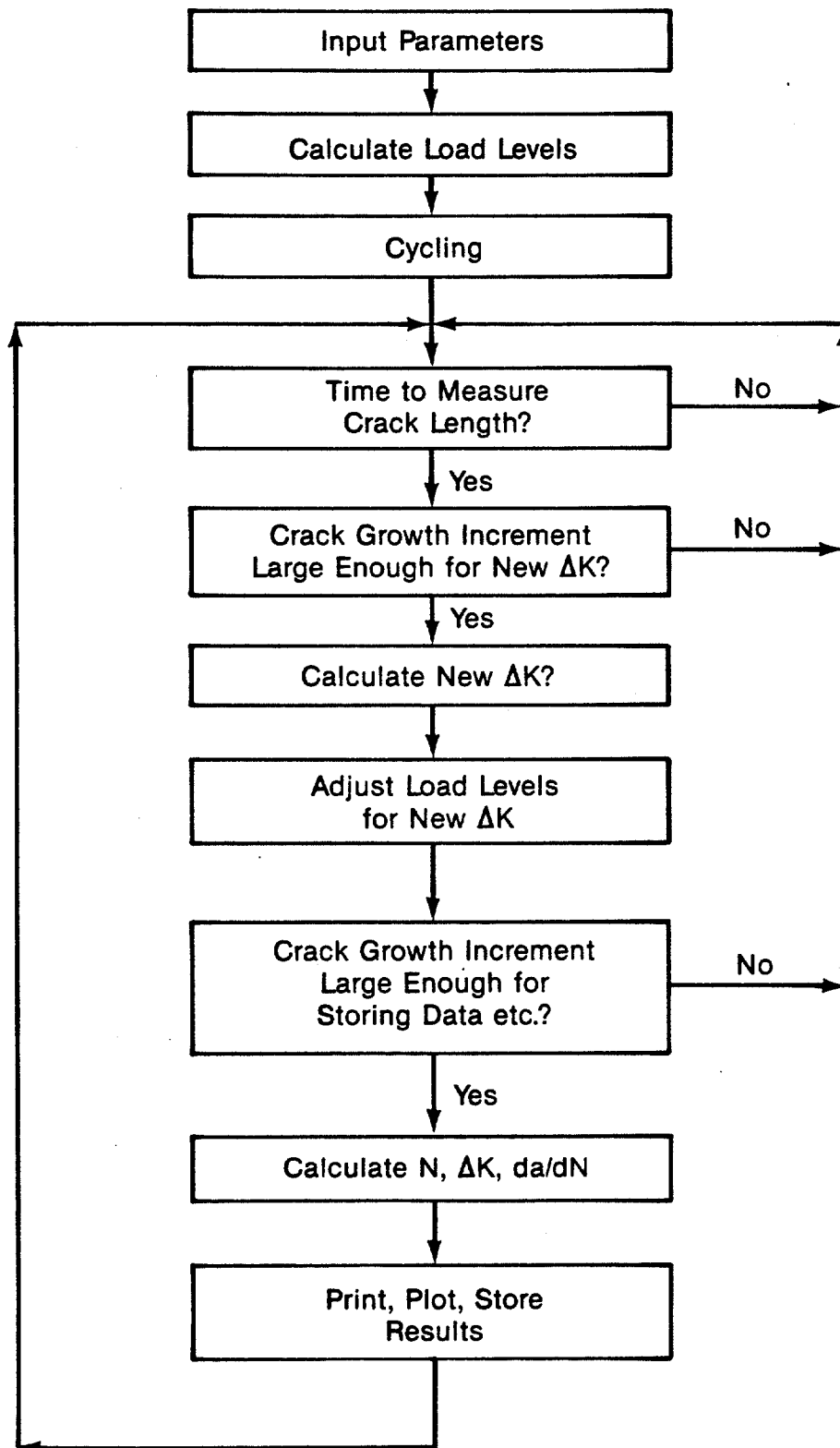


Figure 4. The summary flow chart of the automated near-threshold FCGR test.

SPECTRUM-LOADING FATIGUE-CRACK GROWTH  
FOR A SHIP STEEL IN SALTWATER\*

Yi-Wen Cheng  
Fracture and Deformation Division  
National Bureau of Standards  
Boulder, Colorado 80303

Keywords: corrosion fatigue; fatigue crack growth; fracture mechanics;  
seawater environment; spectrum loading; structural steel.

\*Contribution of NBS; not subject to copyright.

*To be published in the International Journal of Fatigue*  
*April, 1985*

## ABSTRACT

Fatigue crack growth under spectrum loading intended to simulate sea loading of offshore structures in the North Sea was studied using the fracture mechanics approach. A digital simulation technique was used to generate samples of load-time histories from a power spectrum characteristic of the North Sea environments. In the constant-load-amplitude tests, the effects of specimen orientation and stress ratio on fatigue crack growth rates were found to be negligible in the range from  $2 \times 10^{-5}$  to  $10^{-3}$  mm/cycle. Fatigue crack growth rates in a 3.5 percent NaCl solution were two to five times faster than those observed in air in the stress intensity range 25 to 60 MPa/m. The average fatigue crack growth rates under spectrum loading and under constant-amplitude loading were in excellent agreement when fatigue crack growth rate was plotted as a function of the appropriately defined equivalent-stress-intensity range. This procedure is equivalent to applying Miner's summation rule in fatigue life calculations.

## INTRODUCTION

In recent years the petroleum industry has built offshore drilling and production platforms in deeper waters and more hostile climates.<sup>1</sup> As the offshore platforms encounter more severe weather and rougher sea-state conditions, fatigue becomes a more important factor in consideration of structural integrity. In treating the fatigue problem, it is usual to separate the fatigue life into two separate stages: (1) crack initiation; and (2) crack growth. For welded structures, such as offshore platforms, crack initiation, during which microcracks form, grow, and coalesce to become a macrocrack, is less important because fabrication imperfections are always present. The majority of the fatigue life is spent in the crack growth stage.

Analysis of fatigue crack growth under spectrum loading, which is usually irregular in nature, is complicated because of load-sequence interaction effects. A cycle-by-cycle approach, taking into account overload effects, has been used in the aerospace industry [1,2]. Other empirical approaches, such as root mean square (RMS) [3] or root mean cube (RMC) [4], were also successfully used to correlate experimental results of spectrum loading of bridges with those of constant-amplitude loading. Use of the latter approaches is empirical and implementation of the former is time-consuming. A more efficient approach has been proposed [5,6], which will be discussed later. This paper describes work carried out at the National Bureau of Standards over the past two years on the investigation of fatigue crack growth in ABS grade EH36 steel under simulated offshore platform service conditions.



## LOAD SPECTRUM

Service loads acting on offshore structures are random in nature. The main source of cyclic loading derives from wave action which excites a vibration at approximately the wave frequency. The magnitude of the vibration depends mainly on wave height and direction, size of component and its location in a structure. Besides vibration due to wave action, additional vibrations are induced from structural responses to the wave action. The magnitude and frequency of the structural resonance depend on local structural characteristics. Thus, the precise definition of load-time history is extremely complex and would be expected to vary between different locations on the same structure.

Because of complexity in and lack of information on the precise load-time history experienced by offshore structures, no standard load-time history is available (or exists) for purposes of analysis and experiment. Numerous load-time histories, including Rayleigh peak distribution [7,8], Gaussian peak distribution [7-9], Gassner blocked program [10], and others [11], have been used to evaluate fatigue performance of weldments. The load spectrum selected for the present investigation was realistic for offshore structures in North Sea environments [12], as shown in Figure 1. The principal loads in this spectrum, those with a frequency of about 0.1 Hz, are due to wave action. The higher frequency (about 0.35 Hz) loads are due to the structural resonance.

## SIMULATION OF LOAD-TIME HISTORIES

For purpose of experiment, the power spectral density function,  $S(\omega)$ , is not sufficient; load-time history,  $X(t)$ , has to be used. In this investigation, the following expression [13,14] was used to reconstruct  $X(t)$  from  $S(\omega)$ :

$$X(t) = \sum_{k=1}^J [2G(\omega_k)\Delta\omega_k]^{\frac{1}{2}} \cos(\omega_k t + \phi_k) \quad (1)$$

where  $G(\omega)$ , as shown in Figure 1, is the one-sided power spectral density function in terms of frequency,  $\omega$  ( $G(\omega) = 2S(\omega)$  for  $\omega > 0$ ). Frequency is defined over the interval  $[0, \omega_u]$  with partitions of length such that

$$\omega_u = \sum_{k=1}^J \Delta\omega_k \quad (2)$$

$\phi$  is a random phase angle uniformly distributed between 0 and  $2\pi$ .  $\omega_k$  is the midpoint of  $\Delta\omega_k$ . The number of harmonic functions,  $J$ , is arbitrary; in this investigation it was taken to be 50.

An undesired periodic  $X(t)$  with a short period occurs if the minimum common divider for all the  $\Delta\omega_k$  is large. This problem is avoided by using random intervals for  $\Delta\omega_k$ . In this investigation,  $\Delta\omega_k$  was taken from a normal distribution with a mean equal to the average of  $\Delta\omega_k$  and a standard deviation equal to one-tenth of the average of  $\Delta\omega_k$ .

A computer program written in Fortran IV has been developed to simulate  $X(t)$  using Eq. (1). Newton's method was then used to locate peaks and troughs with respect to time in the simulated load-time history.

Two load spectra were used in this study. One considers only the wave-loading portion of the power spectral density function with frequency up to 0.2 Hz (Case I) as shown in Figure 1. The other considers the whole curve (Case II). Typical simulated load-time histories  $X(t)$ , from the power spectral density function are shown in Figure 2a and b.

Values of the irregularity factor (number of mean crossings/number of peaks plus troughs) calculated from the power spectra are 0.90 and 0.69 for Case I and Case II, respectively; they are 0.90 and 0.68, as determined from

the simulated load-time histories. The excellent agreement between the values obtained from the power spectra and the simulated load-time histories indicates that use of Eq. (1) is satisfactory. Values of the clipping ratio are 3.84 and 3.91 for Case I and Case II, respectively. Clipping ratio is defined as the ratio of the maximum load amplitude, which is the difference between the maximum peak and the mean load, to the root-mean-square value of load amplitude.\*

#### EXPERIMENTAL PROCEDURES

Test Material and Specimens: The test material was a 25.4-mm thick plate of ABS grade EH36 steel, a 350-MPa-yield-strength C-Mn steel. The chemical composition is given in Table 1. The steel was in the normalized condition and had particularly uniform properties due to sulfide shape control.

Fatigue crack growth rate (FCGR) tests under constant-amplitude loading and spectrum loading were conducted using standard (25.4-mm thick) and modified [15] compact specimens. The modified compact specimen was a lengthened and side-grooved (with a net thickness of 3.18 mm) version of the standard compact specimen. The deep side grooves determine the plane of crack growth and provide a strip of material that undergoes large cyclic plasticity during fatigue. Specimens were in LT and TL orientations.

Test Apparatus and Environment: Fatigue crack growth rate tests were conducted with a fully automated test system, which was described in a previous paper [16]. Briefly, the fully automated test system consists of a closed-loop, servo-controlled, hydraulic mechanical test machine, a programmable digital oscilloscope serving as an analog-to-digital converter, a programmable arbitrary waveform generator, and a minicomputer.

---

\* This should not be confused with the root-mean-square value of load range which was used in Ref. 3.

Tests were performed in laboratory air and in 3.5 percent NaCl solution with a free corroding condition (no cathodic protection). Crack lengths were measured by the compliance technique. The crack-length measurement technique is at least accurate to 0.1 mm. In the saltwater tests, the clip-gage used for displacement measurements was mounted on a scissors-like extension to avoid immersion in the saltwater. The environmental chamber was a 19- $\ell$ -capacity plastic container. The saltwater is continuously circulated at a rate of 26  $\ell$ /minute through a diatomaceous-earth filter. The NaCl concentration, temperature, and pH value of the saltwater was monitored periodically.

Loading Conditions: In the constant-load-amplitude tests, the stress ratio,  $R$ , that is the ratio of minimum to maximum stress, was kept constant at 0.1 or 0.5. Tests in air were conducted at 10 Hz and tests in 3.5 percent NaCl solution were conducted at 0.1 Hz. A sinusoidal load-time history was used.

In the spectrum-loading tests, the simulated load-time histories were recorded on floppy disks, which were read by a minicomputer. The minicomputer then sent the signals to the hydraulic mechanical test machine through a programmable arbitrary waveform generator. The loads were periodically monitored with an oscilloscope by comparing the input values to the hydraulic mechanical test machine and the output values from the load cell. The input and output values must agree each other during the test. No modifications, such as truncation, on the simulated load-time histories were done, except on the levels of mean loads. The mean loads were increased so that the minimum loads were slightly above zero. This was done because the apparatus was limited to tension-tension loading. The stress ratio, therefore, varied from about 0 (usually for large load ranges) to about 1 (usually for very small load ranges).

Because of the limited capacity of the floppy disk, the total recorded lengths of load-time histories were 18.0 hours for Case I and 9.3 hours for

Case II. The recorded lengths correspond to return periods of 15,773 and 11,890 mean-load crossings for Case I and Case II, respectively. The wave shape was triangular. It has been shown [17] that there are no differences in FCGR between tests conducted with sinusoidal and triangular waveforms. Both tests in air and in saltwater were conducted at ambient temperature.

#### EXPERIMENTAL RESULTS AND DISCUSSION

Constant-Load-Amplitude Tests: Fatigue crack growth rates were calculated using the linear-elastic fracture mechanics approach; the experimental results are shown in Figures 3-6. As shown in Figure 3, specimen orientation, TL vs LT, had little influence on FCGR in air and in saltwater. The FCGR in air and in saltwater are compared in Figures 4 and 5. For stress intensity range,  $\Delta K$ , between 30 and 40 MPa $\sqrt{m}$ , the growth rates in saltwater were up to five times faster than those in air. A summary of all results, Figure 6, indicated that stress ratio had small influence on FCGR in air. Below  $4 \times 10^{-5}$  mm/cycle the FCGR in air and in saltwater were about the same.

The observed behavior of little influence of stress ratio and specimen orientation is consistent with that of other investigators [18] in the FCGR range from  $2 \times 10^{-5}$  to  $10^{-3}$  mm/cycle. The effects of stress ratio and specimen orientation are expected to be more pronounced at higher and lower FCGR [18].

Note that in each of the FCGR curves the high growth rate data were obtained with the modified compact specimen. The data obtained with the modified compact specimen follow the same trend line as the data obtained with the standard compact specimen. Thus it appears that the linear-elastic fracture mechanics approach can be applied to fatigue crack growth in conditions of contained large cyclic plasticity.

Spectrum Loading Tests: Fatigue crack growth rates under spectrum loading were analyzed using the equivalent-stress-range approach [5,6], which is

described in the following. For simplicity the Paris equation,  $da/dN = C(\Delta K)^n$ , is used for discussion. Here,  $da/dN$  is crack growth increment per load cycle,  $\Delta K$  is stress intensity range, and  $C$  and  $n$  are constants.  $\Delta K$  is defined as

$$\Delta K = h (\pi a)^{\frac{1}{2}} Y \quad (3)$$

where  $h$  = stress range

$a$  = crack length

$Y$  = geometry factor

If  $da/dN \ll$  crack length,  $a$ , and there are no load-sequence interaction effects, then

$$\Delta a_1 = C h_1^n [(\pi a)^{\frac{1}{2}} Y]^n \quad (4)$$

$$\Delta a_2 = C h_2^n [(\pi a)^{\frac{1}{2}} Y]^n \quad (5)$$

...

...

...

$$\Delta a_N = C h_N^n [(\pi a)^{\frac{1}{2}} Y]^n \quad (6)$$

Summing Eqs. (4) through (6) gives

$$(\Delta a_1 + \Delta a_2 + \dots + \Delta a_N) = C (h_1^n + h_2^n + \dots + h_N^n) [(\pi a)^{\frac{1}{2}} Y]^n \quad (7)$$

The left-hand side of Eq. (7) is the increment of crack growth in  $N$  successive cycles; the average FCGR per cycle is then

$$da/dN = C [(h_1^n + h_2^n + \dots + h_N^n)/N] [(\pi a)^{\frac{1}{2}} Y]^n \quad (8)$$

$$= C [(\overline{h^n})^{1/n} (\pi a)^{\frac{1}{2}} Y]^n \quad (9)$$

$$= C [h_{eq} (\pi a)^{\frac{1}{2}} Y]^n$$

Here  $N$  should be large in order for the equivalent-stress-range,  $h_{eq}$ , to be representative of a load spectrum. The definitions of stress range and cycle used in this investigation are given in Figure 7. The value of  $n$  in 3.5 percent NaCl solution test is 5.5, which is derived from the results of constant-load-amplitude test in the  $\Delta K$  range of interest.

The results for FCGR under spectrum loading in 3.5 percent NaCl solution are given in Figures 8 and 9 for Case I and Case II, respectively. Excellent agreement between spectrum and sinusoidal loading is observed. This suggests that load-sequence interaction effects are effectively negligible. The lack of observed load-sequence effects is probably due to low clipping ratios of 3.84 (Case I) and 3.91 (Case II). The results also imply that under spectrum loading at a given  $da/dN$ , value of  $\Delta K$  is smaller if RMS ( $n = 2$ ) or RMC ( $n = 3$ ) approach is used because  $h_{eq}$  decreases with decreasing  $n$ . This will shift the spectrum-loading results to the left of those of constant-amplitude loading (Figures 8 and 9), resulting in higher FCGR in spectrum loading than in constant-amplitude loading at a given value of  $\Delta K$ . Conversely, slower FCGR will result if RMS or RMC is used to predict FCGR in a region where  $n$  is larger than 3, such as in the present investigation.

Miner's rule [19] states that a component (or specimen) will fail if

$$\sum (f_i/F_{if}) \geq 1 \quad (10)$$

where  $f_i$  = number of fatigue cycles applied at stress range  $\Delta S_i$

$F_{if}$  = number of fatigue cycles to failure at stress range  $\Delta S_i$

This rule implies that there are no load-sequence interaction effects. Miner's rule, as originally stated, applied to fatigue failure rather than fatigue crack growth. Terms such as "Miner's rule fatigue crack growth" are

often used to mean fatigue crack growth with no load-sequence interaction effects. Such statements represent a generalization of the original Miner's rule. The data of this study along with others [5] support such a generalization for clipping ratio less than 4 and constant mean stress, which might be stated as follows: Load-sequence interactions are small, or they tend to cancel, such that the overall effect on fatigue life is small. In order for such a rule to be applicable to random or quasi-random load-time histories, a definition of a cycle is needed. In this study, the load amplitude of one cycle has been defined as the maximum load difference among three successive mean-crossings (Figure 7).

The value of  $h_{eq}$  can be obtained in a closed-form expression from the power spectrum if the loading is a narrow-band random process [6,20]. However, no closed-form solutions are available for wide-band random processes.

## CONCLUSIONS

The following conclusions were drawn from this investigation:

1. The digital simulation technique is adequate to generate samples of load-time histories from a given power spectrum.
2. In constant-load-amplitude tests, the influence of specimen orientation and stress ratio on fatigue crack growth rate were found to be negligible in the fatigue crack growth rate range from  $2 \times 10^{-5}$  to  $10^{-3}$  mm/cycle. Fatigue crack growth rates in a 3.5 percent NaCl solution were two to five times faster than those observed in air in the stress intensity range 25 to 60 MPa/m.
3. The average fatigue crack growth rates under spectrum loading and under constant-amplitude loading were in excellent agreement when fatigue crack growth rate was plotted as a function of the appropriately defined equivalent-stress-intensity range. This procedure is equivalent to applying Miner's summation rule in fatigue life calculations.



## ACKNOWLEDGMENTS

Helpful discussions with Drs. H. I. McHenry, and D. T. Read, and Professors S. Berge and P. N. Li are appreciated. This work is supported by the Department of Interior, Minerals Management Service.

## REFERENCES

1. O. E. Wheeler, "Spectrum Loading and Crack Growth," J. of Basic Engineering , Trans. ASME, Vol. 94, (March 1972), pp. 181-186.
2. J. Willenborg, R. M. Engle, and H. A. Wood, "A Crack Growth Retardation Model Using An Effective Stress Concept," AFFDL-TM-71-FBR, Air Force Flight Dynamics Laboratory, Dayton, Ohio, January 1971.
3. J. M. Barsom, "Fatigue Crack Growth Under Variable-Amplitude Loading in Various Bridge Steels," in: Fatigue Crack Growth Under Spectrum Loads, ASTM STP 595, American Society for Testing and Materials, Philadelphia (1976), pp. 217-235.
4. P. Albrecht and K. Yamada, "Simulation of Service Fatigue Loads for Short-Span Highway Bridges," in: Service Fatigue Loads Monitoring, Simulation, and Analysis, ASTM STP 671, American Society for Testing and Materials, Philadelphia (1979), pp. 255-277.
5. W. D. Dover, S. J. Holbrook, and R. D. Hibberd, "Fatigue Life Estimates for Tubular Welded T Joints Using Fracture Mechanics," in: Proceedings of European Offshore Steels Research Seminar, The Welding Institute, Cambridge , UK, November 27-29, 1978, pp. V/PD-1 - V/PD-11.
6. F. A. McKee and J. W. Hancock, "Fatigue Crack Growth and Failure in Spectrum Loading," *ibid.*, pp. V/PC-1 - V/PC-10.
7. L. P. Pook, "Proposed Standard Load Histories for Fatigue Testing Relevant to Offshore Structures," NEL Report No. 624, National Engineering Laboratory, Glasgow, UK, October 1976.

8. M. H. J. M. Zwaans, P. A. M. Jonkers, and J. L. Overbeeke, "Random Load Tests on Plate Specimens," Eindhoven University of Technology, the Netherlands, December 1980.
9. P. J. Haagenzen and V. Dagestad, "Corrosion Fatigue Crack Propagation in Structural Steel under Stationary Random Loading," SINTEF Report No. 18 A 78017, The Foundation of Scientific and Industrial Research at the Norwegian Institute of Technology, Norway, October 2, 1978.
10. H. P. Lieurade, J. P. Gerald, and C. J. Putot, "Fatigue Life Prediction of Tubular Joints," Proceedings of the Offshore Technology Conference, OTC Paper No. 3699, Houston, Texas, May 1980.
11. R. M. Olivier, M. Greif, W. Oberparleiter, and W. Schutz, "Corrosion Fatigue Behavior of Offshore Steel Structures under Variable Amplitude Loading," Proceedings of International Conference on Steel in Marine Structures, Paper 7.1, Paris, France, October 5-8, 1981.
12. R. M. Kenley, "Measurement of Fatigue Performance of Forties Bravo," Proceedings of the Offshore Technology Conference, OTC Paper No. 4402, May, 1982.
13. J.-N. Yang, "Simulation of Random Envelop Processes," J. of Sound and Vibration, Vol. 21, No. 1, (1972), pp. 73-85.
14. P. H. Wirsching and A. M. Shehata, "Fatigue under Wide Band Random Stresses Using the Rain-Flow Method," J. of Engineering Materials and Technology, Trans. ASME, Vol. 99, No. 3, (July 1977), pp. 205-211.
15. H. I. McHenry and G. R. Irwin, "A Plastic-Strip Specimen for Fatigue Crack Propagation Studies in Low Yield Strength Alloys," J. of Materials, JMLSA, Vol. 7, No. 4, (December 1972), pp. 455-459.

16. Y. W. Cheng and D. T. Read, "An Automated Fatigue Crack Growth Rate Test System," to be published in the Proceedings of Symposium on Automated Test Methods for Fracture and Fatigue Crack Growth, November 7-8, 1983, Pittsburgh, Pennsylvania.
17. J. M. Barsom, "Effect of Cyclic Stress Form on Corrosion Fatigue Crack Propagation Below  $K_{ISCC}$  in a High Yield Strength Steel," in: Corrosion Fatigue: Chemistry, Mechanics, and Microstructure, National Association for Corrosion Engineers, NACE-2, (1972), pp. 424-435.
18. R. O. Ritchie, "Influence of Microstructure on Near-Threshold Fatigue-Crack Propagation in Ultra-high Strength Steel," Metal Science, Vol II (1977), pp. 368-381.
19. M. A. Miner, "Cumulative Damage in Fatigue," J. of Applied Mechanics, Trans. ASME, Vol. 12, (Sept. 1945), pp. A159-A164.
20. J.-N. Yang, "Statistics of Random Loading Relevant to Fatigue," J. of the Engineering Mechanics Division, Proceedings of the American Society of Civil Engineers, Vol. 100, No. EM3, (June 1974), pp. 469-475.

## List of Tables

1. Chemical composition of ABS grade EH36 steel.

## List of Figures

1. Characteristic power spectrum of offshore structures in the North Sea.
2. Samples of load-time histories: (a) Case I (b) Case II.
3. Fatigue crack growth rates in EH36 steel: effect of specimen orientation. Different symbols represent results obtained from different specimens.
4. Fatigue crack growth rates in EH36 steel: saltwater vs air at stress ratio equal to 0.1. Different symbols represent results obtained from different specimens.
5. Fatigue crack growth rates in EH36 steel: saltwater vs air at stress ratio equal to 0.5. Different symbols represent results obtained from different specimens.
6. Fatigue crack growth rates in EH36 steel: summary. Different symbols represent results obtained from different specimens.
7. Definitions of stress range and cycle.
8. Fatigue crack growth rates in EH36 steel in saltwater: constant-amplitude loading vs spectrum loading (Case I).
9. Fatigue crack growth rates in EH36 steel in saltwater: constant-amplitude loading vs spectrum loading (Case II).

Table 1. Chemical Composition of ABS Grade EH36 Steel

C	Mn	P	S	Si	Cu	Ni	Cr	Mo	Fe
0.12	1.39	0.015	0.006	0.380	0.05	0.03	0.05	0.007	bal.

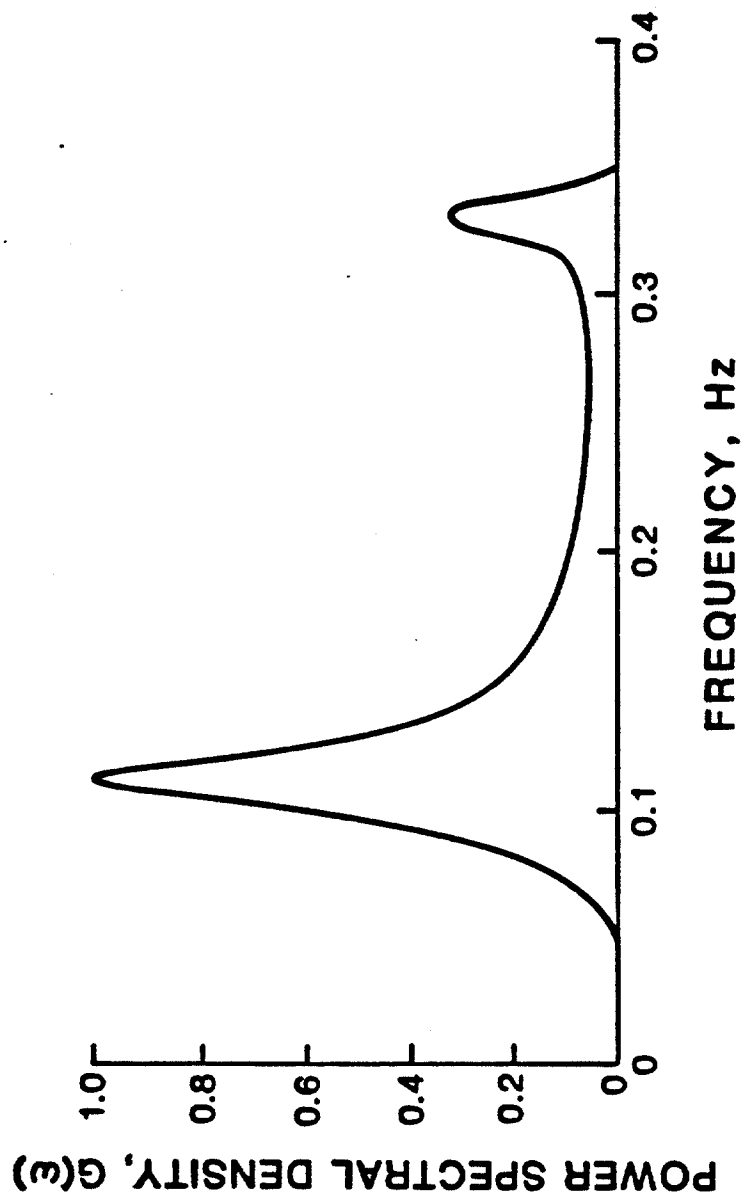
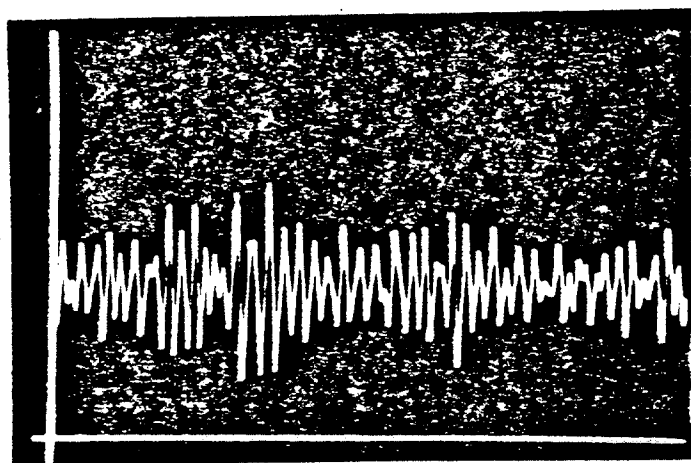
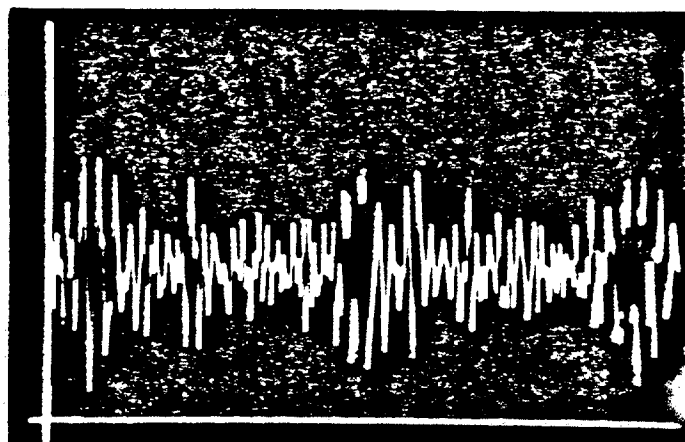


Fig 1



5 min.

(a)



5 min.

(b)

Fig 2



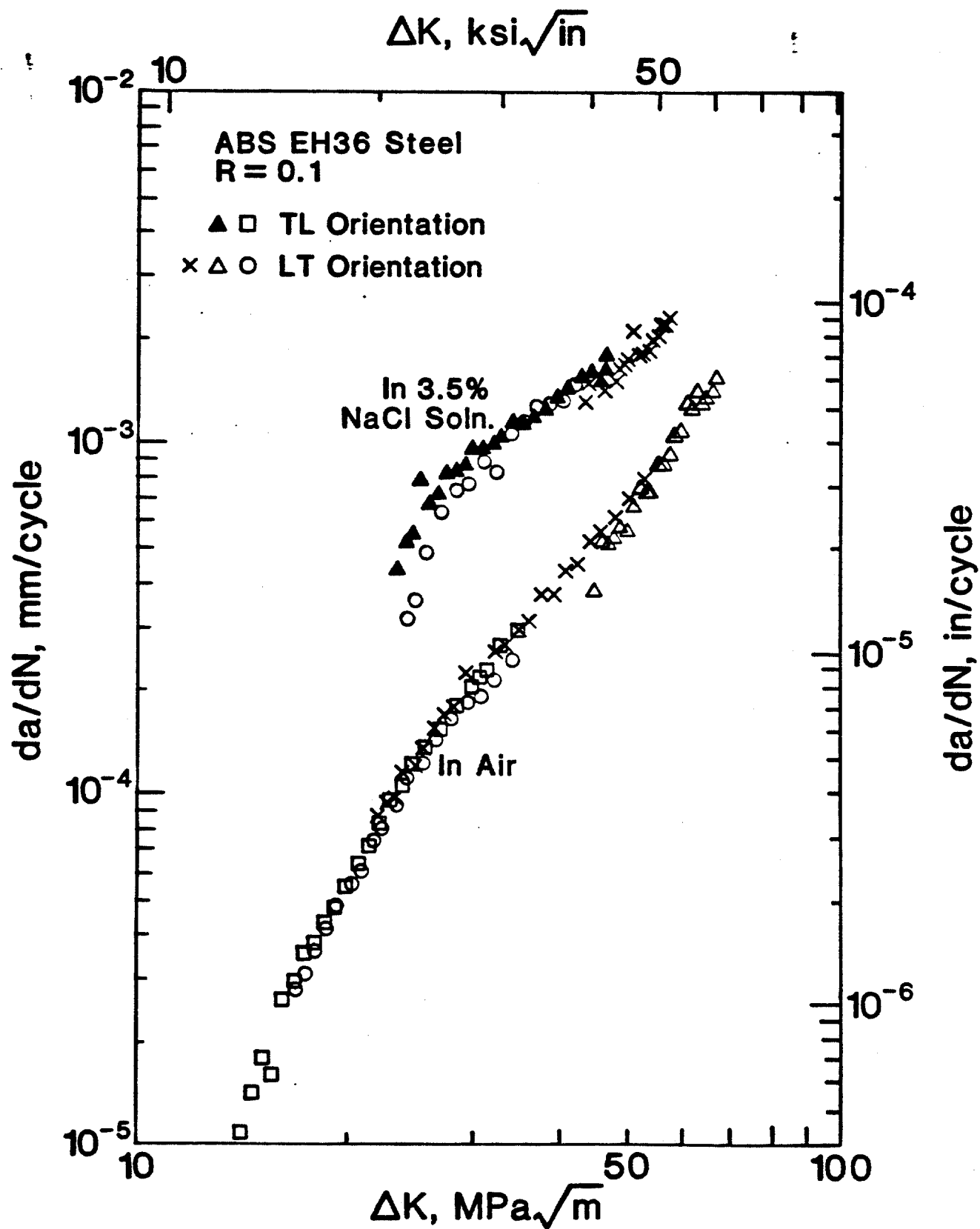


Fig. 3

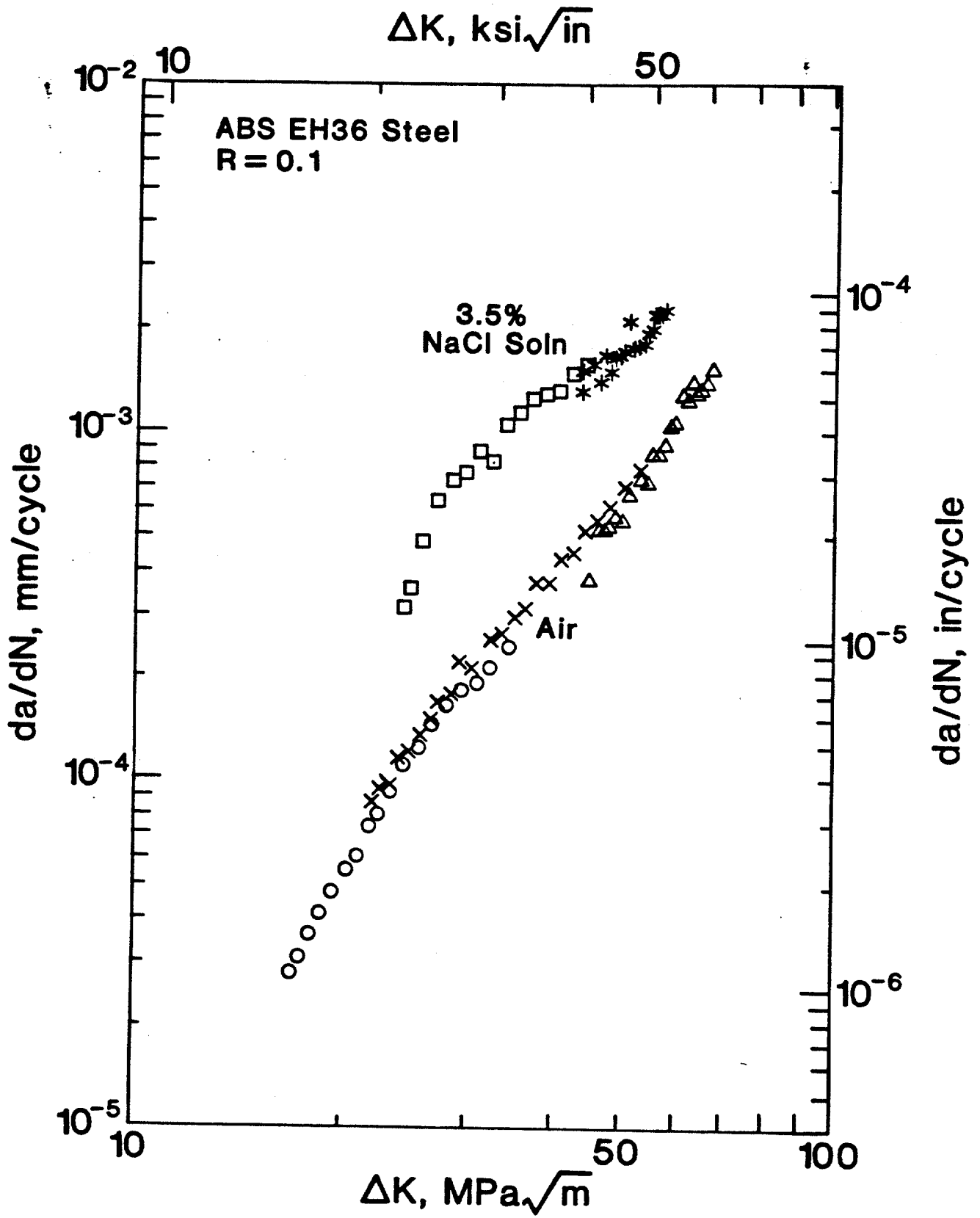


Fig. 4

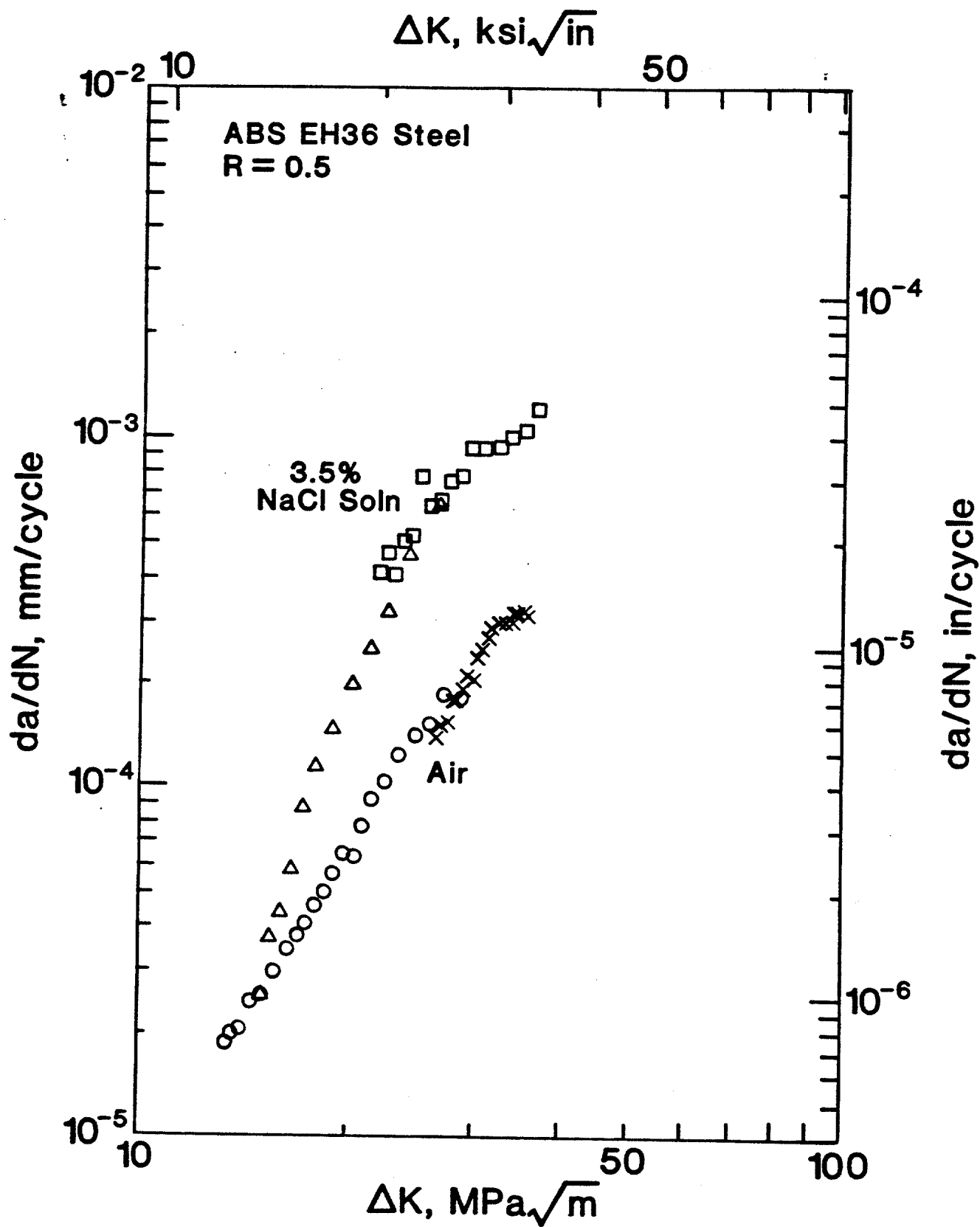
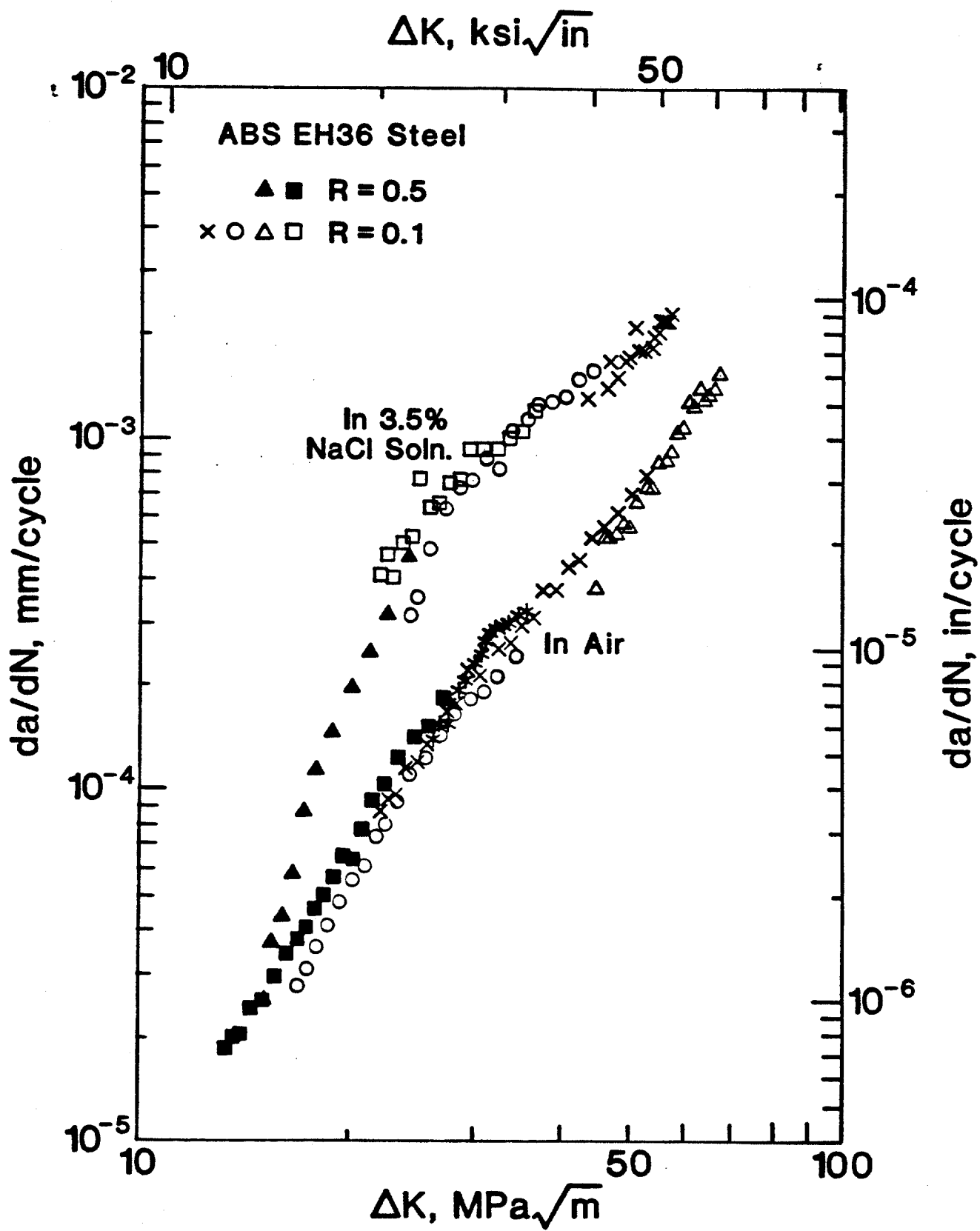


Fig 5



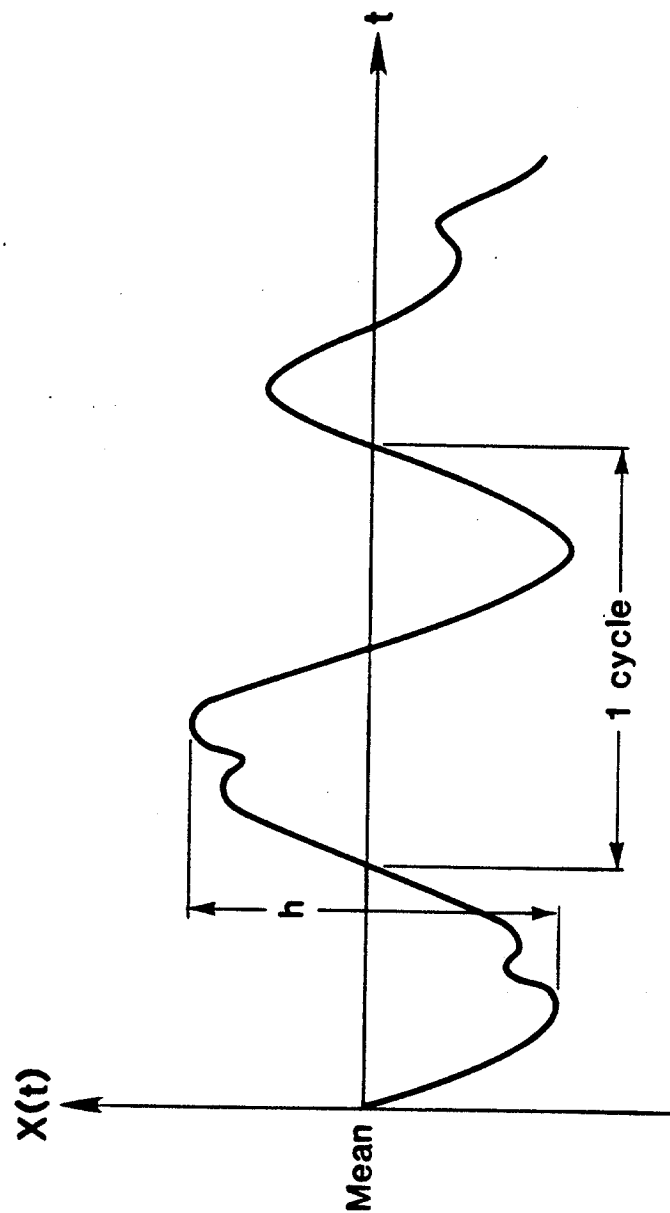


Fig. 7

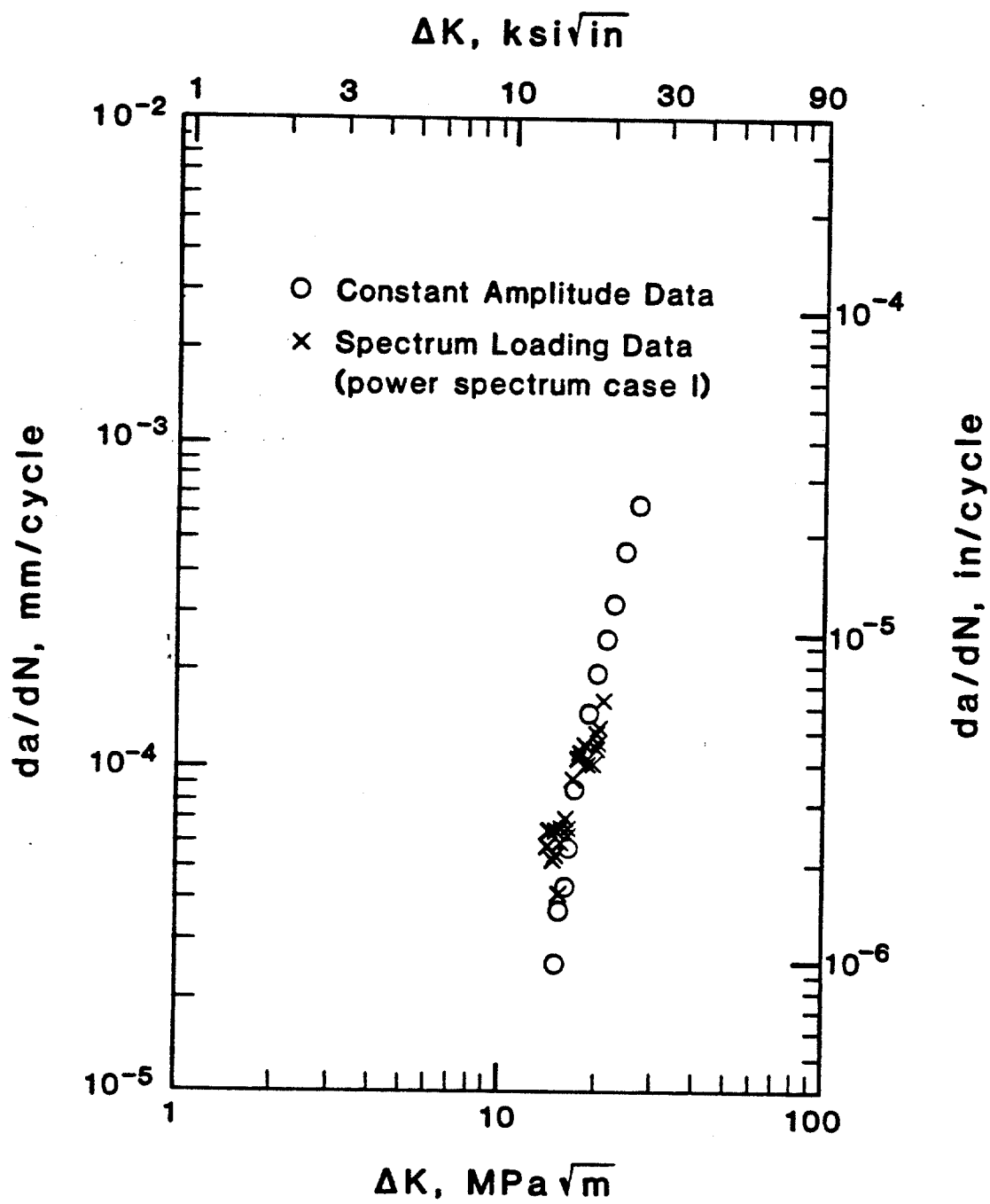


Fig. 8

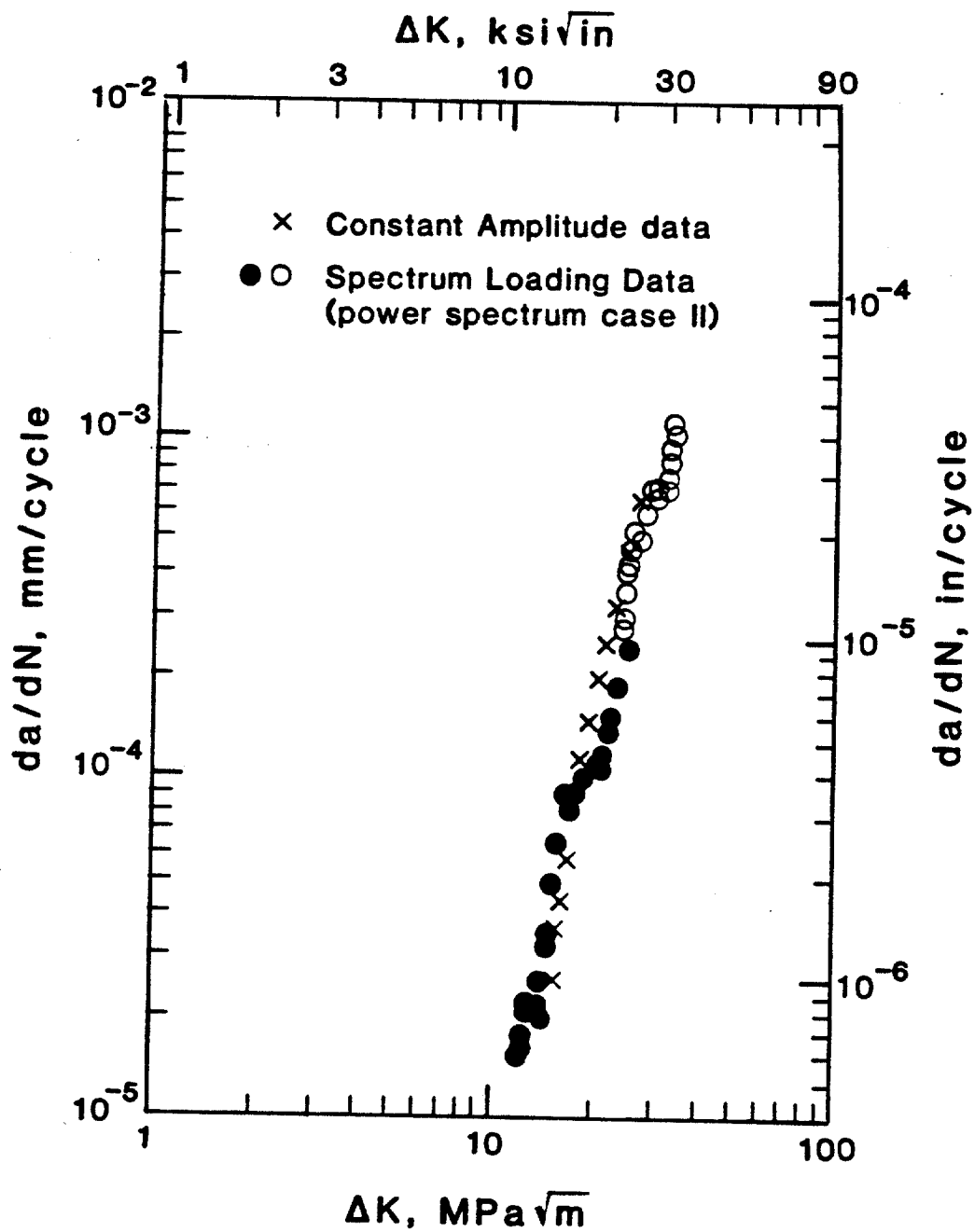


Fig 9

ESTIMATION OF IRREGULARITY FACTOR FROM A POWER SPECTRUM\*

Pei-Ning Li\*\*  
Yi-Wen Cheng

Fracture and Deformation Division  
National Bureau of Standards  
Boulder, Colorado 80303

Key Words: bandwidth, irregularity factor, power spectrum, random loading fatigue.

\* Contribution of NBS; not subject to copyright in the U.S.

\*\* Guest worker, on leave from East-China Institute of Chemical Technology, Shanghai, China.



## ABSTRACT

This paper presents several simplified methods of evaluating the irregularity factor of a power spectrum. The irregularity factor can be computed either from integration of the power spectrum or from the characteristic bandwidth and the center frequency of the power spectrum. The characteristic bandwidths and the center frequencies of power spectra with irregular shapes were defined in this paper. For all the cases studied in this paper, the largest error introduced by using the simplified methods was about 10 percent, but the majority were within 5 percent.

## 1. INTRODUCTION

In many structural applications, fatigue under random loading is a major problem, such as offshore platforms in the North-Sea environments. Load-time histories under random loading are usually difficult to predict and can only be treated in a statistical manner. If the random loading is a stationary Gaussian process as is commonly assumed, then there exists a power spectrum,  $G(f)$ , which possesses all the statistical properties of the original load-time history [1]. The power spectrum is, therefore, conveniently used to represent the random load-time history.

Several important parameters for random-loading fatigue analysis can be derived from the power spectrum. These parameters include the root-mean-square (RMS) value of the load amplitude, average rises and falls, and irregularity factor,  $\alpha$  [2,3]. The RMS value equals to the area under the power spectrum-versus-frequency curve. The average rises and falls are related to the RMS value and the irregularity factor of the power spectrum and have been analytically and numerically studied [4]. The irregularity factor has been used as a parameter to normalize the fatigue damage caused by narrow-band and broad-band loadings [5]. As will be presented in the following sections, the irregularity factor of a power spectrum is usually computed from the integration of the power spectrum, which can become tedious and time consuming if the shape of  $G(f)$  is irregular. This paper presents simplified techniques for estimating  $\alpha$  from a power spectrum.

## 2. IRREGULARITY FACTOR

The irregularity factor,  $\alpha$ , is defined as the ratio of the number of positive-slope zero crossings to the number of peaks per unit time in a load-time history.

$$\alpha = \frac{N_0}{F_0} \quad (1)$$

where  $N_0$  is the number of positive-slope zero crossings per unit time and  $F_0$  is the number of peaks per unit time. The exact value of  $N_0$  and  $F_0$  can be evaluated from  $G(f)$  as follows.

$$N_0 = \left( \frac{M_2}{M_0} \right)^{0.5} \quad (2a)$$

$$F_0 = \left( \frac{M_4}{M_2} \right)^{0.5} \quad (2b)$$

where  $M_0$ ,  $M_2$ , and  $M_4$  are the zeroth, second, and fourth moments of  $G(f)$  about the origin (zero frequency), and are defined as:

$$M_0 = \int_0^{\infty} G(f) df \quad (3a)$$

$$M_2 = \int_0^{\infty} f^2 G(f) df \quad (3b)$$

$$M_4 = \int_0^{\infty} f^4 G(f) df \quad (3c)$$

where  $f$  is frequency. Thus,

$$\alpha = \frac{M_2}{(M_0 M_4)^{0.5}} \quad (4)$$

The irregularity factor,  $\alpha$ , not only describes the irregularity of the random load-time history but also is a measure of the bandwidth of  $G(f)$ . As  $\alpha$  approaches unity, the distribution of the peak load is approximated by the Rayleigh distribution [1], and the shape of  $G(f)$  is sharply peaked at the center frequency. This is called narrow-band power spectrum. A single-frequency sine-wave loading can be described as a Dirac-Delta function power spectrum; it has  $\alpha = 1$ . The value of  $\alpha$  decreases with increasing width of the power spectrum.

### 3. EVALUATION OF IRREGULARITY FACTOR FROM POWER SPECTRA

#### 3.1. Direct Integration of Power Spectral Density Function

The value of  $\alpha$  can be evaluated from equation (4) by integrating equations (3a), (3b), and (3c). The integrations can become tedious and time consuming if the shape of  $G(f)$  is irregular. One simplified way of evaluating  $\alpha$  is to break  $G(f)$  into  $n$  simpler geometries such as those shown in Figure 1 ( $n = 5$ ), and then to evaluate the moments according to the following equation:

$$M_j = \frac{1}{(j+1)(j+2)} \sum_{i=1}^n (G_i - G_{i+1}) \frac{f_{i+1}^{(j+2)} - f_i^{(j+2)}}{f_{i+1} - f_i}, \quad j = 0, 2, 4 \quad (5)$$

where  $G_i$ 's and  $f_i$ 's are power spectral densities and frequencies respectively, as shown in Figure 1. The derivation of equation (5) is given in the Appendix.

For example, using equation (5) and the break-up diagram shown in Figure 2 ( $n = 9$ ), the calculated value of  $\alpha$  was 0.699. The more precise value of  $\alpha$  was 0.697. The error of using equation (5) was 0.14 percent. ✓

### 3.2. Estimation from Characteristic Width and Center Frequency of a Power Spectrum

The irregularity factor can also be estimated from the characteristic width and the center frequency of a power spectrum. For the case of rectangular power spectra,  $\alpha$  can be obtained from the following expression [6].

$$\alpha = \left[ \frac{5 (9 + 6B^2 + B^4)}{9 (5 + 10B^2 + B^4)} \right]^{0.5} \quad (6)$$

where  $B = W/2f_c$ ,  $W$  is the width and  $f_c$  is the center frequency of the rectangle (power spectrum). Here,  $B$  is the geometric dimensionless bandwidth of the power spectrum. Different power spectra with same values of  $B$  will have same values of  $\alpha$  regardless of their shapes and positions with respect to the origin (zero frequency). The definitions of  $W$  and  $f_c$  are obvious in this case, and both are determined in a straightforward manner. For irregular spectra, the determination of  $W$  and  $f_c$  can be difficult and is discussed in the following sections.

From geometric analysis of rectangular power spectra, it was noted that the values of  $B$  were bounded by 0 and 1. Accordingly,  $\alpha$  was within 1 and 0.745.

### 3.2.1. Determination of Characteristic Width, W

In the case of symmetric, single-peaked power spectra, the center frequency is at the center of the frequency range. However, the determination of W is not obvious and the following empirical equation was used to evaluate W.

$$W = W' \left( \frac{A_{\text{rec}}}{A_{\text{ps}}} \right)^{0.5} \quad (7)$$

where W' is the arithmetic average width of the power spectrum,  $A_{\text{rec}}$  is the area of a rectangle enveloping the power spectrum and  $A_{\text{ps}}$  is the area of the power spectrum. For example, the value of W' is half of its base width for an isosceles triangular power spectrum and the ratio of  $A_{\text{rec}}/A_{\text{ps}}$  is 2.

Results for several symmetric, single-peaked power spectra with various shapes, including isosceles triangles, rectangles, isosceles trapezoids and pagodas, are plotted in Figure 3 in the form of  $\alpha$  versus B. All values of  $\alpha$  in Figure 3 and other figures in this paper were evaluated by equation (4), if not otherwise specified. The value of  $\alpha$  obtained from equation (6) will coincide with those of the rectangles in Figure 3. It can be seen that  $\alpha$ -versus-B curves for four different shapes of power spectra were in reasonable agreement, demonstrating that the estimate of W by equation (7) combined with equation (6) does provide good estimates of  $\alpha$ . The errors in  $\alpha$  at B = 1 were less than  $\pm 5$  percent.

### 3.2.2. Determination of Center Frequency, $f_c$

The value of  $\alpha$  of an arbitrary triangular power spectrum with a fixed base (i.e. with a constant characteristic width) varies with the location of the peak within the width, because the center frequency varies. Several candidates for the operational definition of center frequency, including the frequency at the peak of the power spectrum, the frequency at the center of gravity of the power spectrum, the frequency at the middle of the frequency range, and the frequency at the middle of the half-height width, were studied. The frequency at the middle of the half-height width of the power spectrum gave the least scatter in the  $\alpha$ -versus-B curves of several asymmetrical single-peaked power spectra. The  $\alpha$ -versus-B curves of right triangular power spectra with the right angle to the left or to the right are compared with that of rectangular power spectra in Figure 4. The figure shows that at a given value of B the value of all the triangles studied are slightly smaller than those of rectangles. The largest error at  $B = 1$  was about 10 percent. This means that use of the frequency at the middle of half-height width of a triangular power spectrum will slightly overestimate the value of  $\alpha$ .

### 3.2.3. Behavior of Double-Peaked Power Spectra

The irregularity factor of a double-peaked power spectrum was estimated from the following equation:

$$\alpha = \frac{1 + A F^2}{[(1 + A)(1 + A F^4)]^{0.5}} \quad (8)$$

$$A = \frac{A_2}{A_1} \quad (9)$$

$$F = \frac{f_{c2}}{f_{c1}} \quad (10)$$

where  $A_1$ ,  $A_2$ ,  $f_{c1}$ , and  $f_{c2}$  are the areas and center frequencies of each peak, respectively, with  $A_1$  and  $f_{c1}$  being closer to the zero frequency (see Table 1). As shown in Table 1, the error of using equation (8) was within  $\pm 5$  percent for a wide range of two-peaked power spectra. Table 1 contains results ranging  $A$  from 0.1 to 10,  $F$  from 2.333 to 7,  $G_2/G_1$  (see Table 1 for definition of  $G_1$ ) from 0.1 to 10, and  $\alpha$  from 0.56 to 0.96.

Figure 5 presents results from equation (8) in graphic form. It shows that the larger the value of  $F$  and the smaller the value of  $A$  are, the smaller the irregularity factor is. From equations (3) and (4), one would expect that the higher frequency peak dominates the determination of  $\alpha$  because of the second and the fourth power of frequency in  $M_2$  and  $M_4$ . In the case of  $A_2 \gg A_1$ , the lower frequency peak can be neglected in the determination of  $\alpha$ . The smaller the value of  $F$  is, the closer the two peaks are, and vice versa. Figure 5 shows that, at a given value of  $A$ ,  $\alpha$  increased with increasing  $F$ .

The two peaks in a double-peaked power spectrum of practical interest are usually connected to each other at their bases. In this case, the double-peaked power spectrum was divided into two parts. Their center frequencies and areas were estimated; then the value of  $\alpha$  was estimated from equation (8). For example, the power spectrum characteristic of the North-Sea environments, as shown in Figure 6, was divided at 0.3 Hz, 0.25 Hz, or 0.2 Hz, and represented by two triangles,  $\triangle ABC$  and  $\triangle DEF$ ,  $\triangle ABC'$  and  $\triangle D'EF$ , or



$\Delta ABC$ " and  $\Delta DEF$ . All triangles had the same areas as the original curves which they represented. The values of F and A obtained were 2.70 and 0.1514, 2.71 and 0.2278, or 2.74 and 0.3165, respectively. The estimated value of  $\alpha$  using equation (8) was 0.6520, 0.6616, or 0.6785. The errors were -6.5, -5.08, and -2.65 percent, respectively.

#### 4. SUMMARY

Several simplified methods for evaluating the irregularity factor of a power spectrum have been derived. The irregularity factor was computed either from integration of the power spectrum or from the characteristic bandwidth and the center frequency of the power spectrum.

For idealized shapes of power spectra, such as rectangles and isosceles triangles, the characteristic bandwidth and the center frequency were readily obtained. For irregular shapes, the power spectra were represented by simplified geometries from which the characteristic bandwidths and the center frequencies were estimated.

For all the cases studied in this paper, the largest error introduced by using the simplified methods was about 10 percent, but the majority were within 5 percent. Therefore, use of the simplified methods is recommended where approximation is allowable, and as a check on more exact methods.

#### 5. ACKNOWLEDGMENTS

This work was supported by Department of Interior, Minerals Management Service.

## REFERENCES

1. J. S. Bendat, "Principles and Application of Random Noise Theory," John Wiley & Sons, Inc., 1958.
2. S. H. Smith, "Fatigue Crack Growth Under Axial Narrow and Broad Band Random Loading," in: Acoustical Fatigue in Aerospace Structure, 1964, pp. 331-360.
3. F. Beer, R. Wagner, L. Bahar, and R. Ravera, "On the Statistical Distribution of Rises and Falls in a Stochastic Process," Lehigh Institute of Research Progress Report, 1961. (Fracture Mechanics Research for the Boeing Airplane Company).
4. J. R. Rice, "Theoretical Prediction of Some Statistical Characteristics of Random Loadings Relevant to Fatigue and Fracture," Ph.D. Thesis, Lehigh University, Bethlehem, Pennsylvania, 1964.
5. P. H. Wirsching and M. C. Light, "Probability Based Fatigue Design Criteria for Ocean Structures," API-PRAC Project No. 15, Final Report, American Petroleum Institute, 1979.
6. L. P. Pook, "Proposed Standard Load Histories for Fatigue Testing Relevant to Offshore Structures," National Engineering Laboratory, NEL Report No. 624, October 1976.

## APPENDIX

Straight lines can be used to approximate the original curves of any kind of power spectra. For example, Figure 1 shows a single-peaked power spectrum (dash line), approximated by four straight lines (solid line). The important consideration in choosing the straight lines is that the area under the straight line should be the same (or close to) that of the original curve it represents. Taking  $G_1$  and  $G_5$  equal to 0, the four straight lines in Figure 1 are expressed by the following linear equations:

$$G(f) = (G_2 - 0) \frac{f - f_1}{f_2 - f_1} \quad \text{for the first segment}$$

$$G(f) = (G_3 - G_2) \frac{f - f_2}{f_3 - f_2} + G_2 \quad \text{for the second segment}$$

$$G(f) = (G_4 - G_3) \frac{f - f_4}{f_4 - f_3} + G_4 \quad \text{for the third segment}$$

$$G(f) = (0 - G_4) \frac{f - f_5}{f_5 - f_4} \quad \text{for the fourth segment}$$

After integration of equations (3a), (3b), and (3c) and some manipulation, one finds,

$$\begin{aligned} M_0 = \frac{1}{2} \left[ (0 - G_2) \frac{f_2^2 - f_1^2}{f_2 - f_1} + (G_2 - G_3) \frac{f_3^2 - f_2^2}{f_3 - f_2} + (G_3 - G_4) \frac{f_4^2 - f_3^2}{f_4 - f_3} \right. \\ \left. + (G_4 - 0) \frac{f_5^2 - f_4^2}{f_5 - f_4} \right] \end{aligned} \quad (A1)$$

$$M_2 = \frac{1}{12} \left[ (0 - G_2) \frac{f_2^4 - f_1^4}{f_2 - f_1} + (G_2 - G_3) \frac{f_3^4 - f_2^4}{f_3 - f_2} + (G_3 - G_4) \frac{f_4^4 - f_3^4}{f_4 - f_3} \right. \\ \left. + (G_4 - 0) \frac{f_5^4 - f_4^4}{f_5 - f_4} \right] \quad (A2)$$

$$M_4 = \frac{1}{30} \left[ (0 - G_2) \frac{f_2^6 - f_1^6}{f_2 - f_1} + (G_2 - G_3) \frac{f_3^6 - f_2^6}{f_3 - f_2} + (G_3 - G_4) \frac{f_4^6 - f_3^6}{f_4 - f_3} \right. \\ \left. + (G_4 - 0) \frac{f_5^6 - f_4^6}{f_5 - f_4} \right] \quad (A3)$$

Equations (A1), (A2), and (A3) can be written in a general form:

$$M_j = \frac{1}{(j+1)(j+2)} \sum_{i=1}^n (G_i - G_{i+1}) \frac{f_{i+1}^{(j+2)} - f_i^{(j+2)}}{f_{i+1} - f_i}, j = 0, 2, 4 \quad (5)$$

which can be used for single-peaked as well as double-peaked power spectra.

#### List of Table

1. Estimated error in irregularity factor of double-peaked power spectra using a simplified method.

### List of Figures

1. Power spectrum: dashed line represents the original spectrum, and solid lines are simplified break-up diagram.
2. Example of computing irregularity factor from a break-up diagram of a power spectrum.
3. Irregularity factor-versus-geometric dimensionless width for four different symmetric, single-peaked power spectra.
4. Irregularity factor-versus-geometric dimensionless width for four different symmetric, single-peaked power spectra.
5. Irregularity factor as a function of the ratio of area and frequency of each peak for double-peaked power spectra.
6. Example of calculating irregularity factor of a double-peaked power spectrum of practical interest by dividing the connected two peaks into two separate triangles.

Table 1. Estimated errors in irregularity factor of double-peaked power spectra using a simplified method.

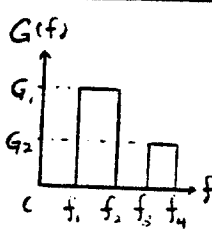
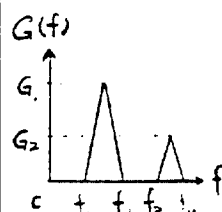
Shape of Spectra	$G_1:G_2$	$f_1 : f_2 : f_3 : f_4$	F	A	Value of $\alpha$		
					by Eq(4)	by Eq(8)	Error
	1:1	0 : 1 : 2 : 3	5	1	0.7249	0.7348	1.50
		1 : 2 : 3 : 4	2.333	1	0.8138	0.8232	1.16
		0 : 1 : 3 : 4	7	1	0.7162	0.7213	-0.71
		1 : 2 : 4 : 5	3	1	0.7762	0.7808	0.60
	1:2	0 : 1 : 2 : 3	5	2	0.8160	0.8325	2.02
		1 : 2 : 3 : 4	2.333	2	0.8733	0.8840	1.23
		0 : 1 : 3 : 4	7	2	0.8164	0.8247	1.02
		1 : 2 : 4 : 5	3	2	0.8532	0.8592	0.70
	2:1	0 : 1 : 2 : 3	5	0.5	0.6192	0.6225	0.53
		1 : 2 : 3 : 4	2.333	0.5	0.7559	0.7641	1.08
		0 : 1 : 3 : 4	7	0.5	0.6000	0.6007	0.12
		1 : 2 : 4 : 5	3	0.5	0.6939	0.6971	0.46
	5:1	0 : 1 : 2 : 3	5	0.2	0.4969	0.4880	-1.79
		1 : 2 : 3 : 4	2.333	0.2	0.7161	0.7244	1.16
		0 : 1 : 3 : 4	7	0.2	0.4559	0.4494	-1.43
		1 : 2 : 4 : 5	3	0.2	0.6150	0.6163	0.21
	1:5	0 : 1 : 2 : 3	5	5	0.8989	0.9200	2.35
		1 : 2 : 3 : 4	2.333	5	0.9312	0.9435	1.32
		0 : 1 : 3 : 4	7	5	0.9057	0.9165	1.19
		1 : 2 : 4 : 5	3	5	0.9249	0.9320	0.77
	10:1	0 : 1 : 2 : 3	5	0.1	0.4384	0.4188	-4.47
		1 : 2 : 3 : 4	2.333	0.1	0.7280	0.7396	1.59
		0 : 1 : 3 : 4	7	0.1	0.3756	0.3623	-3.54
		1 : 2 : 4 : 5	3	0.1	0.5996	0.6298	5.00
	1:10	0 : 1 : 2 : 3	5	10	0.9342	0.9572	2.46
		1 : 2 : 3 : 4	2.333	10	0.9568	0.9693	1.31
		0 : 1 : 3 : 4	7	10	0.9434	0.9554	1.27
		1 : 2 : 4 : 5	3	10	0.9559	0.9635	0.80
	5:1	1 : 3 : 4 : 8	3	0.4	0.6400	0.6727	5.11
		1 : 3 : 5.5 : 6.6	3	0.1	0.6314	0.6005	-4.89

Table 1. (cont.)

Shape of Spectra	$G_1:G_2$	$f_1 : f_2 : f_3 : f_4$	F	A	Value of $\alpha$		
					by Eq(4)	by Eq(5)	%error
	1:3	0 : 1 : 1 : 2	3	3	0.8687	0.8963	3.18
		1 : 3 : 3 : 5	2	3	0.9106	0.9285	1.97
		1 : 2 : 2 : 3	1.666	3	0.9370	0.9495	1.33
	1:2	0 : 1 : 1 : 2	3	2	0.8341	0.8592	3.01
		1 : 3 : 3 : 5	2	2	0.8872	0.9045	1.95
		1 : 2 : 2 : 3	1.666	2	0.9214	0.9335	1.31
	1:1	0 : 1 : 1 : 2	3	1	0.7612	0.7810	2.60
		1 : 3 : 3 : 5	2	1	0.8412	0.8575	1.94
		1 : 2 : 2 : 3	1.666	1	0.8924	0.9050	1.41
		0 : 1 : 2 : 3	5	1	0.7167	0.7348	2.53
		1 : 2 : 3 : 4	2.333	1	0.8186	0.8232	1.31
	2:1	0 : 1 : 1 : 2	3	0.5	0.684	0.697	1.90
		1 : 3 : 3 : 5	2	0.5	0.8006	0.8165	2.00
		1 : 2 : 2 : 3	1.666	0.5	0.872	0.885	1.49
		0 : 1 : 2 : 3	5	0.5	0.6208	0.6225	0.27
		1 : 2 : 3 : 4	2.333	0.5	0.7600	0.7640	0.52
	3:1	0 : 1 : 1 : 2	3	0.3	0.6455	0.6547	1.43
		1 : 3 : 3 : 5	2	0.3	0.7863	0.8030	2.10
		1 : 2 : 2 : 3	1.666	0.3	0.8680	0.8828	1.71
		0 : 1 : 2 : 3	5	0.3	0.5593	0.5587	-0.11
		1 : 2 : 3 : 4	2.333	0.3	0.7275	0.7389	1.57



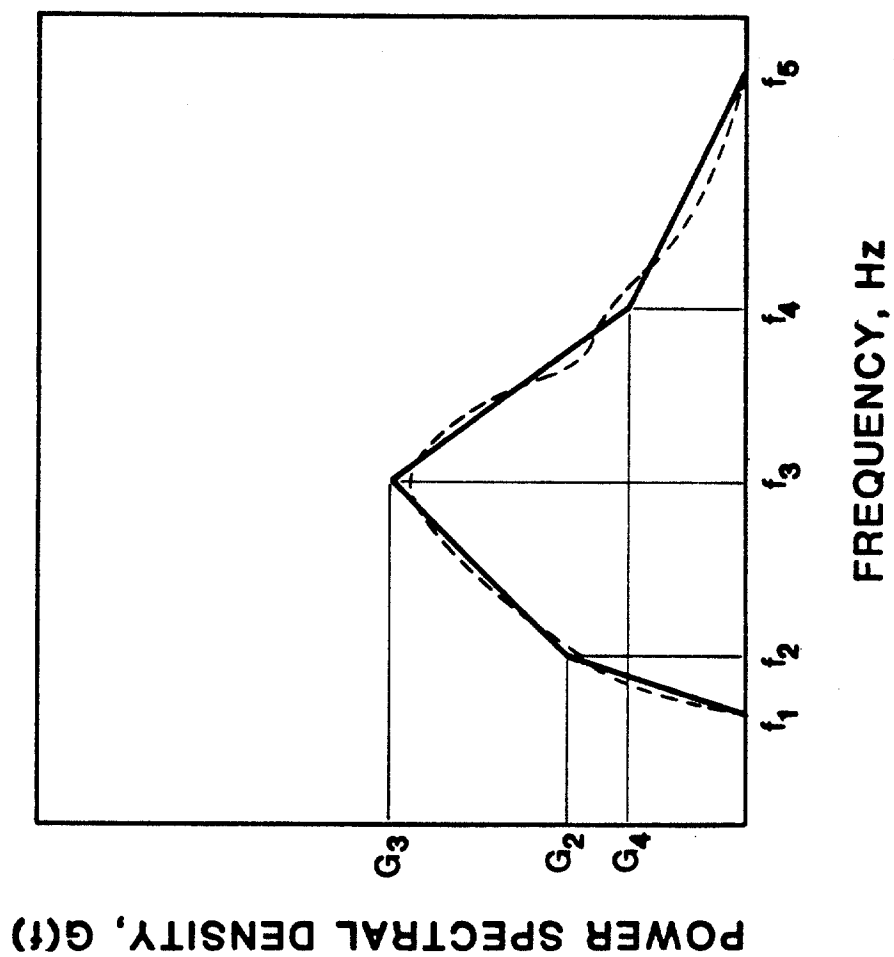


Fig. 1

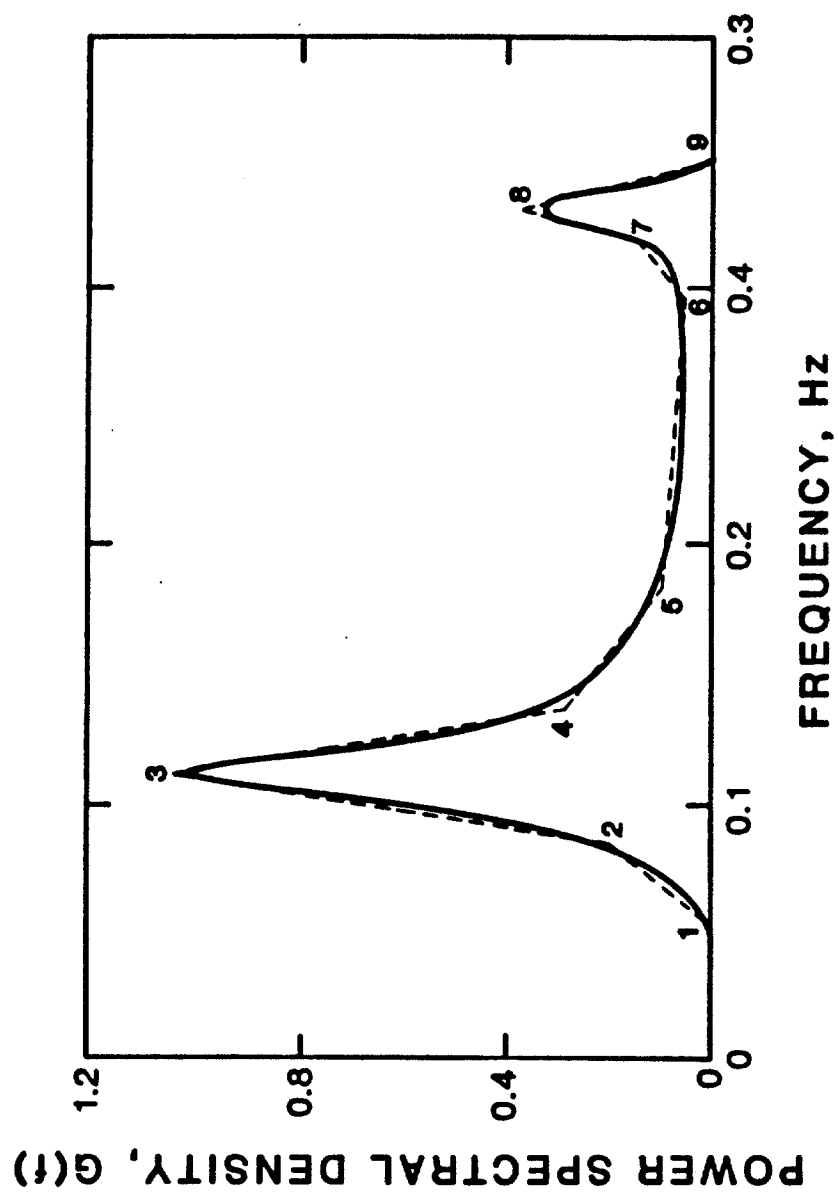


Fig. 2

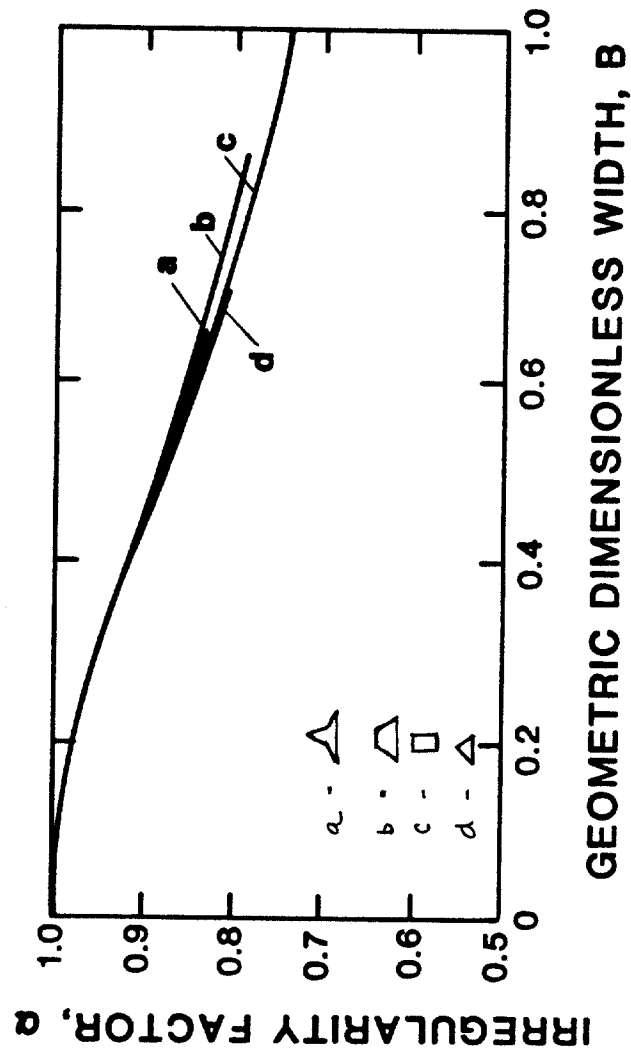


Fig. 3

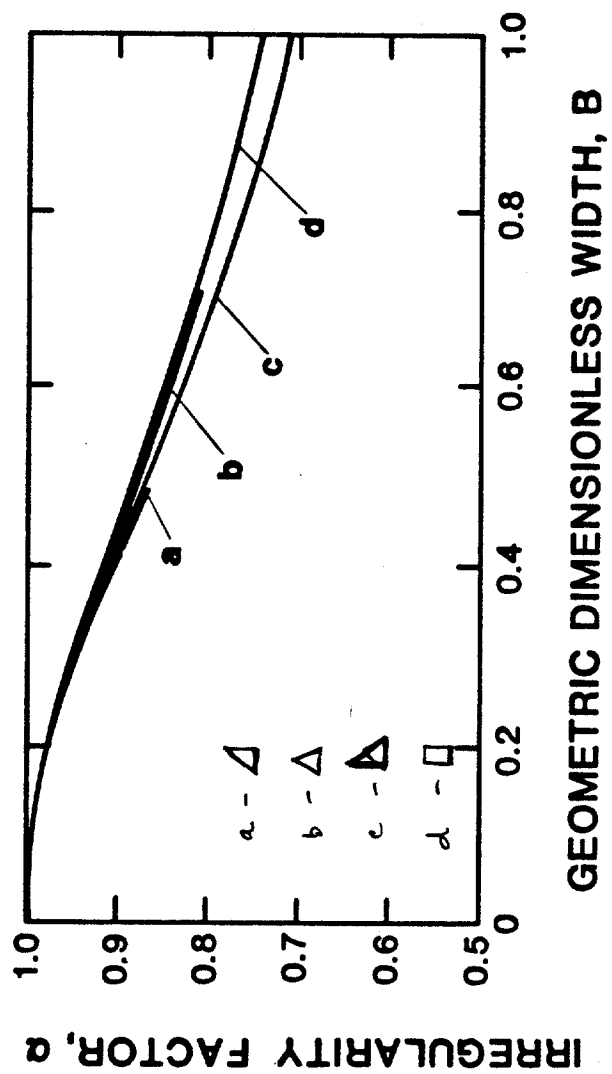


Fig. 4

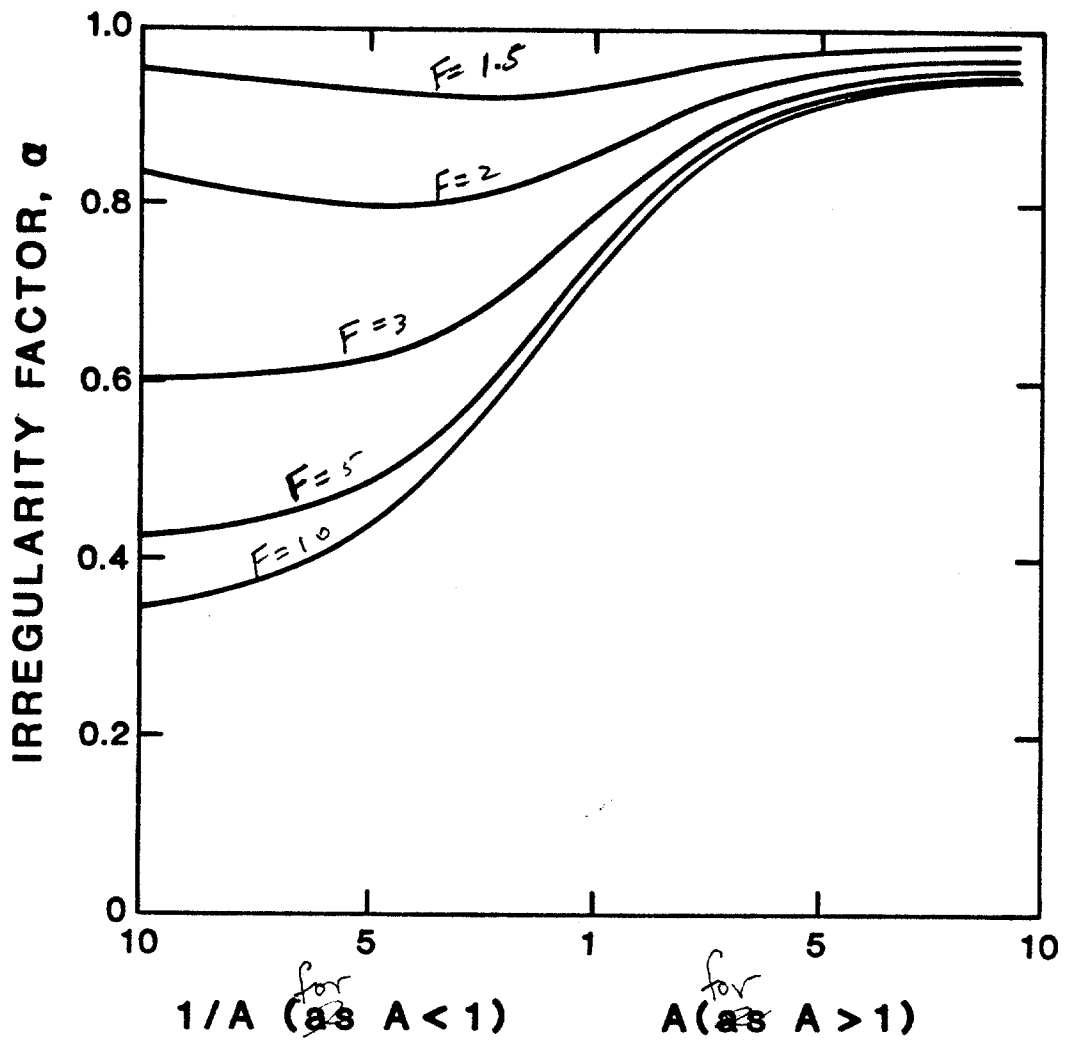


Fig. 5

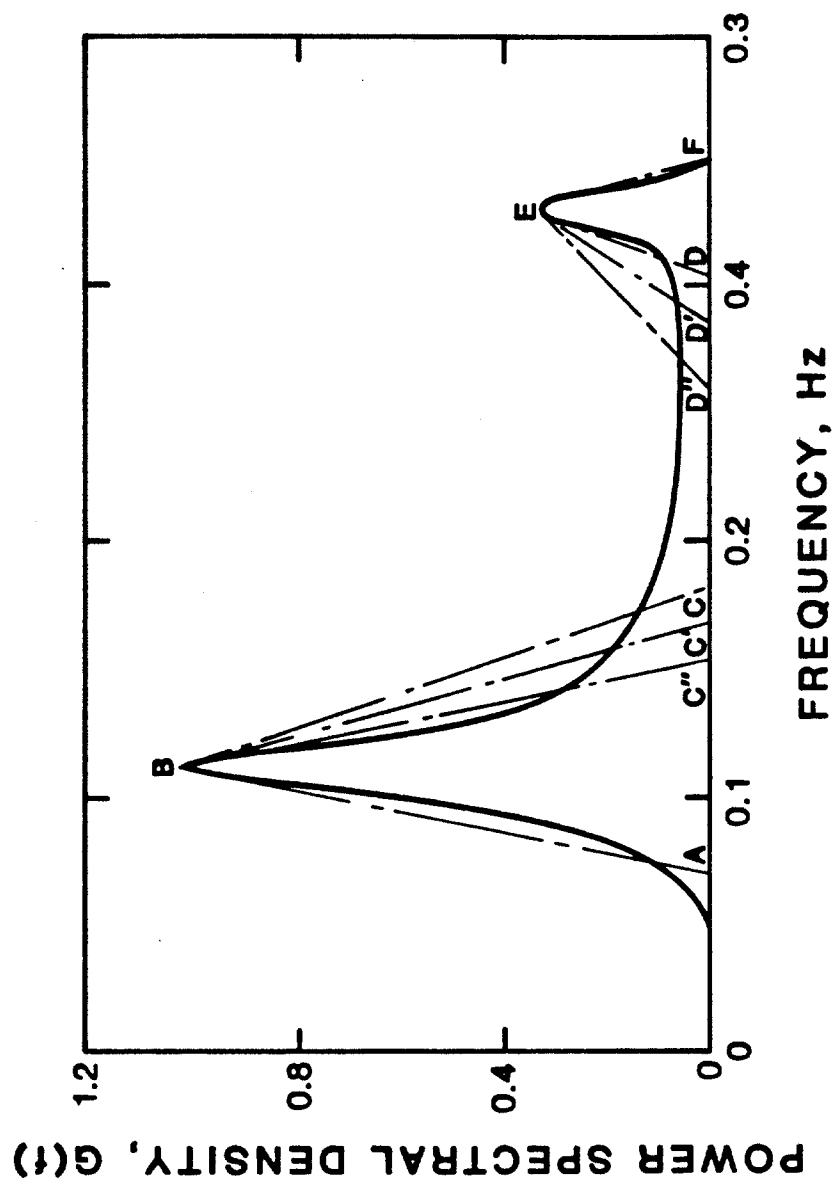


Fig. 6

# Fatigue Crack Growth in Areas of Stress Concentrations\*

P. N. Li\*\* and Y. W. Cheng

Fracture and Deformation Division  
National Bureau of Standards  
Boulder, Colorado 80303

Key Words: C-Mn steel, environmental effects, fatigue crack growth, small cracks, yielding effects.

\*Contribution of NBS; not subject to copyright.

\*\*Guest worker, on leave from East-China Institute of Chemical Technology, Shanghai, China.

# ABSTRACT

Hole-in-plate specimens, made of ABS EH36 steel, were tested in air and in 3.5 percent NaCl solution to measure fatigue crack growth rates in areas of stress concentrations at the edges of circular holes. The linear-elastic fracture mechanics analysis of fatigue crack growth appears to be adequate in yielded regions caused by monotonic loading but having a linear stress-strain relation under cyclic loading. Small-crack behavior, in which cracks grow at faster rates than predictions from the long cracks, was observed when the crack length was less than 1.5 mm in air and 3 mm in 3.5 percent NaCl solution. The problem of small-crack behavior <sup>was</sup> ~~can be~~ accounted for by adding an intrinsic crack length to the physical crack length, as suggested by El Haddad.

*less than*  
^



## INTRODUCTION

The fatigue life of a structural component is determined by the sum of the applied load cycles required to initiate a crack and to propagate the crack from subcritical to critical size. Because welded structures such as offshore structures usually contain weld defects at areas of stress concentrations, the fatigue life mainly depends on the time required for crack propagation, and a fatigue fracture mechanics analysis, therefore, is appropriate. The initial weld defects are small and will propagate in the plastically deformed regions near stress concentrators.

Fatigue crack propagation in plastically deformed regions of structural stress concentrators, such as at weld toes and notch roots, has been studied by many investigators [1-5]. It is observed that the linear-elastic fracture mechanics (LEFM) method was inadequate for predicting the fatigue crack growth rate (FCGR) in this area. Some parameters have been proposed to correlate with FCGR. Solomon [1] suggested that the plastic strain range,  $\Delta\epsilon_p$ , could be used to predict the crack propagation rate, but this worked only for large plastic deformations. El Haddad et al [2-4] used the strain intensity factor range instead of the stress intensity factor range as the driving force for fatigue crack propagation. Dowling [5] proposed that the J-integral was an adequate parameter for several kinds of specimens to correlate with FCGR.

The aforementioned proposed parameters and subsequent correlations with FCGR are empirical or semi-empirical in nature. Their applicability ranges and conditions need to be defined.

Associated with the fatigue crack propagation in plastically deformed regions of structural stress concentrators is the growth of small cracks. Fatigue crack growth rates of small cracks are higher than those predicted by the results from long cracks. The use of existing long-crack results for defect-tolerance fatigue-life calculations in components, where the growth of a small crack represents a large portion of the fatigue life, will lead to non-conservative life predictions. To account for the faster crack growth of small cracks, El Haddad et al [2] introduced the notion of an intrinsic crack length,  $a_0$ , which is added to the physical crack length. The value of  $a_0$  is constant for a given material condition and environment. The term  $(a + a_0)$  is viewed as an effective crack length and the effective stress intensity factor range is

$$\Delta K = \Delta S [\pi (a + a_0)]^{0.5} F_0 \quad (1)$$

where  $\Delta K$  is the stress intensity factor range,  $\Delta S$  is the nominal stress range and  $F_0$  is a geometrical factor. The value of  $a_0$  can be evaluated from the limiting condition of a smooth specimen, where the physical crack length,  $a$ , approaches zero.  $F_0$  is unity and  $\Delta K$  becomes the threshold stress intensity factor range,  $\Delta K_{th}$ . Then  $\Delta S$  approaches the fatigue limit of the material,  $\Delta \sigma_e$ . Therefore, from Eq. (1)

$$a_0 = \left( \frac{1}{\pi} \right) \left( \frac{\Delta K_{th}}{\Delta \sigma_e} \right)^2 \quad (2)$$

In this paper, we report FCGR in areas of stress concentrations and of small cracks, using the hole-in-plate specimens in air and in 3.5 percent NaCl solution (saltwater).

## EXPERIMENTAL PROCEDURES

Test Material: The test material was a 12.7-mm-thick plate of ABS grade EH36 steel, a 350-MPa-yield-strength C-Mn steel. The chemical composition is given in Table 1. The steel was in the normalized condition and had particularly uniform properties owing to sulfide shape control. Tensile, fracture [6], and fatigue crack growth [7] properties of the steel have been studied extensively. Reference 7 is in this volume. The tensile and fracture properties at ambient temperature are listed in Table 2.

Specimen Preparation: The test specimens were 12.7-mm-thick hole-in-plate tensile panels. The test matrix and specimen dimensions are given in Table 3. The specimen configuration is shown in Figure 1. A circular hole at the center of the plate was drilled and fatigue crack grew from the edge of the hole to study fatigue crack growth behavior in areas of stress concentrations. Holes at the ends of the specimen for pin loading were reinforced with extra plates joined together by welding.

Except for specimen 1, which did not have notches, sharp notches about 0.5 to 1 mm in length were machined from the edge(s) of the hole normal to the loading direction with a slitting saw. The sharp notches were used as crack starters to facilitate fatigue pre-cracking.

Solutions for the stress intensity factor, K, of the specimen are available in Reference 8. The stress intensity factor is given as

$$K = S (\pi a)^{0.5} F\left(\frac{a}{D}\right) \quad (1)$$

where the crack length, a, is measured from the edge of the hole, D is the hole diameter and S is the remote tensile stress. The function F(a/D) is expressed in graphical form.

Loading Conditions: Except for specimen 1, specimens were cyclically loaded at ambient temperature with frequencies of 3 Hz in air and 0.1 Hz in saltwater using load control with a 1-MN-capacity servo-controlled hydraulic testing machine. The stress ratio, that is the ratio of minimum to maximum stress, was kept constant at 0.3.

Specimen 1, which had no crack, was instrumented with a series of electrical-resistance strain gages extended from the edge of the hole to the edge of the test plate perpendicular to the loading direction. The purpose of testing specimen 1 was to study the strain distribution at the stress concentration under loading-unloading-reloading sequence. The loading and unloading were controlled manually under displacement control.

Test Environments and Crack-Length Measurements: Tests were conducted in air and in saltwater at ambient temperature. Crack-length measurements were made with a 30X traveling microscope at various time intervals depending upon crack propagation rates. For tests in saltwater, a transparent plastic container was used to contain saltwater which was

continuously circulated at a rate of 26 l/minute through a diatomaceous-earth filter. The NaCl concentration, temperature, and pH value of the saltwater were monitored periodically.

For tests in saltwater, crack lengths were measured with the traveling microscope through the transparent container. The rust around the crack tips was scrubbed from the specimen surface with sandpaper and cotton Q-tips before measurements.

Crack closure was monitored through the load-displacement curves with an X-Y recorder or an oscilloscope. Displacements were measured at the crack mouth. To facilitate the displacement measurements, razor blades, spot welded at the crack mouth, extended out of the specimen plane were used for attachment of the clip-on gage.

## EXPERIMENTAL RESULTS AND DISCUSSION

Strain Survey: Specimen 1, which had no crack, was monotonically loaded from zero to 220.4 MPa (nominal stress) and then unloaded to zero nominal stress. The results of local strains along the plane of the hole diameter normal to the loading direction are plotted in Figure 2.

In the elastic range, that is, the nominal stress is less than one-third of the yield strength, the strain distribution in the vicinity of a circular hole can be calculated accurately [9]. The edge of the hole starts to undergo plastic deformation when the nominal stress is higher than one-third of the yield strength. If the extent of plastic deformation is small, the stress redistribution owing to the plastic deformation is negligible and the elastic solutions [9] are still adequate for regions

that do not yield. The results of the present investigation indicate that the elastic solutions are adequate (the error is within 3 percent) for areas 2 mm or farther from the hole edge at a nominal stress of 155.1 MPa, which is much higher than one-third of the yield strength (117 MPa).

The strain increases rapidly after the material has yielded. Strain distributions in the elastic-plastic case can be estimated using the Neuber's rule [10]. To obtain accurate results, numerical methods, such as finite element analysis, must be performed.

After the specimen was unloaded to zero nominal stress, as shown in Figure 2, residual strains existed over a large region ( $> 50$  mm). The specimen was reloaded and strain increments,  $\Delta\epsilon$ , were recorded.  $\Delta\epsilon$  is the difference between the current measured strain and the residual strain,  $\Delta\epsilon = \epsilon_{\text{current}} - \epsilon_{\text{residual}}$ . As shown in Figure 3, as nominal stress increased from 116.3 to 220.4 MPa (about double),  $\Delta\epsilon$  at a point 2 mm from the hole edge increased from  $1.52 \times 10^{-3}$  to  $3.12 \times 10^{-3}$  (about double). The relation between nominal stress and local strain increment is linear owing to strain hardening of the material in the plastically deformed region. Because of the linear relation between stress and strain at stress levels above monotonic yield strength, the LEFM analysis of FCGR in this region is expected to be adequate. However, the residual stress associated with the residual strain might influence FCGR. The residual stress is in compression and effectively reduces the stress ratio, which usually lowers FCGR especially at higher and near-threshold growth rate regions.

FCGR at Edges of a Yielded Hole in Air: Specimen 4, which had two symmetric cracks emanating from opposite edges of the hole, was fatigue tested with a maximum stress,  $S_{\max}$ , = 207 MPa and a minimum stress,  $S_{\min}$ , = 62.1 MPa in air. With a stress concentration factor of 3.14, the maximum and minimum local stresses at the edge of the hole were 650 and 195 MPa, respectively. Fatigue crack growth rates were measured as the cracks propagated from 0.5 to 9 mm, which was within the yielded region caused by the application of a nominal stress of 207 MPa (Figure 2).

The FCGR results, plotted in Figure 4, show good agreement between the hole-in-plate specimen and compact-type (CT) specimens [7] at  $\Delta K$  higher than 30 MPa $\sqrt{m}$ . Below 30 MPa $\sqrt{m}$ , the FCGR of the hole-in-plate specimen are higher than those obtained from CT specimens, which is not unexpected. Usually, the length of the existing crack is larger than 15 mm for a 25.4-mm-thick CT specimen, which was used in Reference 7 and the crack behaves like a normal or long crack. In the hole-in-plate specimen, the crack length was about 1.5 mm when  $\Delta K$  was 30 MPa $\sqrt{m}$  and the crack behaves like a small crack. As discussed previously, FCGR of small cracks are higher than those predicted by results from long cracks.

If the approach of El Haddad et al [2-4] was used, the value of  $a_0$  in Eq. (1) was found to be 0.35 mm. After this was done, the whole  $da/dN$ -vs.- $\Delta K$  curve of the hole-in-plate specimen agreed well with the curve of CT specimens.

Specimen 2, which had only one crack emanating from one edge of the hole, was fatigue tested with a loading condition identical to that applied to specimen 4. The FCGR results are shown in Figure 5, which show reasonable agreement between the hole-in-plate specimen and CT specimens [7].

The results of this investigation show that the LEFM analysis of fatigue crack growth is adequate in yielding conditions under monotonic loading. This observation is consistent with one other study [7] in which a deep grooved CT specimen was tested. However, it should be cautioned that the applicability of the LEFM analysis of fatigue crack growth in yielding conditions (under monotonic loading) is probably limited to conditions that the local stress-strain relation under cyclic loading <sup>remains</sup> ~~is still~~ linear.

FCGR at Edges of a Yielded Hole in Saltwater: Specimen 3, which had one crack emanating from one edge of the hole, was fatigue tested with a loading history identical to that applied to specimen 4 in saltwater. The FCGR results are shown in Figure 6. Reasonable agreement between results from CT specimens [7] and the present study is observed, indicating that in saltwater as well as in air the LEFM analysis of fatigue crack growth is adequate in yielding conditions under monotonic loading.

As shown in Figure 6, the small-crack behavior occurs at a  $\Delta K$  level of about 45 MPa $\sqrt{\text{m}}$ , which corresponds to a crack length of 3 mm, twice as long as that observed in air (1.5 mm). The reason for this is not clear and further experiment is needed.



The slightly slower FCGR in the present results in comparison with those of CT specimens [7] as shown in Figures 5 and 6 (specimens 2 and 3) are explained as follows. The available K solutions [8] for a crack emanating from one edge of a circular hole appear~~s~~ to be overestimating when they were compared with the experimental data [11,12]. Consequently, the FCGR will be slower at a given  $\Delta K$  value than the actual if the calculated K is used to correlate FCGR. In the case of two cracks emanating from both edges of the hole, the available K solutions [8] appear to be accurate when ~~it was~~ <sup>they were</sup> compared with the experimental data [11].

#### SUMMARY AND CONCLUSIONS

Even though significant plastic deformation exists in areas of stress concentrations in structural components, the fatigue crack growth rates in those areas can be predicted very well using the LEFM analysis provided that the local stress-strain relation is linear under cyclic loading and the crack is long enough that the small-crack behavior is absent. Small cracks grow at faster rates than those predicted from  $da/dN$ -vs- $\Delta K$  results of long cracks. The problem of small-crack behavior can be accounted for by adding an intrinsic crack length to the physical crack length, as suggested by El Haddad. The intrinsic crack length appears to be dependent upon environmental conditions for a given material. It is longer in saltwater (3 mm) than in air (1.5 mm)

#### ACKNOWLEDGMENTS

This work~~ed~~ was supported by Department of Interior, Minerals Management Service. Drs. H. I. McHenry and D. T. Read provided helpful discussions.

## REFERENCES

1. H. D. Solomon, "Low Cycle Fatigue Crack Propagation in 1018 Steel," *Journal of Materials*, Vol. 7, No. 3 (1972), pp. 299-306.
2. M. H. El Haddad, K. N. Smith and T. H. Topper, "Fatigue Crack Propagation of Short Cracks," *Journal of Engineering Materials and Technology*, Vol. 102 (1979), pp. 42-46.
3. M. H. El Haddad, K. N. Smith and T. H. Topper, "A Strain Based Intensity Factor Solution for Short Fatigue Cracks from Notches," in: *Fracture Mechanics*, ASTM STP 677, American Society for Testing and Materials, Philadelphia, 1979, pp. 274-284.
4. M. H. El Haddad, N. E. Dowling, T. H. Topper, and K. N. Smith, "J-Integral Applications for Short Fatigue Cracks at Notches," *International Journal of Fracture*, Vol. 16, No. 1 (1980), pp. 15-30.
5. N. E. Dowling, "Geometry Effects and the J-Integral Approach to Elastic-Plastic Fatigue Crack Growth," in: *Crack and Fracture*, ASTM STP 601, American Society for Testing and Materials, Philadelphia, 1977, pp. 19-32.
6. T. L. Anderson, "The Effect of Crack-Tip Region Constraint on Fracture in the Ductile-to-Brittle Region," Ph.D. thesis, Colorado School of Mines, Golden, Colorado (1983).
7. Y. W. Cheng, "Spectrum-Loading Fatigue-Crack Growth for a Ship Steel in Saltwater," in this volume.
8. H. Tada, P. C. Paris, and G. R. Irwin, *The Stress Analysis of Cracks Handbook*, Del Research Corp., Hellertown, Pennsylvania (1973), p. 19.2, 19.4 and 19.9.
9. G. N. Savin, *Stress Concentration Around Holes*, translated from the Russian by E. Gros, Pergamon Press, 1961, pp. 104-113.
10. H. Neuber, "Theory of Stress Concentration <sup>for</sup> Shear-Strained Prismatical Bodies with Arbitrary Nonlinear Stress-Strain Law," *Journal of Applied Mechanics*, Vol. 28 (1961), pp. 544-550.
11. P. N. Li and Y. W. Cheng, "High/Low Amplitude Effects on Fatigue Crack Growth of a Ship Steel in Air and in Saltwater," in this volume.
12. J. S. Cargill, J. K. Malpani, and Y. W. Cheng, "Disk Residual Life Studies," AFML-TR-79-4173 (1979), Air Force Materials Laboratory, Dayton, Ohio.

#### List of Tables

1. Chemical composition of ABS grade EH36 steel.
2. Tensile and fracture properties of ABS grade EH36 steel at ambient temperature.
3. Test matrix and specimen dimensions.

## List of Figures

1. Schematic of hole-in-plate specimen.
2. Measured strain distribution in the vicinity of a circular hole at various nominal stress levels.
3. Measured strain distribution in the vicinity of a circular hole at various nominal stress levels after one loading-unloading sequence.
4. Comparison of fatigue crack growth rates in plastically deformed regions and compact-type specimens: in air (specimen 2).
5. Comparison of fatigue crack growth rates in plastically deformed regions and compact-type specimens: in air (specimen 4).
6. Comparison of fatigue crack growth rates in plastically deformed regions and compact-type specimens: in saltwater.

Table 1. Chemical composition of ABS grade EH36 steel.

C	Mn	P	S	Si	Cu	Ni	Cr	Mo	Fe
0.12	1.39	0.015	0.006	0.380	0.05	0.03	0.05	0.007	bal.

Table 2. Tensile and fracture properties of ABS grade EH36 steel at ambient temperature [6].

---

Upper Yield Point (MPa):	331
Lower Yield Stress (MPa):	326
Ultimate Tensile Strength (MPa):	496
Fracture Stress (MPa):	1246
Percent Elongation:	39.1
Percent Reduction in Area:	77.6
Charpy V-Notch Absorbed Energy (J):	~346
Fracture Toughness*, CTOD (mm):	0.481
Fracture Toughness*, $J_{Ic}$ (N·mm <sup>-1</sup> ):	241

---

\* 3-point bend specimen with thickness = 25.4 mm.

Table 3. Test matrix and specimen dimensions.

Specimen No.	Specimen Width, mm	Center Hole Diameter, mm	Crack	Test Environment	Test Frequency, Hz
1	203	50.8	No	Air	---
2	254	50.8	Asymmetric (One Crack)	Air	3
3	254	50.8	Asymmetric (One Crack)	Saltwater	0.1
4	254	50.8	Symmetric (Two Cracks)	Air	3



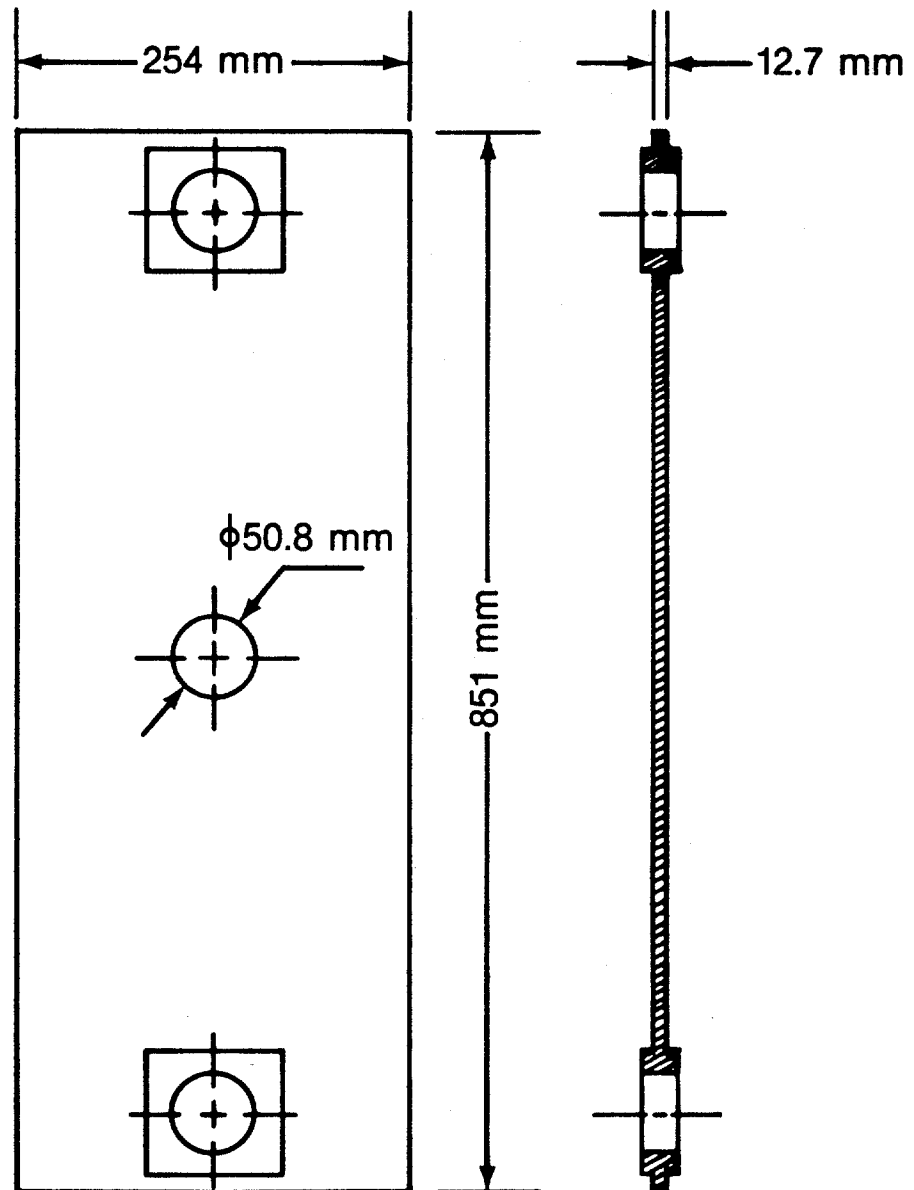
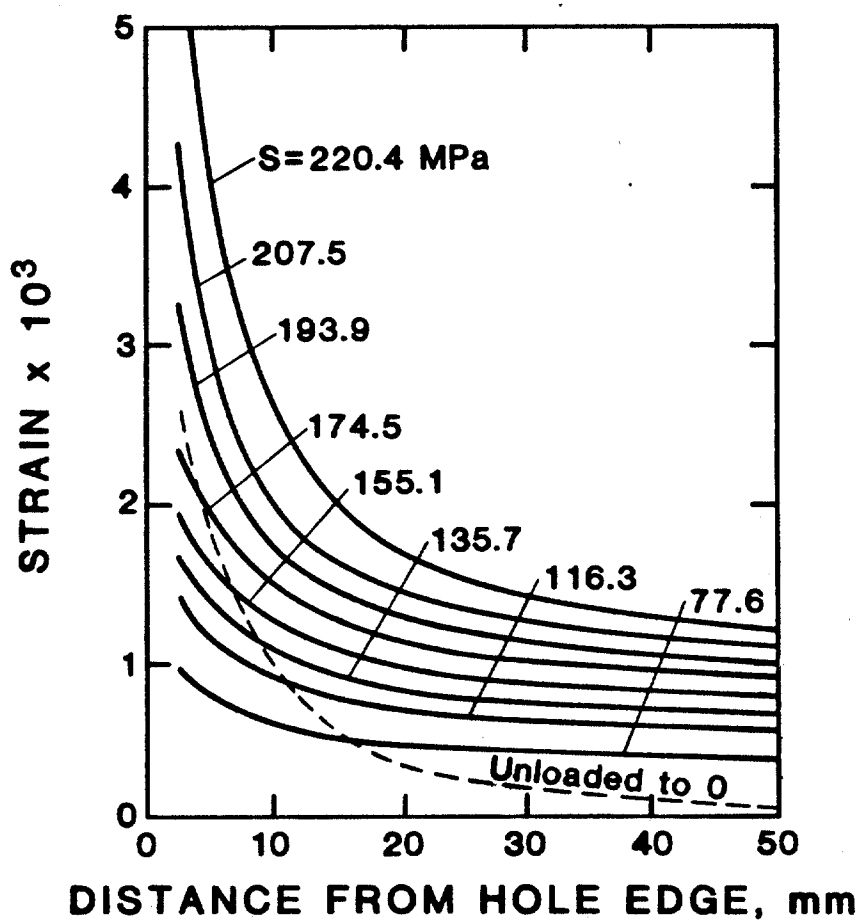


Fig 1



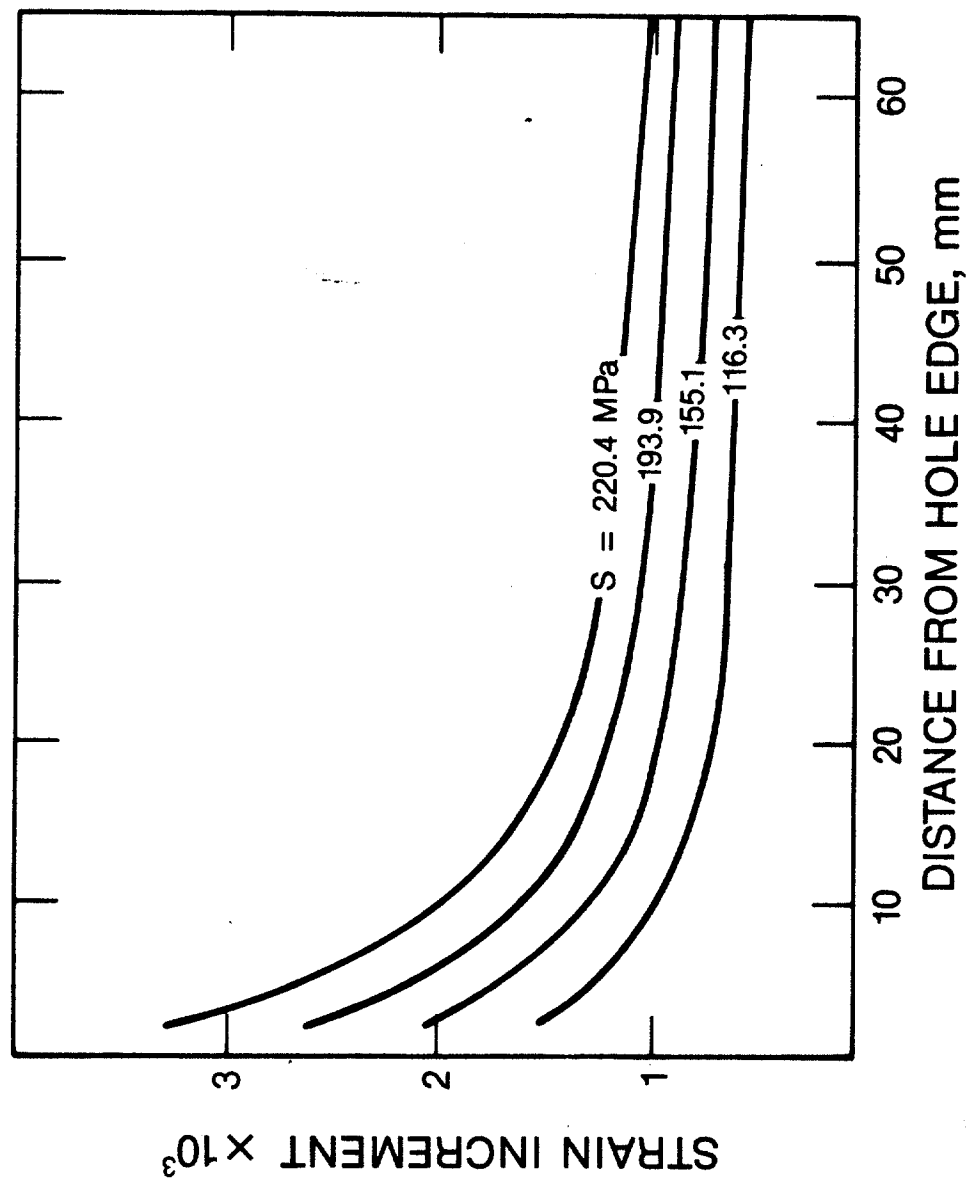


Fig. 3

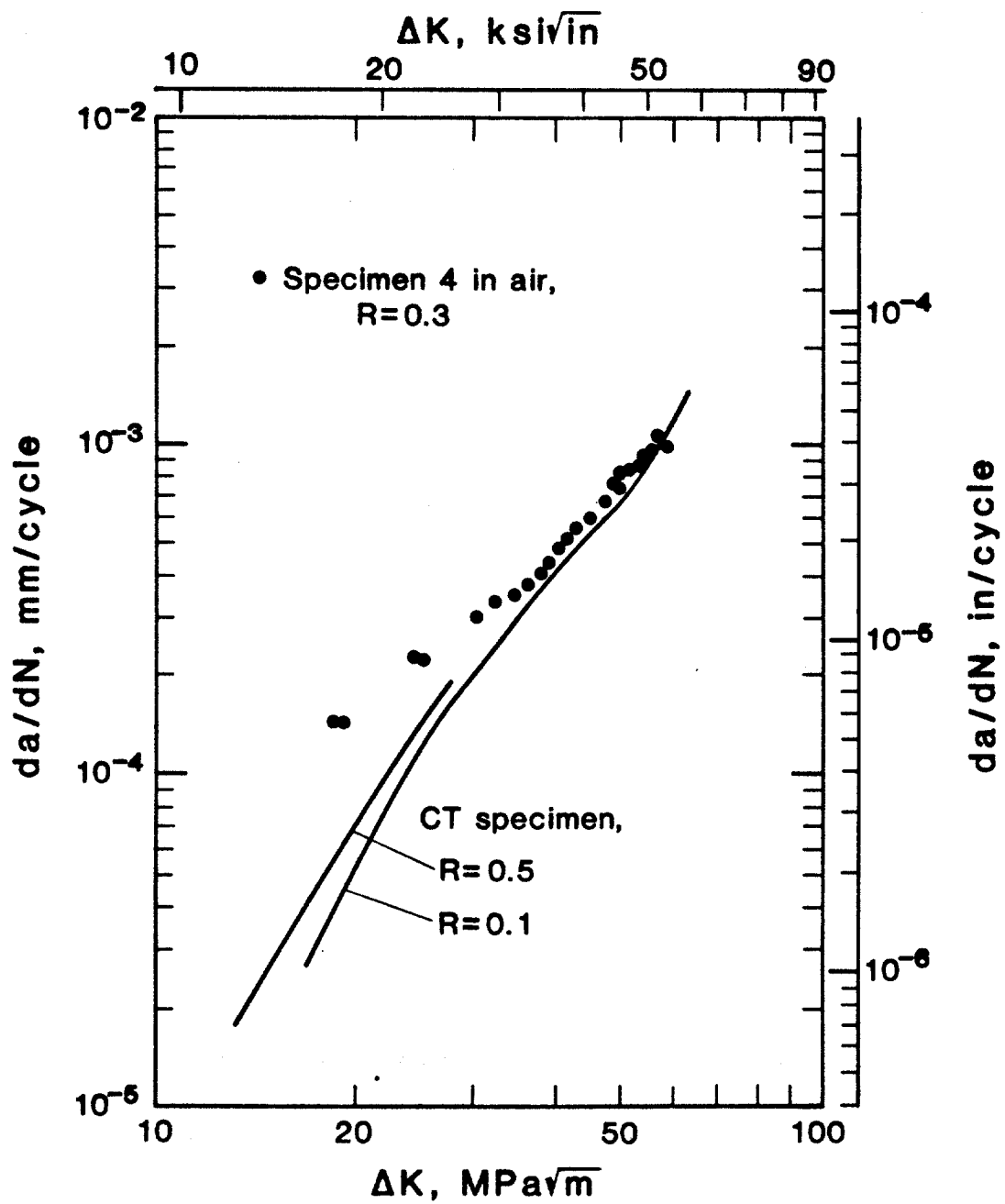


Fig. 4

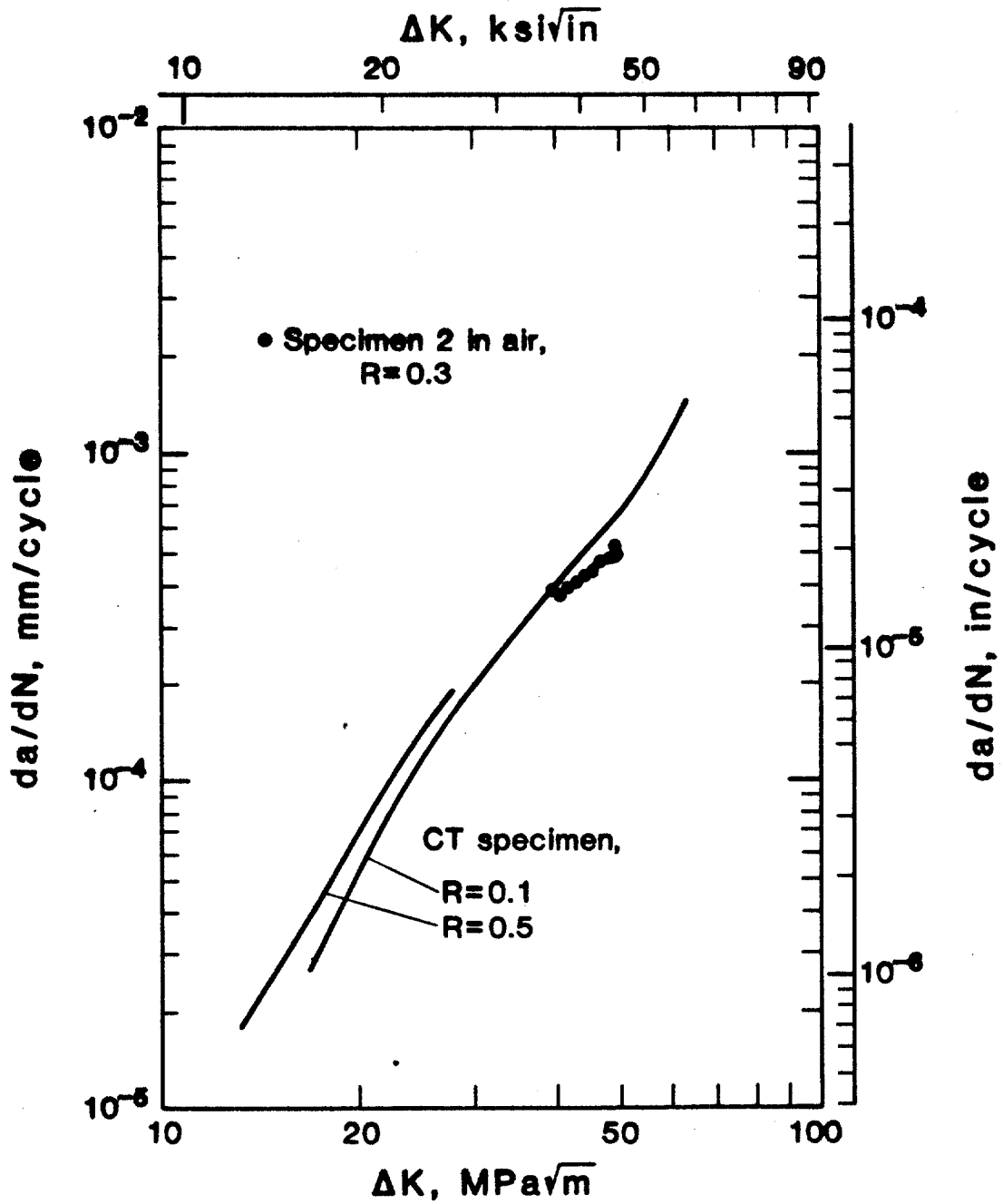


Fig. 5

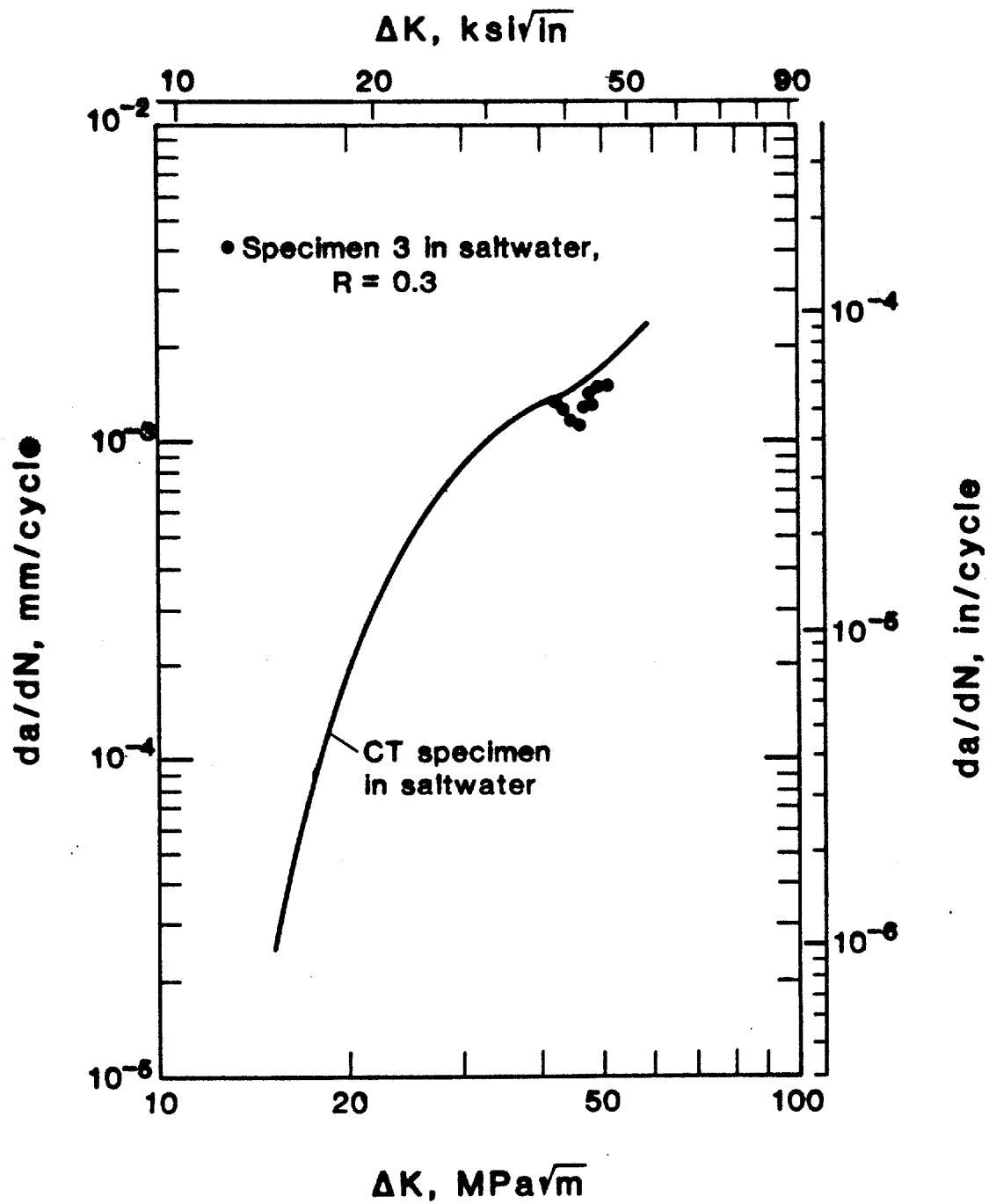


Fig. 6

High/Low Amplitude Effects on Fatigue Crack Growth Rates  
of a Ship Steel in Air and in Saltwater\*

P. N. Li\*\* and Y. W. Cheng

Fracture and Deformation Division  
National Bureau of Standards  
Boulder, Colorado 80303

Key Words: C-Mn steel, environmental effects, fatigue crack growth, load-sequence interaction effects, yielding effects.

\*Contribution of NBS; not subject to copyright.

\*\*Guest worker, on leave from East-China Institute of Chemical Technology, Shanghai, China.

## ABSTRACT

Hole-in-plate specimens, made of ABS grade EH36 steel, were tested in air and in 3.5 percent NaCl solution (saltwater) to study the high/low amplitude effects on fatigue crack growth rates (FCGR) in an elastic stress field and at the edges of a yielded hole. Effects of tensile overload prior to crack initiation on subsequent FCGR at the edges of a yielded hole were also investigated. The results are summarized as follows:

1. The tensile overload retardation effects were similar in a <sup>n</sup>/<sub>Λ</sub> elastic stress field and at the edges of a yielded hole.
2. The tensile overload retardation effects were similar in air and in saltwater.
3. The Bowie analysis overestimated the stress intensity factors <sup>when</sup> ~~in~~ comparison<sup>ed</sup> with experimental results.
4. The simple engineering approach gave accurate stress intensity factors <sup>when</sup> ~~in comparison~~<sup>ed</sup> with experimental results, except in areas close to the edges of a hole. In the latter cases, the simple engineering approach overestimated the stress intensity factors owing to overestimation of crack length.
5. Tensile overload prior to crack initiation appeared to retard the subsequent FCGR at the edges of a yielded hole. The retardation was explained by the presence of beneficial residual stresses and crack closure.



## INTRODUCTION

The fracture mechanics approach has been successfully applied to describe the fatigue crack growth under constant-amplitude loading. However, fatigue life predictions of structural components remain complicated and in-precise owing to lack of methodologies that accurately take account of the irregular nature of service loading. Load-sequence interaction effects have been qualitatively recognized for a long time, but because of numerous factors involved, detailed quantitative characterization has not well been established. Significant effects observed by many investigators can be summarized as follows:

1. Tensile overloads cause retardation of fatigue crack growth. A sufficiently high tensile overload may stop the growth of a fatigue crack completely [1].
2. Preceding lower cyclic loads cause a slight acceleration of fatigue crack growth [2].
3. A compressive overload preceding a tensile overload reduces the retardation caused by the tensile overload [3].
4. A compressive overload following a tensile overload significantly reduces the retardation effects caused by the tensile overload [3].
5. Compressive overloads slightly accelerate fatigue crack growth [3].

For sea loading on offshore structures, all of the aforementioned load-sequence interaction effects will occur. In the case of offshore structures, one has to consider an possibility of additional interactions between load sequence and strong environmental effects due to saltwater. The investigation reported in this paper pursued the following objectives: (1) to compare the high/low amplitude effects on fatigue crack growth

rates (FCGR) in air and in 3.5 percent NaCl solution (saltwater), (2) to compare the high/low amplitude effects on FCGR in an elastic stress field and at edges of a yielded hole, (3) to study the effects of tensile overload prior to crack initiation on subsequent FCGR.

## EXPERIMENTAL PROCEDURES

Test Material: The test material was a 12.7-mm-thick plate of ABS grade EH36 steel, a 350-MPa-yield-strength C-Mn steel. The chemical composition is given in Table 1. The steel was in the normalized condition and had particularly uniform properties owing to sulfide shape control. Tensile, fracture [4], and fatigue crack growth [5] properties of the steel have been studied extensively. Reference 5 is in this volume. The tensile and fracture properties at ambient temperature are listed in Table 2.

Specimen Preparation: The test specimens were 12.7-mm-thick hole-in-plate tensile panels. The test matrix and specimen dimensions are given in Table 3. The specimen configuration is shown in Figure 1. A center hole was drilled and fatigue crack grew from the edge of the hole to study the high/low amplitude interaction effects in an area of stress concentration. Holes at the ends of the specimen for pin loading were reinforced with extra plates joined together by welding.

Except for specimen 1, which did not have notches, sharp notches about 0.5 to 1 mm in length were machined from the edge(s) of the hole normal to the loading direction with a slitting saw. The sharp notches were used as crack starters to facilitate fatigue pre-cracking.

Solutions for the stress intensity factor,  $K$ , of the specimen are available in Reference 6. The stress intensity factor is given as

$$K = S (\pi a)^{0.5} F\left(\frac{a}{D}\right) \quad (1)$$

where the crack length,  $a$ , is measured from the edge of the hole,  $D$  is the hole diameter, and  $S$  is the remote tensile stress. The function  $F(a/D)$  is expressed in graphical form.

Loading Conditions: Except for specimen 1, specimens were cyclically loaded at ambient temperature with frequencies of 3 Hz in air and 0.1 Hz in saltwater using load control with a 1-MN-capacity servo-controlled hydraulic testing machine. The stress ratio, that is the ratio of minimum to maximum stress, was kept constant at 0.3. The maximum and minimum loads were step decreased during the test, while the stress ratio was kept constant, to study the high/low amplitude effects. The initial maximum and minimum nominal stresses,  $S_{\max}$  and  $S_{\min}$ , were 207 and 62.1 MPa. The stresses were step decreased to 147.9 and 44.36 MPa, and then to 105.6 and 31.69 MPa.

Specimen 1, which had no crack, was instrumented with a series of electrical-resistance strain gages extended from the edge of the hole to the edge of the test plate perpendicular to the loading direction. The purpose of testing specimen 1 was to study the strain distribution at the stress concentration under loading-unloading-reloading sequence. The loading and unloading were controlled manually under displacement control.

Specimen 5, which had no crack initially with a hole diameter of 44.45 mm, was monotonically loaded to a nominal stress of 242 MPa. After unloading, two small notches of 0.5 mm in length were introduced with a jeweler's saw on both edges of the hole normal to the loading direction. The specimen was fatigue cycled at stress levels of  $S_{\max} = 207$  MPa and  $S_{\min} = 62.1$  MPa. After each crack had grown 3.2 mm, the specimen was remachined to enlarge the hole diameter to 50.8 mm. The specimen was then fatigue cycled again at the same cyclic stress levels ( $S_{\max} = 207$  MPa and  $S_{\min} = 62.1$  MPa). Specimen 5 was used to study the influence of tensile overload which was applied before crack initiation on the subsequent fatigue crack propagation at stress concentrations.

Test Environments and Crack-Length Measurements: Tests were conducted in air and in saltwater at ambient temperature. Crack-length measurements were made with a 30X traveling microscope at various time intervals depending upon crack propagation rates. For tests in saltwater, a transparent plastic container was used to contain saltwater which was continuously circulated at a rate of 26 l/minute through a diatomaceous-earth filter. The NaCl concentration, temperature, and pH value of the saltwater were monitored periodically.

For tests in saltwater, crack lengths were measured with the traveling microscope through the transparent container. The rust around the crack tips was scrubbed from the specimen surface with sandpaper and cotton Q-tips before measurements.

Crack closure was monitored through the load-displacement curves with an X-Y recorder or an oscilloscope. Displacement was measured at the crack mouth. To facilitate the displacement measurement, razor blades, spot welded at the crack mouth, extended out of the specimen plane were used for attachment of the clip-on gage.

## EXPERIMENTAL RESULTS AND DISCUSSION

Strain Survey: Specimen 1, which had no crack, was monotonically loaded from zero to 220.4 MPa (nominal stress) and then unloaded to zero nominal stress. The results of local strains along the plane of hole diameter normal to the loading direction are plotted in Figure 2.

In the elastic range, that is, the nominal stress is less than one-third of the yield strength, the strain distribution in the vicinity of a circular hole can be calculated accurately [7]. The edge of the hole starts to undergo plastic deformation when the nominal stress is higher than one-third of the yield strength. If the extent of plastic deformation is small, the stress redistribution owing to the plastic deformation is negligible and the elastic solutions [7] are still adequate for regions that do not yield. Results of the present investigation indicate that the elastic solutions are adequate (the error is within 3 percent) for areas 2 mm or farther from the hole edge at a nominal stress of 155.1 MPa, which is much higher than one-third of the yield strength (117 MPa).

The strain increases rapidly after the material has yielded. Strain distributions in the elastic <sup>-plastic</sup> case can be estimated using the Neuber rule [8]. To obtain accurate results, numerical methods, such as finite element analysis, must be performed.

After the specimen was unloaded to zero nominal stress, as shown in Figure 3, residual strains existed over a large region ( $> 50$  mm). The specimen was reloaded and strain increments,  $\Delta\epsilon$ , were recorded.  $\Delta\epsilon$  was the difference between the current measured strain and the residual strain,  $\Delta\epsilon = \epsilon_{\text{current}} - \epsilon_{\text{residual}}$ . As shown in Figure 3, as nominal stress increased from 116.3 to 220.4 MPa (about double),  $\Delta\epsilon$  at a point 2 mm from the hole edge increased from  $1.52 \times 10^{-3}$  to  $3.12 \times 10^{-3}$  (about double). The relation between nominal stress and local strain increment is linear owing to strain hardening of the material in the plastically deformed region. Because of the linear relation between stress and strain at stress levels above monotonic yield strength, the LEFM analysis of FCGR in this region is expected to be adequate. However, the residual stress associated with the residual strain might influence FCGR. The residual stress is in compression and effectively reduces the stress ratio, which usually lowers FCGR, especially at higher and near-threshold growth rate regions.

Effects of High/Low Amplitude on FCGR in Air: Specimens 2 and 4 were tested to study the effects of high/low amplitude on FCGR in air in the plastically deformed regions. The results along with the detailed loading histories are given in Figures 4 and 5 for specimens 2 and 4, respectively. At the beginning of testing specimen 2, which had a single crack

emanating from one edge of the hole, the maximum nominal stress,  $S_{\max}$ , and the minimum nominal stress,  $S_{\min}$ , were first decreased from 207 and 62.1 MPa to 115 and 34.5 MPa, a load reduction ratio of 1.8. The overload effect was so strong that there was no observed crack growth in 90.9 kilo-cycles. Subsequently,  $S_{\max}$  and  $S_{\min}$  were increased to 147.9 and 44.36 MPa, respectively.

The values of  $\Delta K$ , as shown in Figure 4, were calculated using the Bowie analysis [6], the simple engineering approach [9] which considers the hole as a portion of the crack, and the experimental method. In the experimental method, values of  $\Delta K$  were inferred, using the  $da/dN$ -vs- $\Delta K$  results of CT specimens [5], from the measured  $da/dN$  of the hole-in-plate specimen.

As shown in Figure 4, the trend of experimental  $\Delta K$  without considering crack closure or retardation effects, is lower than both predictions of the Bowie analysis and the simple engineering approach. However, if the crack closure is considered, the apparent stress intensity factor range ( $\Delta K_{\text{app}}$ ) plotted as crosses in Figure 4, increases and agrees very well with predictions from the simple engineering approach.

At crack lengths less than 5 mm, the simple engineering approach overestimates  $\Delta K$  because it overestimates the crack length by considering the hole as a portion of the crack. The Bowie analysis overestimates  $\Delta K$  in the whole range studied. The present results are consistent with those of the other study [10] in which a single fatigue crack propagated from the bolthole of a compressor disk. The crack length at which the simple engineering solution crosses over with the Bowie analysis depends on the size of the hole; it increases with increasing hole diameter.

As expected, FCGR immediately after the load reduction was slower than the trend line indicating that the fatigue crack growth was retarded. There was no observed crack growth in 90.9 kilocycles after a load reduction ratio of 1.8. The measured widths of retardation effect were in reasonable agreement with predictions by Willenborg model [10]: 4.5 and 6.5 mm versus 4.9 mm. As indicated in Figure 2, at a nominal stress of 207.5 MPa the yielded region extended from the hole edge to about 19 mm away from the hole edge. Thus, at the first load reduction the crack tip with a crack length of 9 mm was within the yielded region. At the second load reduction the crack tip with a crack length of 26 mm was outside the yielded region. The  $\Delta K$ -vs- $a$  trends, in Figure 4, of the first and the second load reductions are similar indicating that the high/low amplitude effects on FCGR are similar in the elastic and in the yielded regions. It should be cautioned that the LEFM analysis of FCGR in the yielded region is probably limited to conditions that the stress-strain relation in this region remains linear under cyclic loading. If it is cyclically yielded, the analysis will probably not be valid.

The results of specimen 4, which had two cracks emanating from both edges of the hole, are shown in Figure 5. The available  $K$  solution is from Newman analysis [6]. As shown in Figure 5, the experimental  $\Delta K$  values are in excellent agreement with those of analytical predictions except in the areas affected by the load reduction.

Three phenomena <sup>observed in specimen 4,</sup> which were different from specimen 2, were evident. First, no apparent crack closure was observed. Second, the measured width of retardation effect, 17 mm, was much larger in specimen 4 than in specimen 2. Third, the delayed retardation effect was more pronounced. The



only difference between specimens 2 and 4 is that specimen 2 had a single crack emanating from one edge of the hole and specimen 4 had two symmetrical cracks emanating from both edges of the hole. The observed different phenomena between the two specimens seem to be geometry dependent. To confirm the observations, additional tests are needed.

Effects of High/Low Amplitude on FCGR in Saltwater: Specimen 3, which had one crack emanating from one edge of the hole (identical to specimen 2), was fatigue tested with a loading history identical to that applied to specimen 4 in saltwater. The results obtained in saltwater, as shown in Figure 6, are similar to those of specimen 2 in air (Figure 4). That is, (1) the experimental  $\Delta K$  without considering crack closure are smaller than those predicted by the Bowie analysis and by the simple engineering approach, (2) overloading effects are observed and the width of retardation effect is in good agreement with that predicted by the Willenborg model. This indicates that the high/low amplitude effects are practically the same in saltwater as in air.

Effects of Overload Prior to Crack Initiation on FCGR: Specimen 5 containing a center hole, 44.45 mm in diameter, without notch was preloaded to a remote stress of 242 MPa. After unloaded, two small notches of 0.5 mm in length were introduced by a jeweler's saw on both edges of the hole. Then the specimen was fatigue cycled at stress levels of  $S_{\max} = 207$  MPa and  $S_{\min} = 62.1$  Mpa, identical to that applied to specimen 4. As the distance between the two crack tips increased beyond 50.8 mm, the specimen was remachined to enlarge the hole diameter to 50.8 mm, while the center

of the hole was adjusted such that the remaining small cracks were of a same length. Finally, the specimen was cycled again at the same cyclic stress levels ( $S_{\max} = 207$  and  $S_{\min} = 62.1$  MPa).

The data plotted in Figures 7 and 8 show that FCGR are much slower than those of specimen 4 which was without prior overloading. The solid line in Figure 7 was derived from Newman analysis [6] and the dots were inferred from the experimental method. The different behaviors exhibited by specimens 4 and 5 can be explained as follows. Since the hole edge of specimen 5 was yielded during prior overloading, beneficial compressive residual stresses were developed upon unloading. Moreover, when a crack is present in the prior yielded region, the crack surfaces will touch each other before the specimen is unloaded to the minimum load. This means that, in addition to a compressive residual stress field at the crack tip, crack closure occurs and the FCGR decreases. The small-crack behavior was observed which counter-balanced the retardation effect at crack lengths less than 0.5 mm (Figure 8).

#### SUMMARY AND CONCLUSIONS

The retardation in fatigue crack growth rates owing to high/low amplitude was studied with hole-in-plate specimens. The following observations were made:

1. The retardation effects were similar in elastic stress fields and at the edges of a yielded hole.
2. The retardation effects were similar in air and in saltwater.
3. The Bowie analysis overestimated the stress intensity factors ~~in~~<sup>when</sup> comparison<sup>ed</sup> with experimental results.

4. The simple engineering approach gave accurate stress intensity factors <sup>when</sup> ~~in comparison~~ <sup>ed</sup> with experimental results, except in areas close to the edges of a circular hole. The approach overestimated the stress intensity factors because of overestimation of crack length.

Tensile overload prior to crack initiation appeared to retard the subsequent fatigue crack growth rates in areas of stress concentrations. The retardation was explained by the presence of beneficial residual stresses and crack closure.

#### ACKNOWLEDGMENTS

This work was supported by Department of Interior, Minerals Management Service. Drs. H. I. McHenry and D. T. Read provided helpful discussions.

#### REFERENCES

1. C. M. Hudson and H. F. Hardrath, "Investigation of the Effects of Variable-Amplitude Loadings on Fatigue Crack Propagation Patterns," TND-1803, NASA, 1963.
2. E. F. J. von Euw, R. W. Hertzberg and R. Roberts, "Delay Effects in Fatigue Crack Propagation," in: Stress Analysis and Growth of Cracks, ASTM STP 513, American Society for Testing and Materials, Philadelphia, 1972, pp. 230-259.
3. R. I. Stephens, D. K. Chen and B. W. Hom, "Fatigue Crack Growth with Negative Stress Ratios Following Single Overloads in 2024-T3 and 7075-T6 Aluminum Alloys," in: Fatigue Crack Growth under Spectrum Loads, ASTM STP 595, American Society for Testing and Materials, Philadelphia, 1976, pp. 27-40.
4. T. L. Anderson, "The Effect of Crack-Tip Region Constraint on Fracture in the Ductile-to-Brittle Region," Ph.D. thesis, Colorado School of Mines, Golden, Colorado (1983).

5. Y. W. Cheng, "Spectrum-Loading Fatigue-Crack Growth for a Ship Steel in Saltwater," in this volume.
6. H. Tada, P. C. Paris, and G. R. Irwin, The Stress Analysis of Cracks Handbook, Del Research Corp., Hellerton, Pennsylvania (1973), p. 19.2, 19.4 and 19.9.
7. G. N. Savin, Stress Concentration Around Holes, translated from the Russian by E. Gros, Pergamon Press, 1961, pp. 104-113.
8. H. Neuber, "Theory of Stress Concentration for Shear-Strained Prismatical Bodies with Arbitrary Nonlinear Stress-Strain Law," Journal of Applied Mechanics, Vol. 28 (1961), pp. 544-550.
9. D. Broek, Elementary Engineering Fracture Mechanics, 3rd edition, Martinus Nijhoff Publishers, 1982.
10. J. S. Cargill, J. K. Malpani, and Y. W. Cheng, "Disk Residual Life Study," AFML-TR-79-4173 (1979), Air Force Materials Laboratory, Dayton OH.
11. J. Willenborg, R. M. Engle, and H. A. Wood, "A Crack Growth Retardation Model Using An Effective Stress Concept," AFFDL-TM-71-1-FBR (1971), Air Force Flight Dynamics Laboratory, Dayton OH.
12. W. J. Mill, R. W. Hertzberg, and R. Roberts, "Load Interaction Effect on Fatigue Crack Growth in A514F Steel Alloy," in: Cyclic Stress-Strain and Plastic Deformation Aspects of Fatigue Crack Growth, ASTM STP 637, American Society for Testing and Materials, Philadelphia, 1977, pp. 192-208.

#### LIST OF TABLES

1. Chemical composition of ABS grade EH36 Steel.
2. Tensile and fracture properties of ABS grade EH36 steel at ambient temperature.
3. Test matrix and specimen dimensions.

## LIST OF FIGURES

1. Schematic of hole-in-plate specimen.
2. Measured strain distributions at the edges of a circular hole at various nominal stress levels.
3. Measured strain distributions at the edges of a circular hole at various nominal stress levels after one loading-unloading cycle.
4. Theoretical and experimental stress intensity factor ranges as a function of crack length of specimen 2 (tested in air).
5. Theoretical and experimental stress intensity factor ranges as a function of crack length of specimen 4 (tested in air).
6. Theoretical and experimental stress intensity factor ranges as a function of crack length of specimen 3 (tested in saltwater).
7. Theoretical and experimental stress intensity factor ranges as a function of crack length/hole diameter ratio of specimen 5 (tested in air).  $a$  is the crack length and  $D$  is the hole diameter.
8. Comparison of fatigue crack growth rates at a preyielded hole and those of CT specimens.

Table 1. Chemical composition of ABS grade EH36 steel.

C	Mn	P	S	Si	Cu	Ni	Cr	Mo	Fe
0.12	1.39	0.015	0.006	0.380	0.05	0.03	0.05	0.007	bal.

Table 2. Tensile and fracture properties of ABS grade EH36 steel at ambient temperature [4]

---

Upper Yield Point (MPa): 331

Lower Yield Stress (MPa): 326

Ultimate Tensile Strength (MPa): 496

Fracture Stress (MPa): 1246

Percent Elongation: 39.1

Percent Reduction in Area: 77.6

Charpy V-Notch Absorbed Energy (J): ~346

Fracture Toughness\*, CTOD (mm): 0.481

Fracture Toughness\*,  $J_{Ic}$  ( $N \cdot mm^{-1}$ ): 241

---

\* 3-point bend specimen with thickness = 25.4 mm.

Table 3. Test matrix and specimen dimensions.

Specimen No.	Specimen Width, mm	Center Hole Diameter, mm	Crack	Test Environment	Test Frequency, Hz
1	203	50.8	No	Air	---
2	254	50.8	Asymmetric	Air	3
3	254	50.8	Asymmetric	Saltwater	0.1
4	254	50.8	Symmetric	Air	3
5	254	44.45 and 50.8	Symmetric	Air	3



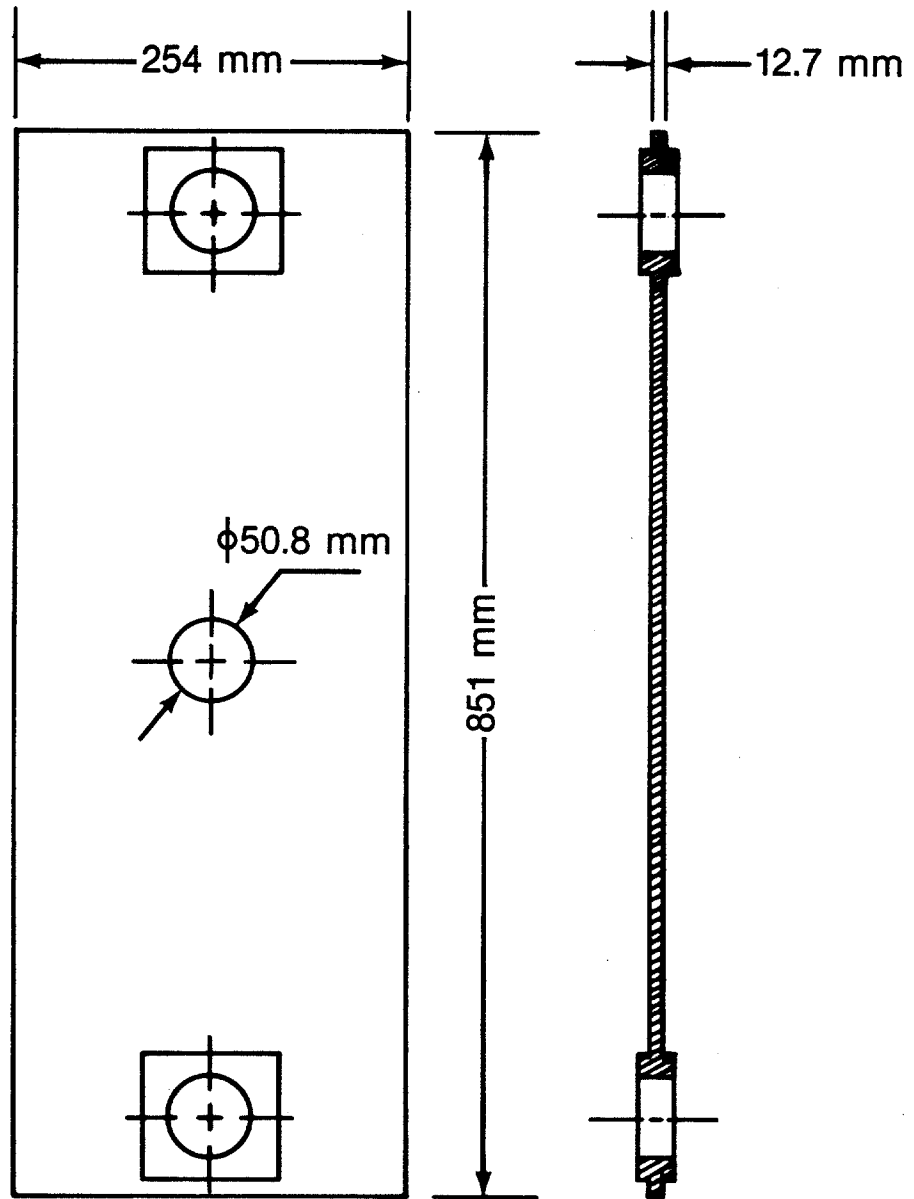


Fig. 1

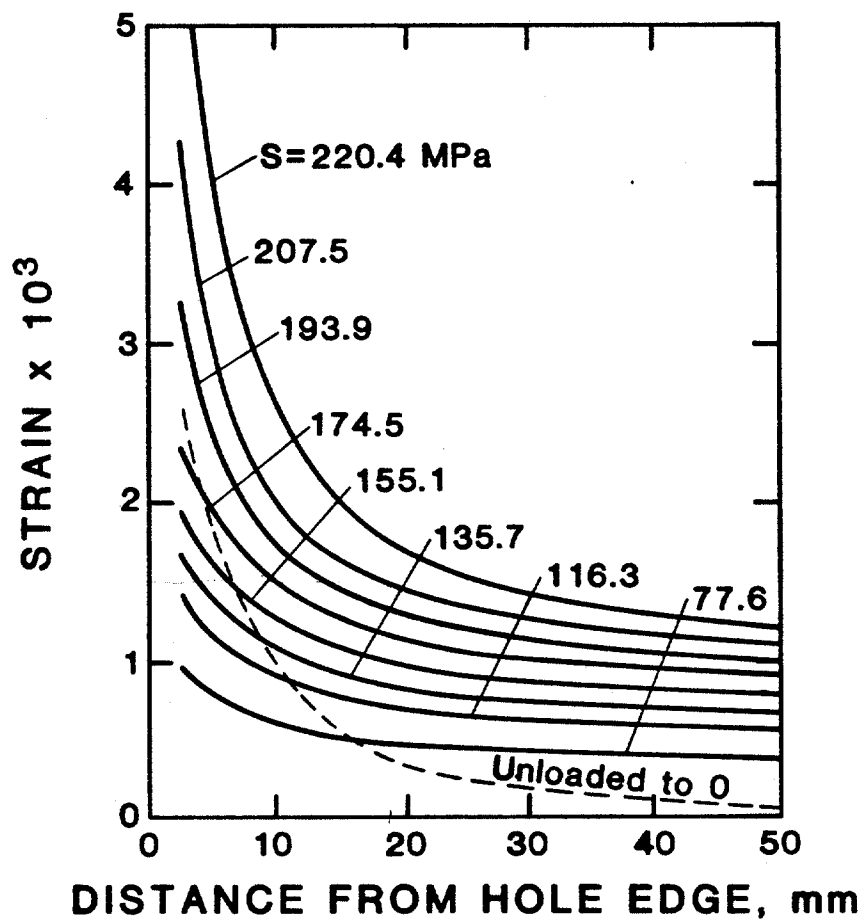


Fig 2

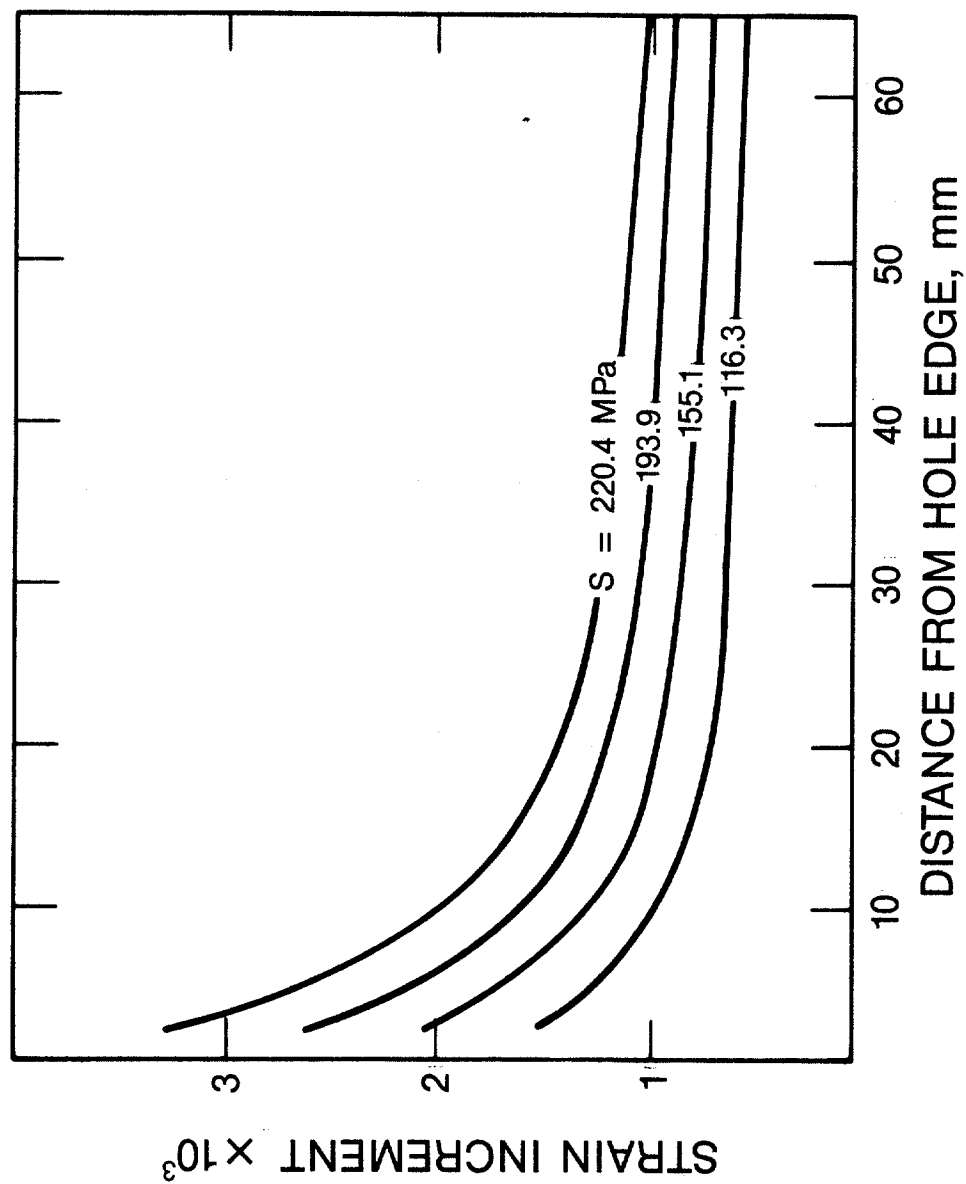
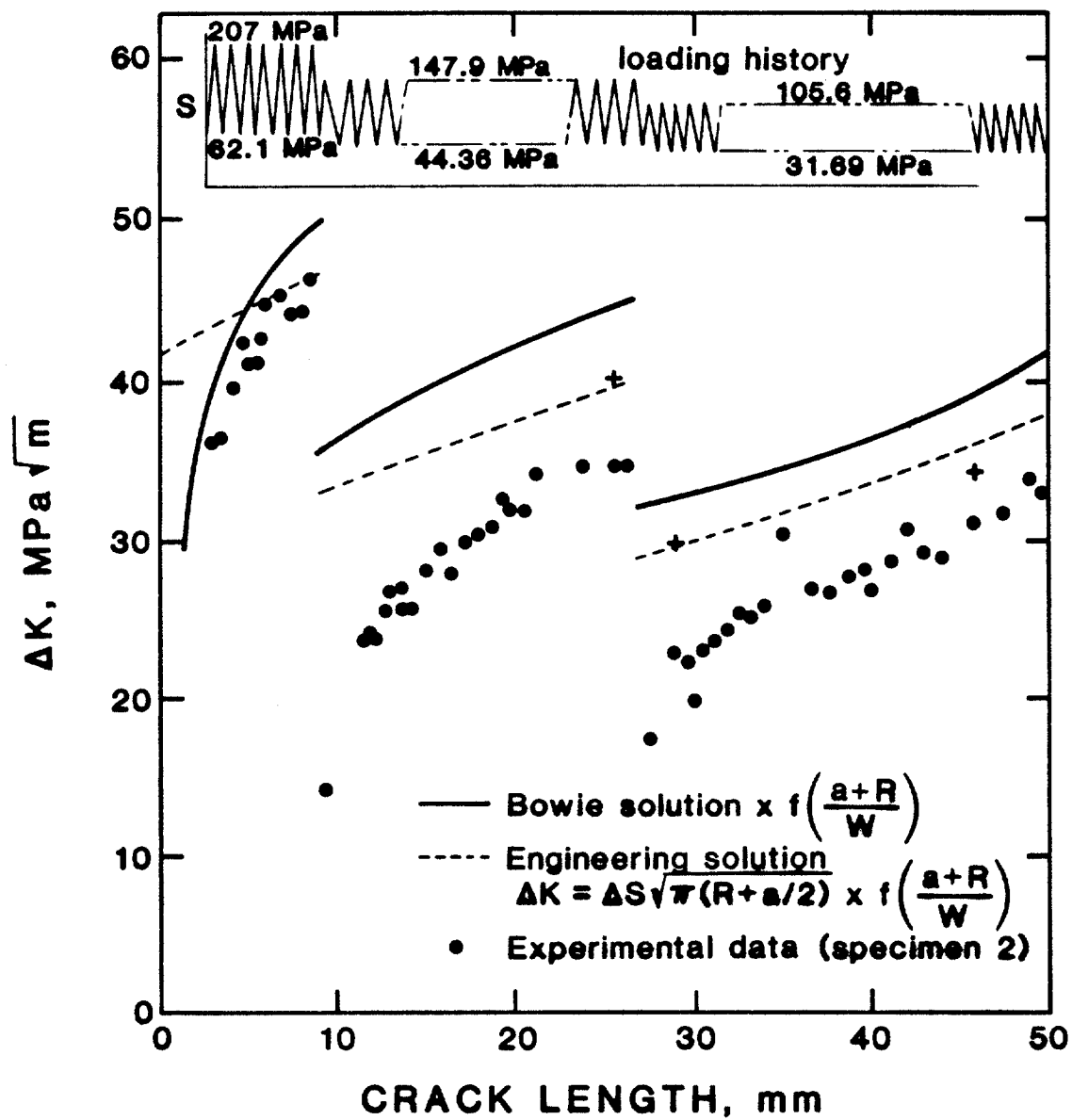


Fig. 3



207.4

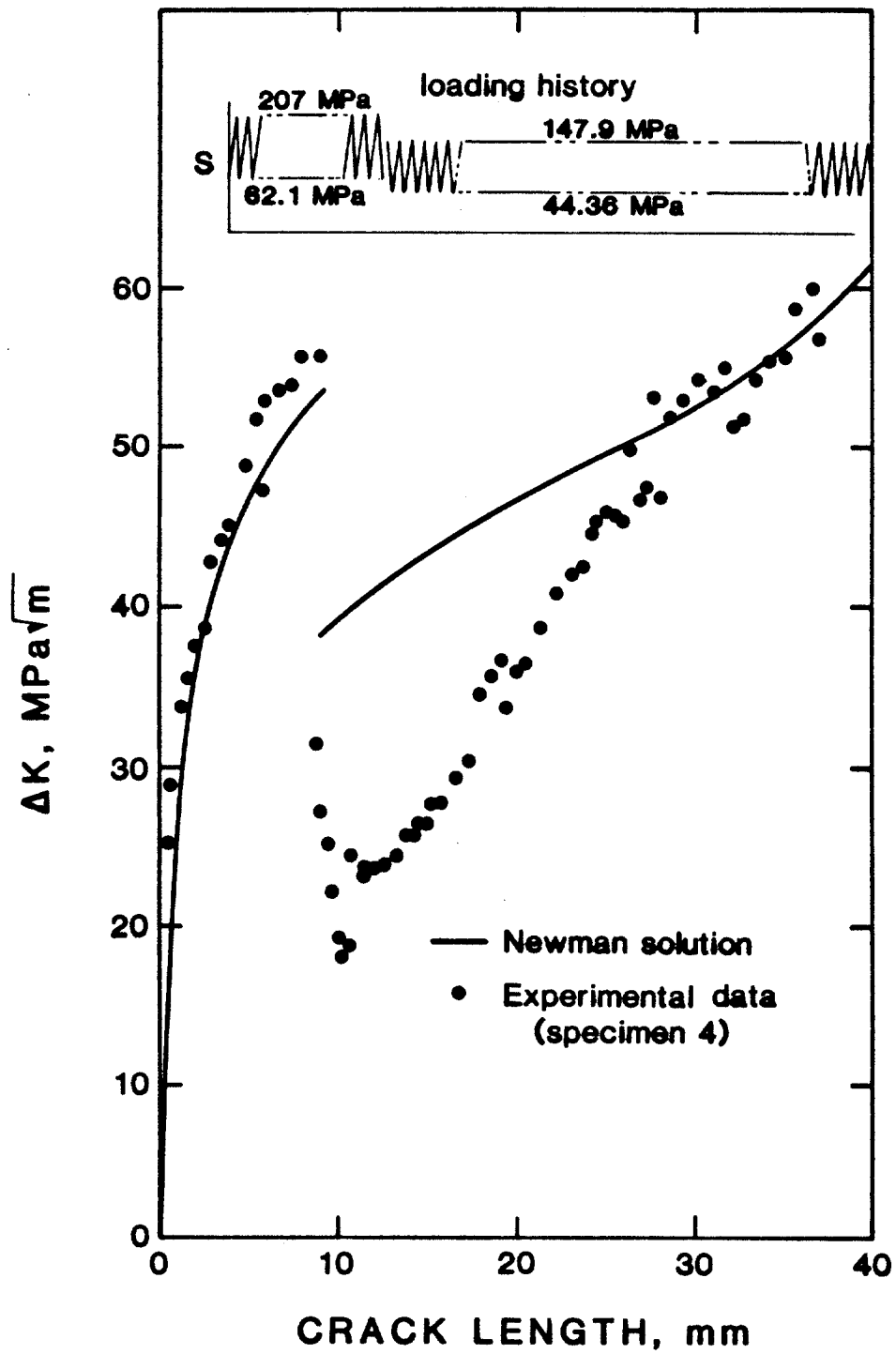


Fig. 5

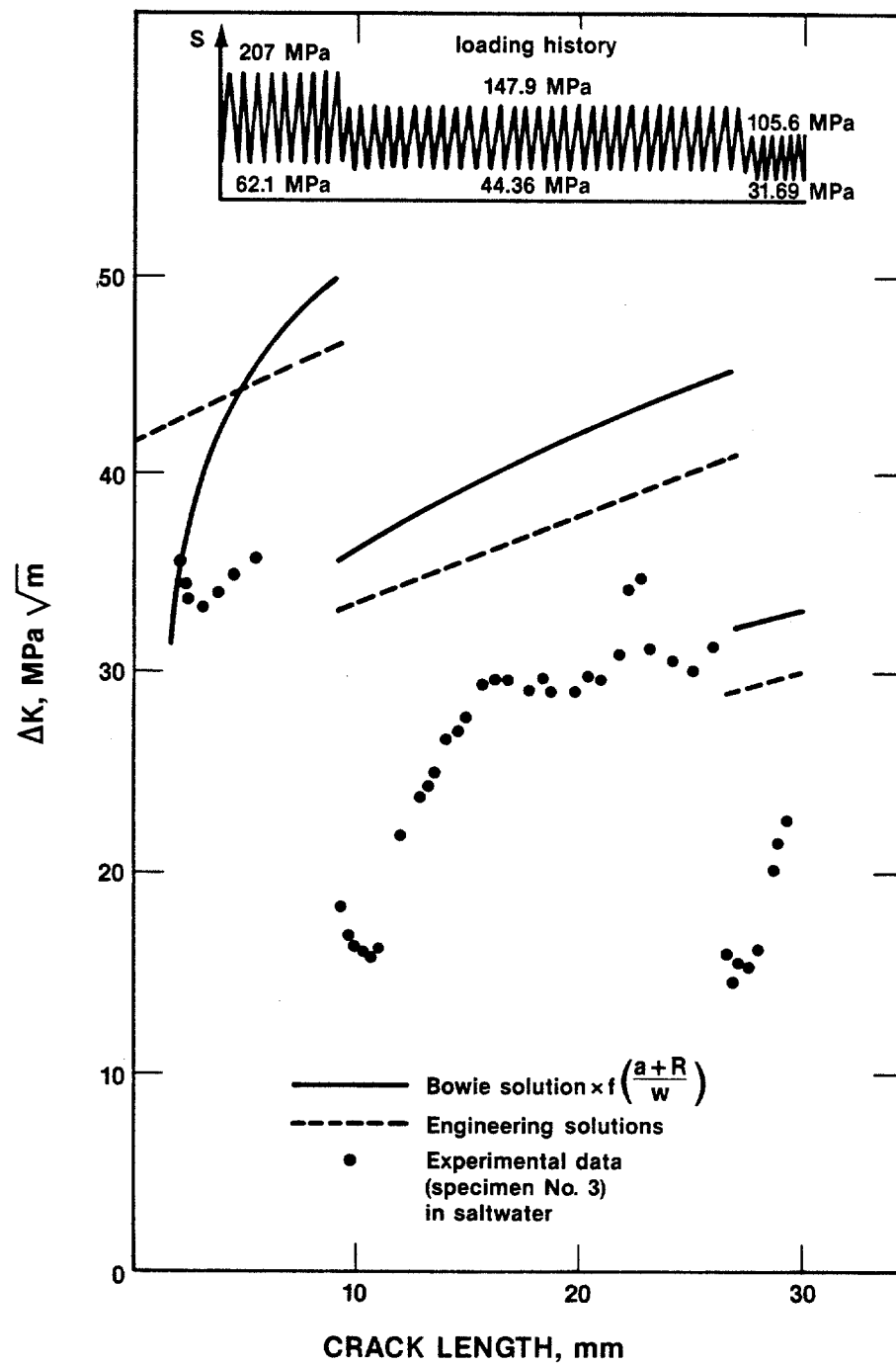


Fig. 6

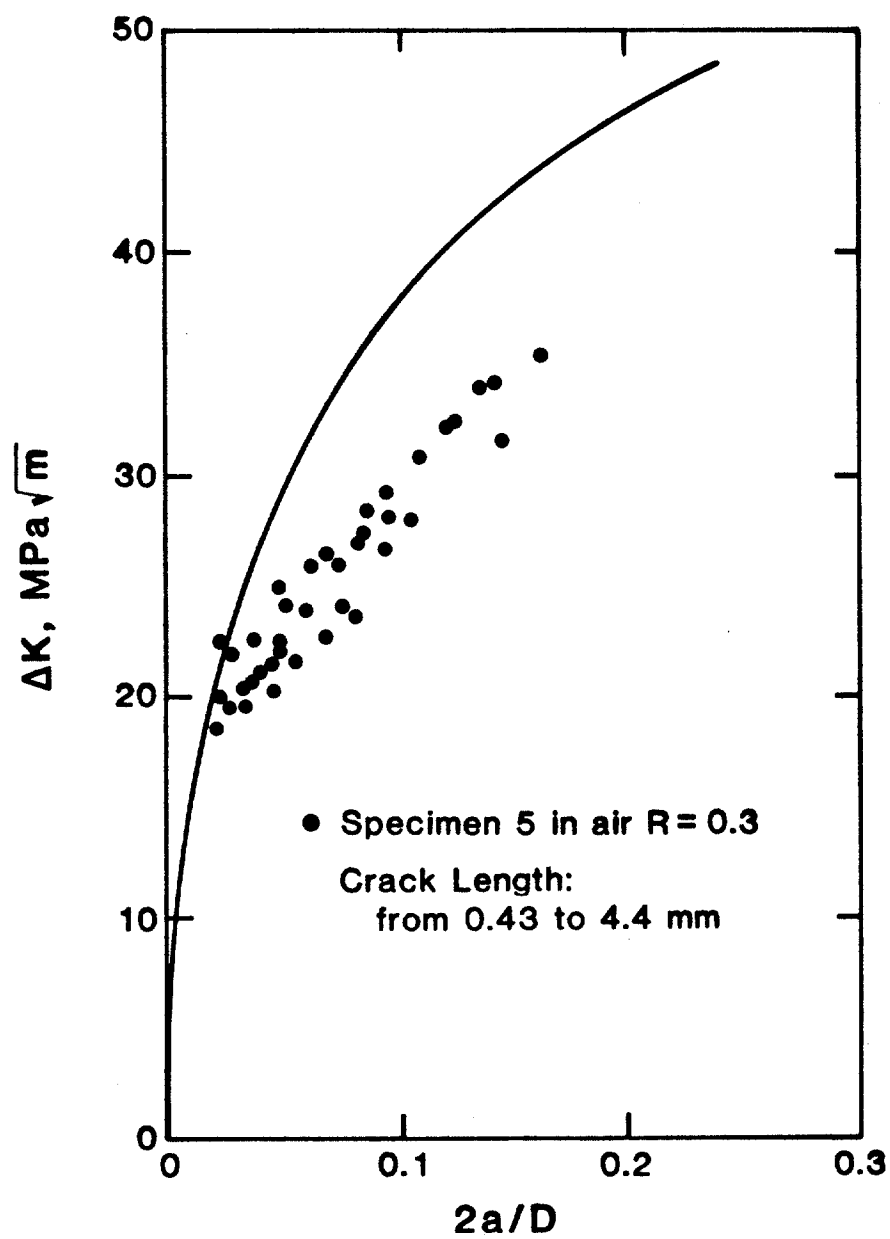


Fig 7

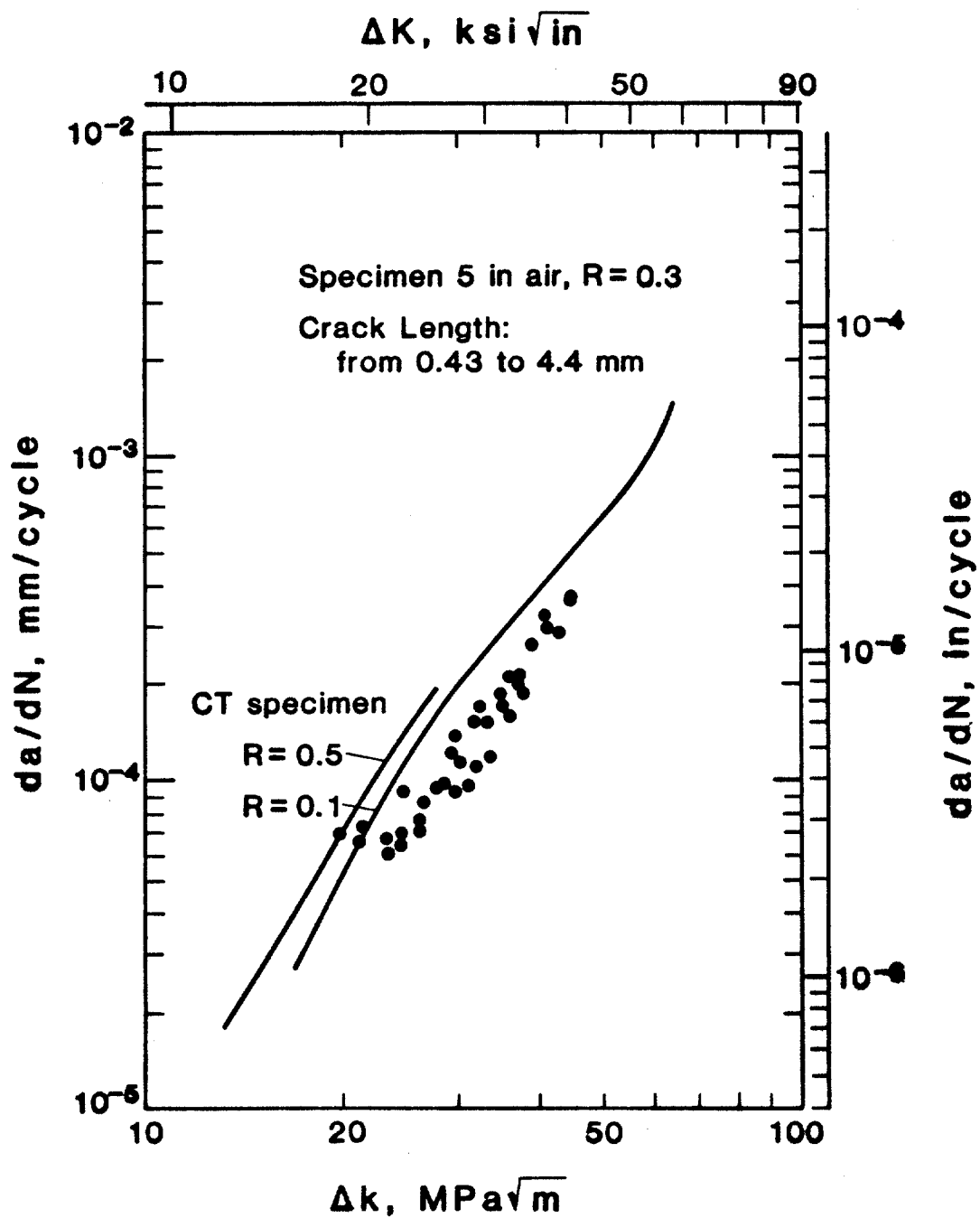


Fig 8